

QCD ASPECTS TO NLO IN THE SEARCH OF SOME BEYOND SM SCENARIOS AT THE HADRON COLLIDERS

A THESIS
SUBMITTED FOR THE DEGREE OF
DOCTOR OF PHILOSOPHY

By

MEDURI C KUMAR



SCHOOL OF PHYSICS
UNIVERSITY OF HYDERABAD
HYDERABAD 500 046, INDIA

June, 2009

DECLARATION

I hereby declare that the material presented in this thesis is the result of investigations carried out by me in School of Physics, University of Hyderabad and in Theory Division, Saha Institute of Nuclear Physics, Kolkata under the supervision of Dr. Prakash Mathews.

The results reported in this thesis are new, and original, to the best of my knowledge, and have not been submitted in whole or part for a degree in any University.

In keeping with the general practice of reporting scientific observations, due acknowledgement has been made whenever the work described is based on the findings of other investigators.

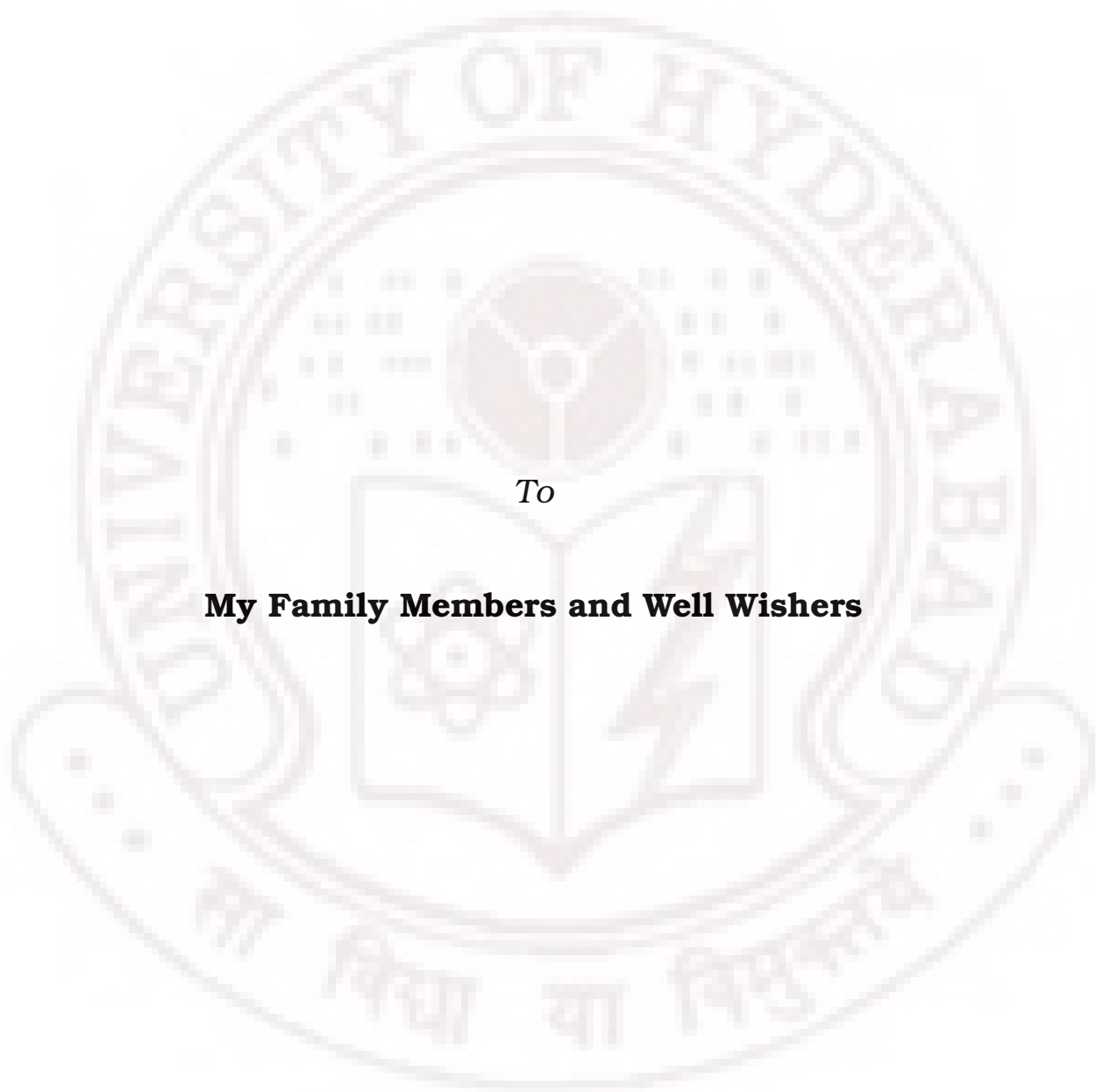
MEDURI C KUMAR

CERTIFICATE

This is to certify that the work embodied in this thesis entitled "QCD ASPECTS TO NLO IN THE SEARCH OF SOME BEYOND SM SCENARIOS AT THE HADRON COLLIDERS", has been carried out by Mr. Meduri C Kumar, under my supervision and the same has not been submitted in whole or part for a degree in any University.

Dr. Prakash Mathews

**DEAN
SCHOOL OF PHYSICS**



To

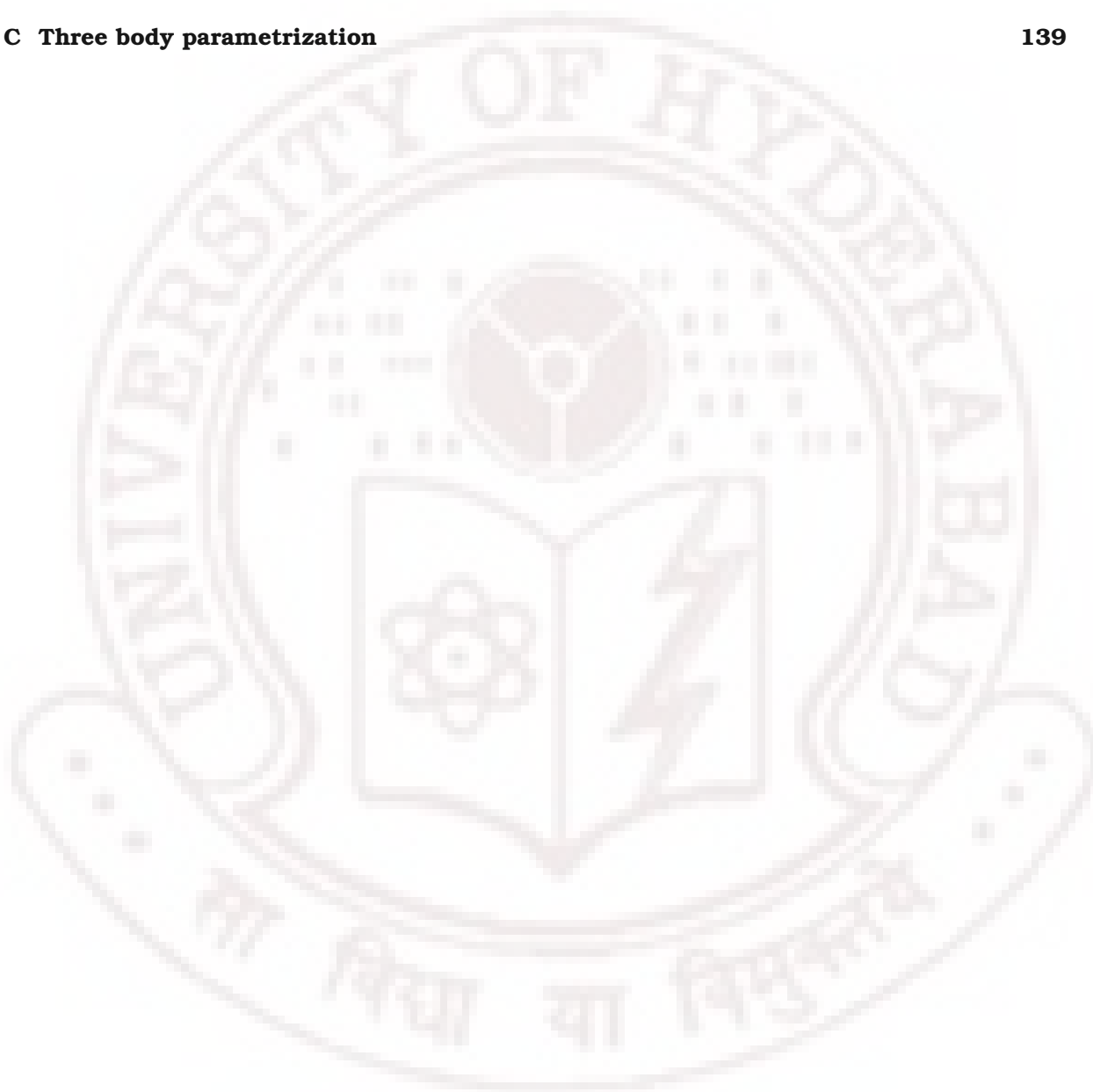
My Family Members and Well Wishers

Contents

Acknowledgements	ix
Abstract	xi
1 Introduction	1
1.1 Motivation for beyond standard model physics	2
1.1.1 Unification of gauge interactions of elementary particles	2
1.1.2 Higgs mass hierarchy problem	3
1.1.3 Cosmological constant problem	4
1.2 Need for higher order QCD corrections	5
2 Beyond Standard Model scenarios	9
2.1 Extra Dimension models	11
2.1.1 Kaluza-Klein theories	11
2.2 Large Extra Dimension model (ADD model)	13
2.3 Warped Extra Dimension model (RS model)	23
2.3.1 KK modes in the RS model	26
2.4 Tests of the gravitational inverse square law	32
2.4.1 Some theoretical speculations	33
2.4.2 Experimental results	34
2.4.3 RS type corrections to ISL	37
2.5 Unparticle scenario	38
3 Two cut-off phase space slicing method	41
3.1 Introduction	41
3.2 The method	42
3.3 Real emission processes	43

3.3.1	Soft	43
3.3.2	Collinear	45
3.4	Virtual processes	48
3.5	Stability with slicing parameters	49
4	Diphoton production to $\mathcal{O}(\alpha_s)$ in the RS model at the hadron colliders	51
4.1	Diphoton production	51
4.1.1	Frixione isolation algorithm	54
4.2	Leading order cross sections	57
4.3	Next-to-leading order cross sections	58
4.4	Results for LHC	64
4.4.1	Stability analysis	65
4.4.2	Kinematic distributions	67
4.4.3	Scale variations	69
4.4.4	Cone variations	70
4.5	Results for Tevatron	72
4.6	Conclusions	73
5	Drell-Yan uncertainties to NLO in QCD in the extra dimension searches	87
5.1	Introduction	87
5.2	Drell-Yan process	88
5.3	Extra Dimension Models	91
5.4	Theoretical uncertainties	93
5.4.1	PDF uncertainty	95
5.4.2	Renormalization/Factorization scale uncertainties	100
5.5	Experimental Uncertainties	101
5.6	Conclusions	102
6	Di-jet production at the LHC through unparticles	115
6.1	SM contribution	116
6.2	Unparticle contribution	117
6.3	Conclusions	122
7	Conclusions	127

Appendices	131
A gg box contribution	133
B Feynman rules	135
C Three body parametrization	139





Acknowledgements

I would like to express my deep sense of gratitude to my supervisor Dr. Prakash Mathews for his guidance in my research work and for all his endeavors to see me get through successfully at various stages in my Ph.D. programme. His simple way of explaining the things in physics gave me a new insight to the subject. The time we have spent together on academic discussions was worth giving me the enough encouragement to move onward in my research. Without his help, in every sense, this work could have surely remained incomplete.

I sincerely thank Dr. V. Ravindran from HRI, Allahabad for his immense help in my research work, for his fruitful discussions and creative ideas about the physics that he used to discuss in our group. I am happy and be proud to come across him in my Ph.D. life and would definitely feel that I owe him something for the time, care and interest he had shown on our research work. I thank my collaborators and friends Anurag Tripathi and Neelima Agarwal for the academic discussions we had together, for their email and telephone conversations on physics and the time they have spent on this.

This work has been supported by the Junior Research Fellowship (JRF) and Senior Research Fellowship (SRF) sponsored by the Council of Scientific and Industrial Research (CSIR), New Delhi, India. I sincerely thank CSIR for its financial support in the last five years.

Thanks go to the School of Physics, University of Hyderabad (UH) where I spent my initial days in research work for providing a good academic atmosphere. I am thankful to the high energy physics group there for the academic events it had organized

like SERC schools which I have got the opportunity to participate in. In particular I thank Prof. M. Siva Kumar, who have kindly agreed to be the in-charge for me at UH for the last four years. I also thank Theory division, Saha Institute of Nuclear Physics (SINP), Kolkata where most of my research work has been carried out, for providing me with all the required facilities to my research work. I thank in particular the graduate students of this division, namely, Purnendu, Ayan, Sayan, Pulak, Jyotirmoy, Muthu, Sovan, Neelanjan, Kalyan, Debarati, for their both academic and non-academic interactions on a variety of topics.

I utterly fail if I don't acknowledge Prof. Asit De and Prof. Harindranath from SINP for providing the access to the super computer CRAY, without which the present work could have been somewhere at its half-way and I thank them with a heart full of reverence. I also thank the Head of Theory division Prof. Kamales Kar for his support to my research visits to various places both within the country and outside the country and also for his humble and personal encouragement in my academic work since the day of my joining SINP.

I thank my friend Karunakar for all that he has been to me over the last many years. A very special thanks to P.M.Swarup Raju for his help in my semester renewal process at UH and for his support at various levels throughout my Ph.D. course. Thanks to my other affectionate friends Thejal and Farzana for the academic discussions we had in general. Thanks to all my old friends who supported me to come to this stage. A sincere thanks to Andhra Loyola College, where my thirst for physics has began, for providing a unique academic atmosphere and an excellent teaching at H.S. and B.Sc. levels.

Last but certainly not the least, I thank my family members, more than any one, for all their continuous support to my research work, for their well wishes and blessings.

Abstract

The Standard model (SM) of particle physics has been very successful in explaining the fundamental interactions of the elementary particles, seen in the nature. However, the SM itself can not be a fundamental theory for it can not explain certain issues like the hierarchy problem. To address such issues in the SM is the main motivation for many beyond the standard model (BSM) physics scenarios like super symmetry, extra dimensions. With the advent of the Large Hadron Collider (LHC) where the center of mass energy will be $\sqrt{S} = 14$ TeV, it will be very much possible to test these theories and to constrain the model parameters. Eventually, the collider phenomenology of the BSM scenarios has gained a lot of interest and a very rich collider signals have been predicted in the literature, most of which are based on a leading order (LO) computation in the perturbation theory. However at the hadron colliders like the LHC, where the gluon fluxes are very high, the QCD corrections will in general be very significant. For the signal cross sections, in addition to the SM subprocesses, many other subprocesses from the BSM sector will enter both at the leading order and next-to-leading order (NLO) levels in the perturbation theory. Hence a naive approximation of the SM K factor to be the same as in the BSM sector is not justifiable and to quantify such higher order (NLO) QCD corrections one needs to perform an explicit computation. These higher order corrections will then be useful in obtaining the bounds on the model parameters from the experimental data. (Chapters 1 and 2).

In the warped extra dimension model (RS), we have explicitly computed the NLO QCD corrections to the well known di-photon production process at the LHC, using a semi-analytical two cut-off phase space slicing method which makes it easy to imple-

ment various experimental kinematic cuts and the isolation algorithm (for suppressing both QED singularities and the fragmentation photons) on the final state photons. We have checked that our results are stable against the variation of the slicing parameters over a wide range and found that our SM results are in agreement with those in the literature. Then, we presented the signals for the RS model in various kinematic distributions and found that the NLO QCD corrections have really enhanced the cross sections. We have studied the factorization scale uncertainties and found that they are decreased considerably at NLO compared to LO. We also presented the RS model predictions at the Tevatron (Chapters 3 and 4).

In the case of Drell-Yan process, we have quantified various QCD uncertainties in both the large and warped extra dimension models. For the uncertainty due to the parton distribution functions (PDFs), we have considered three different parton density sets, MRST2001, CTEQ6L/M and ALEKHIN. Regarding the scale uncertainties, the important observation we made is that the factorization scale uncertainties get reduced by around a factor of 2.75 in going from LO to NLO, independent of the model and irrespective of the collider (Chapter 5).

We have also considered the di-jet production process in the unparticle physics. We find that only the spin-0 unparticles have significant contributions while the spin-2 unparticles don't have any noticeable enhancements over the SM predictions. In the case of scalar unparticles, we have presented the invariant mass, transverse momentum and rapidity distributions of the dijet and found the signal enhancements over the SM background are more than an order of magnitude (Chapter 6.)

List of publications

1. **PDF and scale uncertainties of various DY distributions in ADD and RS models at hadron colliders**

M. C. Kumar, P. Mathews and V. Ravindran

Eur. Phys. J. C 49 (2007) 599; [arXiv:hep-ph/0604135].

2. **Direct photon pair production at the LHC to order α_s in TeV scale gravity models**

M. C. Kumar, P. Mathews, V. Ravindran and A. Tripathi

Nucl. Phys. B 818 (2009) 28; [arXiv:0902.4894 [hep-ph]].

3. **Di-jet production at the LHC through unparticles**

N. Agarwal, M. C. Kumar, P. Mathews, V. Ravindran and A. Tripathi

arXiv:0903.0202 [hep-ph] (in communication.)

Conference Proceedings

1. **Extra Dimension searches at hadron colliders to NLO-QCD**

M.C.Kumar, Prakash Mathews and V.Ravindran

Linear Collider Workshop (LCWS06), March, 2006, Bangalore, India.

Pramana 69:871-876,2007

2. **Diphoton production to NLO in QCD in the RS model at the LHC**

M.C.Kumar, Prakash Mathews, V. Ravindran and Anurag Triapthi

Physics of Warped Extra Dimensions February, 2008 I.I.T. Kharagpur, India.



Chapter 1

Introduction

One of the most remarkable achievements of modern theoretical physics has been the construction of the Standard model (SM) of particle physics that describes the fundamental interactions of the elementary particles. It is a gauge theory based on the group $SU(3) \otimes SU(2) \otimes U(1)$ and explains the electromagnetic, weak and strong interactions seen in the nature. The particle spectrum consists of six quark flavors (u, d, c, s, t, b), three charged leptons (e^\pm, μ^\pm, τ^\pm), three neutrino flavors corresponding to these leptons (ν_e, ν_μ, ν_τ), eight gluons, three weak gauge bosons (W^+, W^-, Z) and one massless photon (γ). The three generations of the quarks and leptons observed in the experiments have been successfully embedded in this model, some of the particles like top and charm quarks are predicted even before their discovery at the experiments. The SM predicted the existence of the weak bosons W^\pm and Z from the electroweak symmetry breaking phenomenon, which have been discovered in the experiments later. The SM predicted masses of these weak bosons were very well compared with the measured ones. The experimentally measured values of these bosons are $m_W \sim 80.398$ GeV and $m_Z \sim 91.1876$ GeV. However, the last piece of the SM, the Higgs boson, the only scalar boson in the theory expected to give masses to the elementary particles, has been elusive in the so far conducted experiments. The consistency of the SM predictions with the precision electroweak measurements from the LEP and Tevatron indicates the existence of this Higgs boson or something analogous to that.

It is very much expected that this Higgs boson be discovered at the LHC experiments. In the possible case of the Higgs boson discovery, the SM can be considered as the best theory to describe the physics of elementary particles and the interactions they respect. However, in spite of its significant achievements and predictions, the SM can not be regarded as a fundamental theory. The theory is not complete as it can not explain some of the challenging issues like the unification of the gauge interactions, large hierarchy between the electroweak and the Planck scales, origin of the neutrino masses, cosmological constant problem. Various attempts have been made since decades to address such issues but with the concepts that are indeed beyond the scope of the SM and in a domain of new physics (NP), that we call 'beyond the standard model (BSM) physics'. In what follows we address some such issues that motivated the study of BSM scenarios.

1.1 Motivation for beyond standard model physics

1.1.1 Unification of gauge interactions of elementary particles

In the SM, it is expected that the couplings of the electromagnetic, weak and strong interactions roughly meet at the GUT scale of the order 10^{16} GeV and hence all these interactions are supposed to have a common origin at this scale. But, the fourth interaction, gravitational interaction, is not considered in the SM so far and it is expected that the gravitational couplings become of the order unity at around Planck scale M_{Pl} energies. In view of the above GUT scale, it is possible to expect that the gravity can also be unified with the remaining three interactions leading to a theory of everything. Postulating such a unified theory of all the four interactions is extremely challenging and is not addressed in the domain of SM.

Both the electromagnetic and gravitational forces are long range forces and it is possible that they could have a common origin. It is with this idea that the initial attempts to unify the gravity and the electromagnetism were made up by Kaluza and

Klein. The unification of these two interactions is shown to be possible with the concept of extra spatial dimensions. The 5 dimensional gravity could lead to both 4 dimensional gravity as well as electromagnetism in 4 dimensions. Following this, subsequent attempts have been made to unify weak and strong interactions (non-abelian gauge theories) with Einstein's gravity using this concept of extra dimensions. Thus one of the main motivations for the extra dimensions stands as the unification of the gravity with the remaining three forces.

1.1.2 Higgs mass hierarchy problem

Higgs boson couples to all the massive particles with the couplings that are proportional to the masses of the particle with which it couples. The self energy corrections to the Higgs boson will give the corrections to its mass. The one loop quantum corrections to the Higgs mass coming from a fermion loop are given by

$$\Delta m_H^2 = \frac{\lambda_f}{8\pi^2} [\Lambda_{UV}^2 + \dots],$$

where λ_f is the Higgs boson coupling with the fermion and Λ_{UV} is the ultra-violet cut-off for the SM theory. If the SM is valid all the way up to the GUT scale 10^{16} GeV or the Planck scale 10^{19} GeV, then the one loop corrections to the Higgs mass quadratically diverge. However, the precision electroweak measurements strongly indicate that the Higgs boson mass must be around few hundreds of GeV. In order to obtain a mass of $\sim 10^2$ GeV from the GUT scale or the Planck scale, one needs to “fine tune” the bare parameters of the theory to several orders of magnitude. This is the Higgs hierarchy problem in the SM. There is no way to address this problem and to obtain a reasonably accepted Higgs mass in the SM frame work.

This hierarchy has been a long standing problem and to address it, many new physics scenarios such as super symmetry, large and warped extra dimensions have been proposed. In the context of super symmetry the presence of the super particles can account for the hierarchy problem. The quadratic divergences of the Higgs mass, coming from the self energy diagrams with the SM particles in the loops, will be

canceled by those coming from the self energy diagrams in which the super particles are in the loops. Thus the Higgs boson could have a mass in the expected range without requiring to fine tune the bare mass parameters. In the case of large extra dimension model, the higher dimensional Planck scale could be as low as a few TeV owing to the large volume of the extra dimensions, and consequently there is a TeV scale upper limit on the Higgs mass. In the case of warped extra dimension model, the fundamental masses could be of the order of Planck scale but the physical masses, because of the exponential warp factor of the higher dimensional metric, could be of the TeV scale order on the 4-dimensional space-time. Hence the physical mass of the Higgs boson could be well within the TeV scale range.

1.1.3 Cosmological constant problem

One of the possible ways to explain the acceleration of the universe is based on a very small cosmological constant Λ . It appears in the the Einstein's field equation as

$$R_{\mu\nu} - \frac{1}{2}Rg_{\mu\nu} + \Lambda g_{\mu\nu} = 8\pi GT_{\mu\nu}$$

The measured value of the Λ is very small, of the order of 10^{-35} s^{-2} . However, the quantum field theories predict a huge cosmological constant corresponding to the vacuum energy. For the quantum field theories valid below a cut-off scale, say M_{Pl} , then it would imply a cosmological constant of the order M_{Pl}^4 which is smaller than the measured one by a factor of 10^{120} . A very large hierarchy between the predicted and the observed values. There is no known natural way to obtain a cosmological constant that is used in the cosmology from the particle physics. This is the cosmological constant problem. This problem can be addressed with the theories of infinite volume extra dimensions. These theories are not 4-dimensional at low energies.

1.2 Need for higher order QCD corrections

In the QCD improved parton model, the hadronic cross section $\sigma^{(H)}$ can be expressed in terms of the perturbatively calculable parton level cross sections $d\hat{\sigma}^{ab}$ convoluted with the appropriate parton distribution functions $f(x, \mu_F)$ (PDF) as given by

$$\sigma^{(H)}(S) = \int_0^1 dx_a \int_0^1 dx_b f_a(x_a, \mu_F) f_b(x_b, \mu_F) d\hat{\sigma}^{ab}(x_a, x_b, \mu_F)$$

where μ_F is called the factorization scale. The parton level cross section $d\hat{\sigma}^{ab}$ corresponds to a perturbative expansion to all orders in the strong coupling strength $\alpha_s(\mu_R)$ as follows:

$$d\hat{\sigma}^{ab}(x_a, x_b, \mu_F) = d\hat{\sigma}_{(0)}^{ab} \left[1 + \alpha_s(\mu_R) C_1(x_a, x_b, \mu_F, \mu_R) + \alpha_s^2(\mu_R) C_2(x_a, x_b, \mu_F, \mu_R) + \dots \right],$$

where $d\hat{\sigma}_{(0)}^{ab}$ corresponds to the leading order contribution and $C_i(x_a, x_b, \mu_F, \mu_R)$ are the coefficient functions that come at order $\alpha_s^{(i)}$. It is expected that the hadronic cross section, which can be measured at the experiments, should not depend on the arbitrary scales introduced in the intermediate stages of the calculation. The factorization of the collinear singularities from the parton cross sections introduces the factorization scale μ_F both in the PDFs and in the parton level cross sections. The renormalization of the coupling constant involves the renormalization scale μ_R in the strong coupling $\alpha_s(\mu_R)$. Though the choice of these scales is decided by the hard scale of the problem, the exact value does not come from the QCD and hence these scales are completely arbitrary. Both the parton level cross sections, calculated to all orders in the perturbation theory, and the parton distribution functions satisfy the renormalization group equations such that the resulting cross section is insensitive to the choice of these scales. This implies that any truncated perturbative cross section results in the explicit dependency of the hadronic cross sections on these scales such that the dependency goes on decreasing as we include more and more higher order terms in the perturbation theory. Thus, though the factorization and the renormalization scales are not physical, the truncation of the perturbative series leads to the scale uncertainties in the hadronic cross sections. The only way to get away with these scale

uncertainties is to include higher order quantum corrections in the calculation. This implies that the NNLO cross sections are more reliable than the NLO ones, which in turn are better than the LO ones. In the case of SM, the QCD corrections to the processes like Drell-Yan, di-photon are computed to higher orders and found that the cross sections have not only showed a significant enhancements over the leading order predictions but also decreased the scale uncertainties considerably. This importance of the QCD corrections eventually led to the resummation techniques to approximate the all order contribution of the cross sections. At the hadron colliders like LHC ($\sqrt{S} = 14$) TeV where the QCD plays an important role, the higher order quantum corrections are expected to be very large and play an important role in the reliable predictions of the cross sections.

Apart from that, in the BSM scenarios like extra dimensions, the gluon initiated subprocesses contribute to the signals at the LO itself. The NLO QCD corrections to this kind of subprocesses will add more to the signal cross sections. It should be noted that such gluon initiated subprocesses in the SM need not come at the LO for every process but can contribute at only higher orders in the perturbation theory. In addition, in BSM scenarios some new vertexes (four point interactions) come directly at NLO which are not there in the SM. Because of these additional amplitudes, the NLO QCD corrections (or K factor) are expected to be larger than those in the SM. In the context of the LHC where the gluon fluxes are very high, a systematic computation of such NLO cross sections would definitely quantify the impact of QCD corrections to the processes that are useful in the search of BSM scenarios. Besides this quantitative estimation, the NLO cross sections have additional advantage of providing the transverse momentum distributions of the pair of particles like di-lepton and di-photon. Such a study of the transverse momentum distributions is not possible using leading order cross sections.

In view of the above points, it can be easily understood that the LO predictions are a crude estimate of the actual hadronic cross sections. As the cross sections for many of the processes in the BSM scenarios are available only at LO, the computation

of NLO cross sections would certainly improve the predictions of the signal cross sections and hence are very useful in the search of BSM physics at the LHC.





Chapter 2

Beyond Standard Model scenarios

There are numerous beyond standard model (BSM) scenarios proposed to address the problems that are not answered in the standard model (SM), as well as to look for the possible new physics that could stand as a more fundamental theory. The SM would then correspond to the low energy effective theory of this fundamental theory. Super symmetry (SUSY), extra dimensions, techni-colour, unparticles, little Higgs and Z' models are a few to name. Each of these scenarios are interesting in its own right when it comes to the understanding of how these models help address various issues and how rich and interesting will be the signals of these models at the collider experiments such as those at the Tevatron or the LHC. The gauge hierarchy problem is one among such issues. In SUSY, corresponding to each of the particles in the SM there is a super partner, called *sparticle* but with a different spin than that of the particle. For each of the fermions in the SM there is a corresponding boson and for each of the gauge boson in the SM there is a fermion. In this model the particle spectrum is rich and in number it contains almost the double of the particles of the SM. The existence of these super partners explains some of the problems in the SM and also gives rise to a much interesting particle phenomenology. But the fact that we do not see super particles in nature breaks the super symmetry and pushes the super particle spectrum to higher energy scales, may be of the order of a TeV scale.

The concept of extra dimensions is first introduced by Kaluza and Klein. These

models are based on the idea that the space-time consists of $4 + n$ dimensions rather than the conventional 4 space-time dimensions. The space of n extra dimensions is called *bulk* whereas the usual 4 dimensional space-time is called a domain wall (may be a *brane*, but need not be always). The compactification of the extra dimensions lead to a tower of modes. Thus a particle propagating the extra spatial dimensions will correspond to a tower of modes on the brane. In the case of *universal extra dimensional* model [1] (UED), all the SM particles are allowed to propagate the extra dimensions. As the SM has been tested down to 10^{-16} cm., and found no evidence for the new extra dimensions which the SM particles can traverse, the size of the extra dimensions is expected to be smaller than this length scale. Consequently, the modes will be very heavy and hence can be observed only in high energy collider experiments.

In the case of both *large extra dimension* model [2] (LED) and warped extra dimension model [3] (WED), only the gravity is allowed to propagate the extra dimensions while all the SM fields are confined to the brane. The concept of the localization of the SM fields to a domain wall comes from the string theory, according to which all the SM fields are harmonic excitations of the open strings whose one end lie on the brane and consequently they can not leave it and propagate into the bulk. Whereas the gravity and other anti-symmetric fields correspond to closed strings which can live in the bulk as well as on the brane. Hence only gravity is allowed to propagate the extra dimensions. Because the gravity has been tested down to sub millimeter range so far, the size of the extra dimensions in the LED could be as large as this length scale. In the case of *warped extra dimension* model unlike UED or LED case, the extra dimension is not flat but highly warped. Because of this large warp factor, the size of the extra dimension could be very small, may be of the order of Planck's length. Both the LED and WED scenarios offer an explanation to the hierarchy problem. In what follows, we concentrate on both the large and warped extra dimension models and discuss them in detail. First, we begin with the Kaluza-Klein theories.

2.1 Extra Dimension models

2.1.1 Kaluza-Klein theories

One of the initial attempts to unify the long range forces seen in the nature, that of gravity and electromagnetism, were made by Kaluza and Klein (KK) with their theories of extra spatial dimensions [5]. The conventional electromagnetic A_μ and gravitational fields $h_{\mu\nu}$ in 4 dimensions are supposed to originate from a higher dimensional field, a gravitational field h_{AB} ($A, B = 0, 1, 2, 3, 5$) in $(4 + 1)$ dimensions. This h_{AB} now stands as the unified field of gravity $h_{\mu\nu}$ ($\mu, \nu = 0, 1, 2, 3$) and electromagnetic fields $A_\mu = h_{\mu 5}$. In a sense it is analogous to the way the electric and magnetic fields are unified in the electromagnetic field. In the Kaluza-Klein theories the extra dimensions are not similar to the usual spatial dimensions but are compactified on some manifold. In the case of one extra dimension, it could be compactified on a circle of radius R . In general, the space of n extra dimensions could be a higher dimensional sphere or torus or some other manifold (X^n). For example, for an n -dimensional torus, this space is $X^n \sim L^n = (2\pi R)^n$. In the KK approach, the $(4 + n)$ dimensional space is the direct product of 4-dimensional space-time M^4 and this compact space X^n of extra dimensions. It is implicit that there is a particular dynamics of these n extra dimensions, which leads to the suitable compactification of them leaving the Minkowski spacetime M^4 intact.

These *extra dimensions* have physical implications when the energy scales used can probe the length scales of the order R . A massless field in $4 + n$ dimensions is equivalent to a tower of massive modes in 4 dimensions. For example, consider a massless scalar field in $4 + 1$ dimensions.

$$\mathcal{L} = -\frac{1}{2}\partial_A\Phi\partial^A\Phi, \quad A = 0, 1, 2, 3, 5$$

where $\Phi(x, y) \equiv \Phi(x_\mu, y)$ with periodic boundary condition $y = y + 2\pi R$. We expand the field in terms of the spherical harmonics. The coefficients are the conventional 4 -

dimensional fields.

$$\Phi(x, y) = \sum_{n=-\infty}^{+\infty} \phi_n(x) e^{iny/R}, \quad \phi_{-n}(x) = \phi_n^*(x)$$

After compactification, the *effective* action in 4- dimensions can be given as

$$S = \int d^4x \left[-\frac{1}{2} \partial_\mu \varphi_0 \partial^\mu \varphi_0 \right] - \int d^4x \sum_{k=1}^{+\infty} \left[\partial_\mu \varphi_k \partial^\mu \varphi_k^* + \frac{k^2}{L^2} \varphi_k \varphi_k^* \right]$$

where $\varphi_n \equiv \sqrt{2\pi R} \phi_n$. There are one massless mode and an infinite tower of massive modes φ_k with mass $m_k^2 = k^2/R^2$, together called *Kaluza-Klein* modes.

Similar is the case with electromagnetic field in $(4 + 1)$ dimensions. The electromagnetic lagrangian in $(4 + 1)$ dimensions is given by

$$\mathcal{L} = -\frac{1}{4g_5^2} F_{AB} F^{AB},$$

where the field strength $F_{AB}^2 = F_{\mu\nu}^2 + 2(F_{\mu 5}^2)$. As action is dimensionless, the coupling g_5 must be dimensionful here. After the KK decomposition, the fields A_μ and A_5 can be expanded in terms of spherical harmonics as before

$$A_\mu(x, y) = \sum_{n=-\infty}^{+\infty} A_\mu^{(n)}(x) e^{iny/R}, \quad A_5(x, y) = A_5^{(n)}(x) e^{iny/R}$$

After the compactification of the extra dimension on circle S^1 , the effective lagrangian in 4 dimensions is given by

$$\mathcal{L}_4 \sim F_{\mu\nu}^{(0)} F^{(0)\mu\nu} + 2 \sum_{n=1}^{\infty} \left[F_{\mu\nu}^{(k)} F^{*(k)\mu\nu} + \frac{n^2}{R^2} A_\mu^{(k)} A^{*(k)\mu} \right] + 2(\partial_\mu A_5^{(0)})^2$$

The mass spectrum consists of a massless gauge field $A_\mu^{(0)}$ with $g_4^2 = g_5^2/2\pi R$, an infinite tower of massive gauge bosons with mass $m_k^2 = k^2/R^2$ and a massless scalar field $A_5^{(0)}$. The massive scalar modes $A_5^{(k)}$ are absorbed into the massive modes of $A_\mu^{(k)}$, a phenomenon analogous to the Higg's mechanism but driven by the geometry of the extra dimensions without requiring any Higg's field. The n-dimensional gauge transformation will be reduced to an infinite number of 4-dimensional *gauge transformations* - one for each KK level.

Thus, a massless field propagating the extra dimensions is equivalent to that of a tower of massive KK modes in 4 dimensions. However, as we did not see any such new massive scalars or photons in the experiments so far, we can say that either the size of the extra dimensions is sufficiently small that probing such modes was beyond the experimental reach, or in a more intuitive way that these fields are confined to the 4-dimensional spacetime (*brane*). This kind of localization of certain fields to the brane and at the same time allowing fields like gravity to traverse the extra dimensions is considered in a particular class of extra dimension models in order to explain some of the issues that are not addressed in the SM, like the hierarchy problem. In what follows, we will discuss such models that have gained lot of attention in the recent past in both theoretical and experimental physics.

2.2 Large Extra Dimension model (ADD model)

There are two apparent physical scales in the particle physics, namely the electroweak scale $M_w \sim 10^2$ GeV that governs the electroweak interactions and the Planck scale $M_{Pl} \sim 10^{19}$ GeV that governs the gravitational interactions. If the SM is valid all the way up to the Planck scale, then there is no mechanism or dynamics that can generate a large gap of 16 orders of magnitude between these two scales, a problem known as *hierarchy* in the particle physics. Or when put in the terminology of particle physics that explains the fundamental interactions between the elementary particles, this is to question as to why the gravity is very weak compared to the electroweak interactions seen in the nature. This hierarchy problem is a long standing problem and has been the main motivation for physics beyond the SM. The hierarchy between the electroweak scale and the Planck scale has in the past been addressed by modifying the particle content of the theory— supersymmetry and technicolor belong to this category. A paradigm shift in this approach was proposed by Arkani-Hamed, Dimopoulos and Dvali (ADD) [2], wherein they have explained the hierarchy with the help of extra spatial dimensions which gravity alone can ‘see’. In this model the spacetime is

supposed to have more than four dimensions. Similar to the Kaluza-Klein compactifications, the extra dimensions will form a compact manifold. The metric in higher dimensions is the direct product of four dimensional Minkowski spacetime with the compact manifold of the extra dimensions. The gravity can propagate all the dimensions whereas the SM fields live only on the $3 + 1$ dimensional domain wall, which does not extend in the compact directions. In string theory, D-branes are the natural candidates for such domain walls, and accordingly the domain wall is some times called a brane in the literature. It is worth noting that the SM domain wall, in this model, can correspond to a 3-brane, but need not necessarily be so. The KK theories of gravity in general are effective theories valid below a certain scale Λ [6]. Because only the gravity is allowed to propagate the extra dimensions, it can undergo some modifications at length scales smaller than the size of these extra dimensions. In this context two cases are of much importance [6]. If ' E ' is the energy scales that can be attained in the experiments, then (i) $E < 1/R \ll \Lambda$ corresponds to a case where a large number of $(\Lambda R)^n$ of KK modes are integrated out. Thus, though the coupling of each KK mode is Planck scale suppressed, they can contribute non-negligible higher dimension operators to the effective low energy theory. (ii) $1/R \ll E < \Lambda$ corresponds to the case where a large number $(ER)^n$ of KK modes are dynamically accessible and one can observe the effects of the extra dimensions in the experiments. Now, the question that needs to be addressed is what could be the size of the extra dimensions that gravity only is allowed to propagate. For this we will have to consider the the gravitational force between two masses in the presence of extra dimensions.

Gravitational force in presence extra dimensions

According to the Newton's inverse square law, the gravitational force of attraction between two point of masses, M and m is

$$\vec{F} = -\frac{G_N M m}{r^2} = m \vec{\nabla} \phi$$

where $G_N \sim 1/M_{pl}^2$ is Newton's constant and $\phi = -\frac{G_N M}{r}$ is the Newtonian potential. In $4 + d$ dimensions this Newtonian potential can be given as

$$\phi = -\frac{4\pi}{(n-2)V_{s^{4+n-2}}}G_N^{4+n}\frac{M}{r^{4+n-3}}$$

Here G_N^{4+n} is the gravitational constant in $4 + n$ dimensions, and $V_{s^{4+n-2}}$ is the volume of $4 + d - 2$ dimensional sphere. Here G_N^{4+n} can be obtained from the Gauss' law which says that the total flux of the gravitational field over any closed surface area containing the gravitational charge (mass) be the same. For simplicity one can take infinite spherical surface area for the 4 dimensional space-time and the volume of n -dimensional torus for the extra dimensions, which is $(2\pi R)^n$. At infinity, in $(4 + n)$ dimensions, the total flux is $\Phi = 4\pi G_N^{4+n}M$ which is the same as $\Phi = 4\pi G_N(2\pi R)^n M$ obtained from the Newtonian potential in 4-dimensions and integrating over the extra n -dimensions. This gives us an important relation between G_N and G_N^{4+n} given by

$$G_N^{4+n} = G_N(2\pi R)^n \quad (2.1)$$

As the $G_N \sim 1/M_{Pl}^2$, the above relation can be re-written as :

$$M_{Pl}^2 = M_s^{n+2}(2\pi R)^n \quad (2.2)$$

where M_s the scale of the extra dimensions, often called as the string scale. To solve the hierarchy problem, one expects M_s to be of the order of a TeV.

$$L \sim 10^{-17+30/n}$$

For $2 \leq n \leq 6$, $10^{-1} \text{ cm.} \leq L \leq 10^{-6} \text{ cm.}$ Then the size of the extra dimension will be $L = 2\pi R \simeq 10^{13} \text{ m}$ for $n = 1$. Obviously, the possibility of $n = 1$ is thus ruled out. For $n = 2$, $L \simeq 1 \text{ mm}$ and is interesting scale which is being probed currently for the deviations from the inverse square law. For $n = 6$, the size of the extra dimensions will be as small as few fm . However the size of the extra dimensions in this model could be as large as few μm and is clearly not ruled out by the current gravitational experiments that probe the inverse square law. (A brief study of the experiments on

the inverse square law behaviour of gravity and the distance scales that have been probed so far are taken up in the section(2.4). Hence, a value of $n \geq 3$ is acceptable for the phenomenology of extra dimensions. Thus, there is a region in the parametric space of n and L corresponding to $M_s \sim \text{TeV}$ that is allowed by the present experiments on Newtonian gravity. As a result the new physics can commence at the TeV scale itself setting the UV of the SM at this scale instead of at M_{Pl} . Thus the hierarchy problem has been offered an explanation coming from the large extra dimensional model.

Gravity in higher dimensions

The metric in this model is given by

$$ds^2 = g_{\mu\nu} dx^\mu dx^\nu - r^2 d\Omega_{(n)}^2$$

where $g_{\mu\nu}(x) = \eta_{\mu\nu} + \kappa h_{\mu\nu}(x) + \mathcal{O}(\kappa^2)$. In the weak gravitational field approximation one can neglect the higher order terms in κ and work in the linearized gravity approximation as given by $g_{\mu\nu}(x) = \eta_{\mu\nu} + \kappa h_{\mu\nu}(x)$ where $h_{\mu\nu}$ are the gravitational fluctuations around the flat metric $\eta_{\mu\nu}$. The action in higher dimensions now takes form

$$S^{4+n} = -\frac{M_s^{n+2}}{2} \int d^4x \int_0^{2\pi L} d^n y \sqrt{g^{4+n}} R^{4+n}$$

The linearized gravity lagrangian in $(4+n)$ dimensions or the Fierz-Pauli lagrangian is given by

$$\frac{1}{\kappa^{(d)2}} \sqrt{g^d} R^d = \frac{1}{4} (\partial^A h^{BC} \partial_A h_{BC} - \partial^A h \partial_A h - 2h^A h_A + 2h^A \partial_A h) + \mathcal{O}(\kappa^{(d)}),$$

where $\kappa^{(d)2} = 16\pi G^{(4+n)}$ with $G^{(4+n)}$ the Newton's constant in $(4+n)$ dimensions. This lagrangian is invariant under general coordinate transformations: $\partial h_{AB} = \partial_A \zeta_B + \partial_B \zeta_A$ and yields the following d'Alembert equation of motion

$$\square_{(4+n)} (h_{AB} - \frac{1}{2} \eta_{AB} h) = 0,$$

after imposing the de Donger gauge condition $\partial^A(h_{AB} - \frac{1}{2}\eta_{AB}h) = 0$. The KK reduction of this linearized gravity to 4-dimensions can be given as :

$$h_{AB} = V_n^{-1/2} \begin{pmatrix} h_{\mu\nu} + \eta_{\mu\nu}\phi & A_{\mu i} \\ A_{\nu j} & 2\phi_{ij} \end{pmatrix},$$

where V_n is the volume of the compact space of n extra dimensions, $\phi = \phi_{ii}$ and $\mu, \nu = 0, 1, 2, 3$ and $i, j = 5, 6, \dots, (4+n)$. These together with the tracelessness condition $h_A^A = 0$ and the equation of the motion of gauge parameter will fix the physical degrees of freedom for a massless graviton in $(4+n)$ dimensions. These fields can be compactified on an n -dimensional torus, and can have harmonic expansion as

$$h_{\mu\nu}(x, y) = \sum_{\vec{k}} h_{\mu\nu}^{\vec{k}}(x) e^{i\vec{k} \cdot \vec{y}/R} \quad (2.3)$$

$$A_{\mu i}(x, y) = \sum_{\vec{k}} A_{\mu i}^{\vec{k}}(x) e^{i\vec{k} \cdot \vec{y}/R} \quad (2.4)$$

$$\phi_{ij}(x, y) = \sum_{\vec{k}} \phi_{ij}^{\vec{k}}(x) e^{i\vec{k} \cdot \vec{y}/R}, \quad (2.5)$$

where $\vec{k} = \{k_1, k_2, \dots, k_n\}$. For simplification the extra dimensions are all taken to be of the same size R and compactified on n dimensional torus. For, the extra dimensions of different size, the compactification on an asymmetric n -dimensional torus is straight forward by considering different R_i along the directions of different extra dimensions, denoted by k_i . The compactification leads to a massless mode corresponding to $\vec{k} = 0$ and a tower of massive modes of spin-2, spin-1 and spin-0 particles, all are mass degenerate for any given KK level \vec{k} . Each of these massive KK modes satisfy the following equation of motion:

$$(\square_4 + m_{\vec{k}^2})X^{\vec{k}} = 0 \quad \text{with } m_{\vec{k}}^2 = \frac{\vec{k}^2}{R^2} \quad (2.6)$$

where $X^{\vec{k}} = (h_{\mu\nu}^{\vec{k}} - \frac{1}{2}\eta_{\mu\nu}h^{\vec{k}}, \quad A_{\mu i}^{\vec{k}}, \quad \phi_{ij}^{\vec{k}})$. To make these fields invariant under the gen-

eral coordinate transformations

$$\begin{aligned}\delta h_{\mu\nu}^{\vec{k}} &= \partial_\mu \zeta_\nu^{\vec{k}} + \partial_\nu \zeta_\mu^{\vec{k}} + i\eta_{\mu\nu} \frac{k_i}{R} \zeta_i^{\vec{k}}, \\ \delta A_{\mu i}^{\vec{k}} &= -i \frac{k_i}{R} \zeta_\mu^{\vec{k}} + \partial_\mu \zeta_i^{\vec{k}}, \\ \delta \phi_{ij}^{\vec{k}} &= -i \frac{k_i}{2R} \zeta_j^{\vec{k}} - i \frac{k_j}{2R} \zeta_i^{\vec{k}},\end{aligned}$$

they will be redefined as [6]

$$\begin{aligned}\bar{h}_{\mu\nu}^{\vec{k}} &= h_{\mu\nu}^{\vec{k}} - i \frac{k_i R}{\vec{k}^2} (\partial_\mu A_{\nu i}^{\vec{k}} + \partial_\nu A_{\mu i}^{\vec{k}}) - (P_{ij}^{\vec{k}} + 3\bar{P}_{ij}^{\vec{k}}) \left(\frac{2}{3} \frac{\partial_\mu \partial_\nu}{m_k^2} - \frac{1}{3} \eta_{\mu\nu} \right) \phi_{ij}^{\vec{k}}, \\ \bar{A}_{\mu i}^{\vec{k}} &= P_{ij}^{\vec{k}} (A_{\mu j}^{\vec{k}} - i \frac{2n_k R}{\vec{k}^2} \partial_\mu \phi_{jk}^{\vec{k}}), \quad \bar{\phi}_{ij}^{\vec{k}} = \sqrt{2} (P_{ik}^{\vec{k}} P_{jl}^{\vec{k}} + a P_{ij}^{\vec{k}} P_{kl}^{\vec{k}}) \phi_{kl}^{\vec{k}},\end{aligned}\quad (2.7)$$

where the projection operators are given by

$$P_{ij}^{\vec{k}} = \delta_{ij} - \frac{k_i k_j}{k^2}, \quad \bar{P}_{ij}^{\vec{k}} = \frac{n_i n_j}{n^2} \quad (2.8)$$

and a is the solution of the equation $3(n-1)a^2 + 6a - 1 = 0$. As can be seen from the eqns.(2.7), that a massless spin-2 fields $h_{\mu\nu}^{\vec{k}}$ absorb the spin-1 and spin-0 fields at the same KK level and become massive. This is similar to Higg's mechanism but governed by the geometry of the extra dimensions without requiring to have any Higg's field. Hence the compactification of the extra dimensions lead to a tower of massive spin-2, spin-1 and spin-0 particles in 4-dimensions with masses $m_k^2 = \vec{k}^2/R^2$. As discussed before, the size of the extra dimension in this model could be as large as few tens of μm consistent with the present experiments on testing Newton's gravity at smaller length scales. With this possible macroscopic size of the extra dimensions, there can be a large number of light KK modes that can play an important role in the phenomenology of particle physics.

Gravity couples to the SM fields via energy momentum tensor $T^{\mu\nu}$. Hence all the above spin-0, spin-1 and spin-2 KK modes obtained from a gravity in higher dimensions will also couple to the SM via energy momentum tensor. From the relation

$$P_{ij}^{\vec{k}} \phi_{ij}^{\vec{k}} = \frac{3\omega}{2} \bar{\phi}^{\vec{k}}$$

(where $\omega = \sqrt{\frac{2}{3(n+2)}}$), we see that the spin-0 modes couple through the dilation mode $\bar{\phi}^{\vec{k}} = \bar{\phi}_{ii}^{\vec{k}}$, the trace of it, whereas the spin-1 KK modes decouple. Hence, the effective interaction lagrangian between the physical (redifined) KK modes and the SM fields is given by

$$\mathcal{L}_{int} = -\frac{\kappa}{2} \sum_{\vec{k}=0}^{\infty} \int d^4x \left[\bar{h}_{\mu\nu}^{\vec{k}}(x) T^{\mu\nu}(x) + \omega \bar{\phi}^{\vec{k}}(x) T_{\mu}^{\mu}(x) \right]$$

where $\kappa = \sqrt{16\pi}/M_{Pl}$. The zero mode corresponds to the usual 4-dimensional massless graviton. Though, the coupling of each of the KK modes with the SM fields is M_{Pl} suppressed, the effective coupling due to the many available KK modes need not be suppressed by again Planck scale but could be by the scale M_s that governs this effective theory of large extra dimensions. This results in enhanced effective couplings that can lead to observable effects in the collider experiments. In any typical scattering cross section, one needs to perform a summation over all possible virtual states at the amplitude level (or in the propagator) itself. For incoherent processes, similar to that of the subprocess contribution involving different initial and final state particles but leading to the same physical observable, all possible contributions have to be added over at the cross section level. In the case where the KK modes participate in a scattering process at the intermediate level, thus, one has to perform the summation over these virtual KK modes at the amplitude level itself. In general, these virtual KK modes lead to the deviations from the expected SM background contribution. However for the processes involving the KK modes in the final state, KK modes with different mass correspond to different final states, and hence incoherent processes, that have to added at the cross section level. The real emission of the KK modes lead to the large missing \cancel{E}_T signals at the collider experiments.

In a process involving a virtual exchange of KK modes between the SM particles, the sum of KK propagators with momentum q is $\mathcal{D}(Q^2)$ is given by ($q^2 = Q^2$)

$$\kappa^2 \mathcal{D}(Q^2) = \kappa^2 \sum_k \frac{1}{Q^2 - m_k^2 + i\epsilon} \quad (2.9)$$

For large extra dimension case, the m_k will be small and hence the spectrum of these light KK modes can be approximated to be a continuous one with the number of KK states lying in the interval dm_k^2 being

$$\Delta \vec{k}^2 = \rho(m_k) dm_k^2$$

where $\rho(m_k)$ is the density of the KK states in the continuum limit. Hence the above summation over the KK modes can be approximated to the integral given by

$$\kappa^2 \mathcal{D}(Q^2) = \frac{8\pi}{M_s^4} \left(\frac{Q}{M_s} \right)^{(n-2)} \left[-i\pi + 2I(\Lambda/Q) \right], \quad (2.10)$$

The integral $I(\Lambda/Q)$ is a result of the summation over the non-resonant KK modes and the term proportional to π is due to the resonant production of a single time-like KK mode [6]. Here the Λ is the explicit cut-off on the KK sum which is identified with the scale of the extra dimension theory M_S [6, 7]. The κ^2 suppression in a virtual exchange is compensated for by the high multiplicity, after the KK modes are summed over. For time-like KK modes, the integral can be read as

$$\begin{aligned} I(\omega) &\sim \int_0^\omega dx \frac{x^{n-1}}{1-x^2} \\ &= - \sum_{k=1}^{n/2-1} \frac{1}{2k} \omega^{2k} - \frac{1}{2} \log(\omega^2 - 1) \quad k = \text{even}, \\ &= - \sum_{k=1}^{(n-1)/2} \frac{1}{2k-1} \omega^{2k-1} + \frac{1}{2} \log\left(\frac{\omega+1}{\omega-1}\right) \quad k = \text{odd}. \end{aligned} \quad (2.11)$$

Here it should be noted that for an exchange of space-like KK modes, there will be no factor of π corresponding to the resonance in the above summation. The summation for space-like KK propagators is given by

$$\kappa^2 \mathcal{D}(Q^2) = -\kappa^2 \sum_k \frac{1}{Q^2 + m_k^2} \quad (2.12)$$

where $Q^2 = |q^2|$ and the above integral for space-like KK modes takes the following

form:

$$\begin{aligned}
I(\omega) &= \int_0^\omega dx \frac{x^{n-1}}{1+x^2} \\
&= (-1)^{n/2+1} \sum_{k=0}^{n/2-1} \frac{(-1)^k}{2k} \frac{1}{2k} \omega^{2k} + \frac{1}{2} \log(\omega^2 - 1) \quad k = \text{even}, \\
&= (-1)^{(n-1)/2} \sum_{k=1}^{(n-1)/2} \frac{(-1)^k}{2k-1} \omega^{2k-1} + \tan^{-1} \omega \quad k = \text{odd}.
\end{aligned} \tag{2.13}$$

As the coupling of the KK modes to the SM fields is via energy momentum tensor, the KK modes do not distinguish the color, flavor, electric charge or even the spin of the SM particles. Hence each KK mode couples with the same strength to the photons, leptons, weak bosons, quarks, gluons and scalars. However the vertex factors could be different. As per the phenomenology of these KK modes is considered, this particular feature of their coupling to all SM fields is very much interesting. For example, we know that the photons do not interact with each other and hence the production of a pair of photons from the hard scattering process at the photon colliders can be explained only with the terms that come at higher orders in perturbation theory in the SM, whereas in the extra dimension models this process can take place in the simplest $2 \rightarrow 2$ process itself because of the photon-graviton couplings. Another example is various pair production processes at the LHC. At the hadron colliders like LHC where the centre of mass energy is very high ($\sqrt{s} = 14$ TeV), the parton fluxes that can produce invariant mass of upto 1 TeV are very high. In particular, the gluon fluxes are very very high. This when combined with the fact that the KK modes couple to the gluons directly, makes various processes possible, like production of $l\bar{l}$, $\gamma\gamma$, di-jet, ZZ , W^+W^- , hh , that can be explained based on the simplest gluon-gluon initiated gravity mediated tree level $2 \rightarrow 2$ feynman diagrams [6–9]. For the scale $M_s \sim \mathcal{O}(\text{TeV})$, it can be likely that the cross sections in these processes could become large enough to dominate the SM background contribution. Thus it will be very much possible to look for the signals that these extra dimension models predict based on the virtual effects of the KK modes at the LHC. On the other hand, the phenomenology associated with

the real production of KK modes is even interesting in the sense that it is associated with large missing transverse energies that are balanced by either a mono-jet or by a mono-photon ensuring the energy momentum conservation. These mono-photon and mono-jet productions do give a very clear signals. In the possible case of such single jet or single photon productions in the SM, the final states in the SM and in the extra dimension model are different and hence in such channels there will be no interference effects (SM*ADD). Hence the study of such signals is easy to compare with the theoretical predictions and obtain the information about the unknown parameters of the model. The search for the large extra dimensions at the Tevatron experiments has already been carried out in the dielectron and diphoton channels using the 1.05 fb^{-1} data obtained from the $p\bar{p}$ collisions at the center of mass energy of 1.96 TeV [10]. The data has been presented in the table 2.1.

n_d	2	3	4	5	6	7
Obs. M_s	2.09	1.94	1.62	1.46	1.36	1.29
Exp. M_s	2.16	2.01	1.66	1.49	1.38	1.31

Table 2.1: Observed and expected lower limits at the 95% C.L. on the effective Planck scale, M_s , in TeV [10].

The data has set a lower limit of 2.1 TeV to 1.3 TeV on the string scale M_s for 2 to 7 extra dimensions.

Summary and few remarks on the ADD model

1. The ADD model offers a possible explanation to the hierarchy between the electroweak scale and the Planck scale. The size ' R ' of the extra dimensions in this model could be as large as few tens of micrometers, consistent with the present experimental results on the gravitational inverse square law. The compactification of these extra dimensions leads to a tower of spin-0, spin-1 and spin-2 Kaluza-Klein (KK) modes. The spin-2 and spin-0 (via its dilaton mode) couple to the SM fields while the spin-1 KK modes decouple.

2. At the LHC energies for $M_s \sim \mathcal{O}(\text{TeV})$, a large number of KK modes are dynamically accessible and hence there is every possibility to look for these KK modes at the LHC experiments. The virtual KK modes will give rise to deviations from the SM predictions while the real emissions of these KK modes lead to a large missing transverse energy signals.
3. Above the scale M_s , the extra dimensions are dynamically accessible and the world looks $(4 + n)$ dimensional indeed and in that case the collider signals will be different from those of the compactified extra dimensions.
4. The signals of the ADD model are interesting for they could open up a window for the discovery of the gravitons in the laboratory experiments and eventually to probe the quantum structure of gravity.

2.3 Warped Extra Dimension model (RS model)

In the last chapter we have studied the ADD model, the first extra dimension model to address the hierarchy problem. The hierarchy between the electroweak scale and the Planck scale has been accounted for the large volume of the extra dimensions in that model. The string scale M_s , below which the effective theory of the extra dimensions is valid, can be as low as a few TeV and stands as a new UV cutoff for the SM. Because of the many available KK modes, both the virtual effects and the real emission of these can become significant and hence the collider phenomenology of this model is very rich. Although, the model is very interesting in various respects, there are few important points worth noting here, they are

- In explaining the hierarchy, a very large number of $N = (\Lambda R)^n$ of modes have been integrated over in this model, where Λ is the scale below which the effective theory of the extra dimension model, as described by ADD, is valid. To address a large hierarchy, the model introduces a large number of KK modes.

- In explaining the hierarchy between M_w and M_{Pl} , this model runs into another hierarchy between the scales $1/R$ and M_w . There is no apparent explanation for this new hierarchy.

In light of the above, a new approach to the hierarchy problem was taken up by Randall and Sundrum (RS) using a completely different geometry of the extra dimensions [3]. In this model also, only gravity is allowed to propagate the higher dimensional spacetime while the SM fields are confined to the 4-dimensional spacetime (*brane*). In the RS model there is only one extra spatial dimension and is compactified on a circle of circumference $2\pi r$ and further orbifolded by identifying points related by $y \rightarrow -y$. The higher dimensional metric in this model is not factorisable as given by

$$ds^2 = e^{-2ky} \eta_{\mu\nu} dx^\mu dx^\nu + dy^2 \quad (2.14)$$

where $y = r\phi$ is the coordinate of extra dimension, x^μ are the familiar 4-dimensional coordinates and k is a scale of order the Planck scale M_{Pl} . This metric corresponds to anti de Sitter space AdS_5 for it is a maximally symmetric Lorentzian manifold with negative curvature. This metric is also a solution of the Einstein's field equations.

The novel feature in this model is the exponential warp factor e^{-2ky} which can be accounted for the hierarchy between the electroweak and the Planck scales, without requiring a large volume of the extra dimensional space. Thus, the size r could be as small as possible that the compactification scale $\mu \sim 1/r$ need not be very different from the fundamental Planck scale. As the extra dimension has orbifold symmetry S^1/Z_2 , the points corresponding to $0 \leq y \leq r\pi$ will specify the metric completely. Another significant thing in this model is that there are two 3-branes that are attached to the orbifold fixed points $y = 0$ and $y = r\pi$, as opposed to the familiar one 3-brane like in ADD model. The brane on which we live is the SM brane or the “visible” brane and the other one is called Planck brane or the “hidden” brane. The SM brane is placed at the point $y = r\pi$ in order to account for the apparent weakness of the gravity on it, consistent with the above metric. On the other hand the hidden brane is placed at $y = 0$ where the gravitational interactions are expected to become strong. The SM

brane is with negative tension while the Plank brane is with positive tension. Both of these branes can support the familiar 4-dimensional field theories but the excitations of the particle on the SM brane are at the TeV scale while those on the Plank brane are at the Planck scale. The classical action for this five dimensional system is given by

$$S = S_{gr} + S_{sm} + S_{Pl} \quad (2.15)$$

where

$$\begin{aligned} S_{gr} &= \int d^4x \int_{-\pi}^{\pi} d\phi \sqrt{-G} [-\Lambda + 2M^3 R] \\ S_{sm} &= \int d^4x \sqrt{-g_{sm}} [\mathcal{L}_{sm} + 24M^3 k] \\ S_{Pl} &= \int d^4x \sqrt{-g_{Pl}} [\mathcal{L}_{Pl} - 24M^3 k], \end{aligned} \quad (2.16)$$

and M is the $(4+n)$ dimensional Planck scale. The action of gravity in 4-dimensions is

$$S_{gr}^4 \sim M_{Pl}^2 \int d^4x \sqrt{-g} R \quad (2.17)$$

By comparing the scales in this action and the effective action obtained from eqn.(2.16), one can easily show that

$$M_{Pl}^2 = \frac{M^3}{k} [1 - e^{-2kr\pi}] \quad (2.18)$$

From this we see that for $M \sim M_{Pl}$ and large kr values, the 4-dimensional Planck scale does not get significant modifications because of the additional extra dimension. The metric on the SM brane will be $g_{\mu\nu} \sim e^{-2kr\pi} \eta_{\mu\nu}$. This is an important outcome of the model for it can lead to a general conclusion that any fundamental mass parameter M_0 in higher dimensions corresponds to a physical mass m on the SM brane at $\phi = \pi$ as given by

$$m = M_0 e^{-kr\pi} \quad (2.19)$$

For $kr \sim 12$, one can generate a TeV scale from the Planck scale. This is remarkable in the sense that to explain a large hierarchy one really does not require a large volume of the extra dimensions but an exponential warp factor as considered above will be sufficient, with the size of the extra dimension not far away from the Planck length. All the fundamental parameters k , M , $\mu \sim 1/r$ (with $k < M$) are the order of the same scale and there is no new hierarchy among these scales. This model not only offers a possible explanation to the hierarchy between the electroweak scale and the Planck scale but also gives raise to the possibility that the gravitational interactions can become stronger on the brane at scales close to TeV. The gravitational interactions can have only TeV scale suppression as opposed to the usual Planck scale suppression. Further it has been showed that [11] the value of $kr\pi$ can be stabilized without fine tuning by minimizing the potential for the modulus field which describes the relative motion of the two branes. In the RS model graviton and the modulus field can propagate the full 5-dimensional space time while the SM is confined to the TeV brane.

2.3.1 KK modes in the RS model

The Kaluza-Klein compactification of the extra dimension in general involves the fields $h_{\mu\nu}(x, y)$, $A_{\mu 5}(x, y)$ and $\phi_{55}(x, y)$. In the particular set up of the branes at $\phi = 0$ and at $\phi = \pi$ as described here, there are no continuous isometries of the higher dimensions and hence all the off diagonal elements corresponding to these vector modes $A_{\mu y}^{(n)}$ are excluded in this effective theory. To perform the KK decomposition, the gravitational field $h_{\mu\nu}(x, y)$ can be expanded as

$$h_{\mu\nu}(x, \phi) = \sum_{n=0}^{\infty} h_{\mu\nu}^{(n)} \frac{f^{(n)}(\phi)}{\sqrt{r}} \quad (2.20)$$

The equation of the motion of $h_{\mu\nu}^{(n)}$ in the gauge $\partial^\mu h_{\mu\nu}^{(n)} = \eta^{\mu\nu} h_{\mu\nu}^{(n)} = 0$, is given by

$$(\square - m_n^2) h_{\mu\nu}^{(n)} = 0 \quad (2.21)$$

In addition the functions $f^{(n)}(\phi)$ are chosen to satisfy

$$\int_{-\pi}^{\pi} d\phi e^{-2k\phi} f^{(n)}(\phi) f^{(m)}(\phi) = \delta_{nm} \quad (2.22)$$

From the above equation and the Einstein's equation for the field $h_{\mu\nu}(x, \phi)$ sets the equation of the motion for the field $f^{(n)}(\phi)$ as

$$\frac{-1}{r^2} \frac{d}{d\phi} \left[e^{4\phi} \frac{df^{(n)}}{d\phi} \right] = m_k^2 e^{-2ky} f^{(n)} \quad (2.23)$$

The solutions for the above differential equation are given by [11, 12]

$$f^{(n)}(\phi) = \frac{e^{2ky}}{C_n} [J_2(\alpha_n) + a_n Y_2(\alpha_n)], \quad (2.24)$$

where $J_2(\alpha_n)$ and $Y_2(\alpha_n)$ are second order Bessel functions of first and second kind respectively, $\alpha_n = m_n e^{ky}/k$, C_n are normalization and a_n are constants. On the SM brane, if we define $x_n = \alpha_n(\pi)$ and in the limit $m_n \ll k$ (with $e^{kr} \gg 1$), the requirement that $f^{(n)}(\phi)$ has to be continuous across the orbifold fixed points gives us $a_n \sim x_n^2 e^{-2kr\pi}$ and $J_1(x_n) = 0$. Here, the x_n are simply the zeros the first order Bessel function. Hence the masses of the RS modes are given by

$$m_n = k x_n e^{-kr\pi} \quad (2.25)$$

where $x_1 = 3.8317$ and $x_n = 7.0156 + (n-2)\pi$ for $n > 2$. From the value of a_n , we can ignore $Y_2(x_n)$ in eqn.(2.24) in comparison to $J_2(x_n)$. The normalization constants hence can be approximated to

$$C_n = \frac{e^{kr\pi}}{\sqrt{kr}} J_2(x_n) \quad (2.26)$$

for $n > 0$ and for zero mode, it is $C_0 = 1/\sqrt{kr}$. As the masses of the RS modes depend on the zeros of the Bessel's functions, the mass spectrum is not uniform, and the separation is decided by that between the zeros of the Bessel function. The coupling of the gravity to the matter fields is given by the interaction of the higher dimensional gravitational field $h_{\mu\nu}(x, \phi)$ given in eqn.(2.20) at $\phi = \pi$, with the energy momentum tensor $T^{\mu\nu}$ of the SM fields on the brane at $\phi = \pi$

$$\mathcal{L}_{int} \sim -\frac{1}{M^{3/2}} h_{\mu\nu}(x, \phi) T^{\mu\nu}(x) \quad (2.27)$$

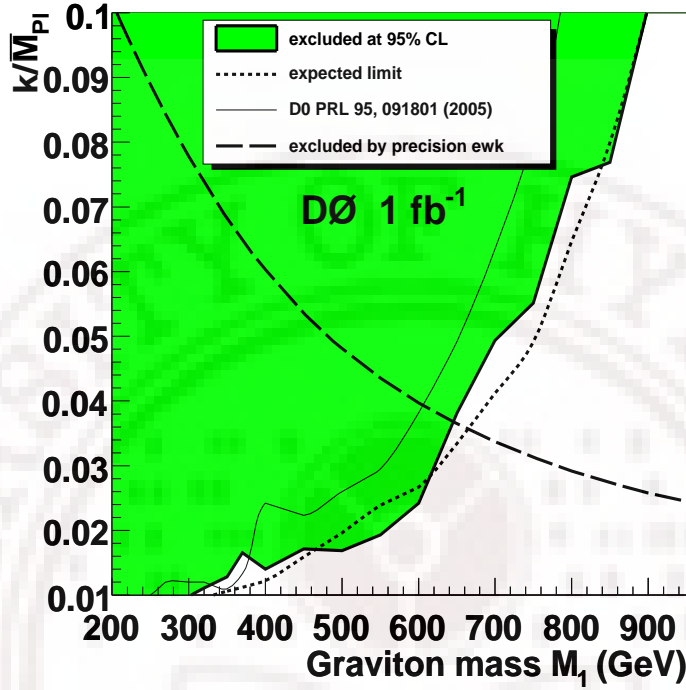


Figure 2.1: Bounds on the RS model parameters obtained using 1 fb^{-1} of data from $p\bar{p}$ collisions at the Tevatron, collected by the D0 detector [13]. The shaded region is excluded at 95% confidence level. The solid thin line corresponds to the previously published exclusion contour. The area below the dashed line is excluded by precision electro weak measurements ($\bar{M}_{Pl} = M_{Pl}/\sqrt{8\pi}$).

Using eqn. (2.18), eqn.(2.20) and eqn.(2.26), the above interaction Lagrangian takes the following form

$$\mathcal{L}_{int} \sim -\frac{1}{M_{Pl}} T^{\mu\nu} h_{\mu\nu}^{(0)} - \frac{1}{M_{Pl}} \frac{1}{e^{-kr\pi}} \sum_{n=1}^{\infty} T^{\mu\nu} h_{\mu\nu}^{(n)}. \quad (2.28)$$

We see here that the coupling of the zero mode is M_{Pl} suppressed while the those of the higher graviton modes are suppressed by only TeV scale ($\sim M_{Pl} e^{-kr\pi}$) with $kr\pi \sim 12$. In this model there are two parameters which are $c_0 = k/M_P$, the effective coupling and m_1 the mass of the first KK mode. Except for an overall warp factor the Feynman rules of RS are the same as those of the ADD model.

The RS modes, when produced in high energy collider experiments, being heavy

can decay into the SM fields with a decay width Γ_n . The graviton propagator with momentum Q and mass m_n is $P_G(Q) = iB_{\mu\nu\rho\sigma}D(Q^2)$ (see eqn. B.0.1) with

$$\begin{aligned}\mathcal{D}(Q^2) &= \sum_n \frac{1}{Q^2 - m_n^2 + im_n \Gamma_n} , \\ &= \frac{1}{m_0^2} \sum_n \frac{x^2 - x_n^2 - i\frac{\Gamma_n}{m_0}x_n}{(x^2 - x_n^2)^2 + \frac{\Gamma_n^2}{m_0^2}x_n^2} ,\end{aligned}\tag{2.29}$$

where $x = Q/m_0$ and $x_n = m_n/m_0$. The summation over n is kinematically bounded. Further the RS KK mode of mass m_n if decays only to SM particles, it can be computed and hence the decay width Γ_n is not unknown. Hence, these heavy RS modes will show up themselves as a resonance pattern in the invariant mass distribution of the pair production processes like Drell-Yan, di-photon production processes, at the high energy collider experiments. This resonance pattern is very much distinct from the signals of the contact type interactions as in the case of ADD model which have a smooth deviations from the SM predictions, say in the tail of the invariant mass distribution.

For example, at the LHC ($\sqrt{S} = 14$ TeV) it is very much possible to probe the TeV scale physics, like the RS model with KK modes that are of the order of a few TeV. As the gravity couples to the energy momentum tensor of the SM fields, the KK modes couple to quarks and gluons with the same coupling of $c_0 = k/M_{Pl}$. At the LHC where the gluon fluxes are very high, higher than the quark anti-quark fluxes, the RS modes can be produced in the gluon fusion subprocesses which subsequently decay into all the possible SM particles, like a pair of leptons $\bar{l}l$, photons $\gamma\gamma$, jets jj , weak bosons ZZ and Higgs bosons hh . In addition to the gluon gluon fusions, the quark anti-quark annihilations also can produce these RS modes. These RS modes will appear, then, as resonance pattern in the invariant mass of the above mentioned channels. It should be noted here that the coupling of the each of the RS modes, except the zero mode, is very large as given by c_0 and hence each RS mode can prominently decay into the SM particles, whereas in the ADD model, the coupling of each of the KK modes is Planck scale suppressed but due to the many available light KK modes the effective coupling

is M_s scale suppressed. The decay width of ADD gravitons is very small owing to its negligible coupling to the SM particles and hence is neglected in the propagator. The typical value chosen for this effective coupling is $0.01 < c_0 < 0.1$. Smaller couplings $c_0 \ll 1$ corresponds to $k \ll M_{Pl}$ and gives raise to additional hierarchy between the fundamental scales k and M_{Pl} . Therefore to avoid new hierarchy in the model, smaller couplings are not allowed.

The Tevatron experiments ($\sqrt{S} = 1.96$ TeV) for the first time have searched for the RS model signatures using the di-lepton and di-photon final states. At the Tevatron for its relatively low center of mass energy, the gluon fluxes corresponding to TeV scale invariant mass are smaller than the quark anti-quark fluxes. So the quark anti-quark annihilations subprocesses have dominant contributions over those of the gluon fusion subprocesses. The latest bounds obtained from the Tevatron using the 1 fb^{-1} of data collected by the $D0$ detector on the parameters of the RS model are shown in the fig.(2.1). This data has set a lower bound at 95 % confidence limit on the first RS mode to be $m_1 > 850$ GeV corresponding to a coupling $c_0 \sim 0.01$.

Summary and a few remarks on the RS model

1. The RS model provides an alternate explanation to the large hierarchy between the electroweak scale and the Planck scale with a new geometry of the extra dimensions that is completely different from the one in the ADD model. In this model there is only one extra dimension which is a slice of anti de Sitter space-time AdS_5 , with orbifold symmetry. Two branes, namely the Plank and the SM brane, are attached at the orbifold fixed points of the extra dimension. The (4+1) dimensional metric in this model has an exponential warp factor $e^{-2kr\phi}$ which is a function of the extra dimension. The large hierarchy has been accounted for this exponential warp factor with a particular choice of $kr \sim 12$.
2. All the higher dimensional parameters $M, k, \mu \sim 1/r$ are of the order the same scale, Planck scale, and hence there is no additional hierarchy among these

scales, unlike the ADD model case where in explaining the existing hierarchy, the model runs into another hierarchy between the weak scale and the compactification scale of the extra dimensions.

3. Any fundamental mass parameter M_0 in higher dimensions corresponds to a physical mass $m = e^{-kr\pi} M_0$ on the SM brane. Thus the fundamental scales could be of the order Planck scale but the physical scales on the brane are only of the order of a few TeV.
4. Although, the model successfully addresses the hierarchy problem, the explanation is based on the particular choice $kr \sim 12$, which plays a key role in addressing the hierarchy problem. This choice does not come from the theory and there is no explanation for it so far.
5. The bulk moduli field accounts for the stability of the two branes against their mutual attraction towards each other. However, this moduli field has a back reaction on the branes, which has been ignored in this model.
6. The compactification of the extra dimension leads to a tower of graviton modes on the SM brane, the masses of whose are determined by the zeros of the Bessel function. The modes could be of order a TeV scale and the spectrum of these modes is non-uniform.
7. The zero mode has a Planck scale suppressed coupling while all other higher modes have TeV scale suppressed couplings to the SM fields. Thus the zero mode decouples in the RS mode spectrum.
8. These graviton modes being heavy when produced at the high energy colliders like LHC, will decay into SM particles and appear as resonance enhancements over the SM predictions.
9. The RS model has a very distinct collider signatures such as a series of resonances whereas those of the ADD model give a tail raising pattern in the invari-

ant mass distributions. Hence distinguishing these two models is very easy at the collider experiments.

10. The concept of localization of the fields to the branes has gained lot of interest following the work in this model, and hence the attempts have been made to localize the gravity in a model known as RS(II) model by considering the infinite size extra dimension and taking the second brane to infinity. A significant research on the concept of localization of the fields in the non-factorisable metric of higher dimensions is on progress.

2.4 Tests of the gravitational inverse square law

According to the Newton's Inverse Square Law (ISL), the gravitational force of attraction between two point masses m_1 and m_2 separated by a distance ' r ' is given by

$$F = -G_N \frac{m_1 m_2}{r^2} \quad (2.30)$$

where $G_N \simeq 6.673 \times 10^{-11} \text{ m}^3 \text{ kg}^{-1} \text{ s}^{-2}$ is the gravitational constant. Until few years ago, this inverse square law is assumed to be valid for length scales ranging from infinity to Planck length ($\sim 10^{-35} \text{ m}$). However, motivated by many new physics scenarios which predict that the gravitational inverse square law could be altered at sub-millimeter range, this ISL has been put to experimental verification by various collaborations at shorter length scales. The modifications to the inverse square law can be accounted for the Yukawa type of corrections to the familiar Newtonian potential that can be written as [14].

$$V(r) = -G_N \frac{m_1 m_2}{r} \left[1 + \alpha e^{-r/\lambda} \right] \quad (2.31)$$

where α is the dimensionless strength parameter and λ is a length scale. This Yukawa potential describes the interaction from the exchange of a scalar of mass $m \sim 1/\lambda$ between the two masses m_1 and m_2 . The deviations from the ISL can then be obtained from the experimental bounds on these α and λ parameters.

2.4.1 Some theoretical speculations

In this section we outline some of the possible new physics scenarios that are relevant in the search of deviations from the Newtonian ISL [14].

1. *Large extra dimensions:*

The observed gauge hierarchy between the Planck scale and the weak scale has been offered an explanation in an interesting theoretical approach that deals with the existence of large extra spatial dimensions. Only gravity ‘sees’ the extra dimensions and the Planck scale in higher dimensions can assume as low value as a few TeV in this scenario. Consequently the gravity is expected to be stronger at the length scales that are of the order of the size of these extra dimensions. The modification to the Newtonian potential can then assume the form given in eqn. (2.31) with the strength α and the range λ given by

$$\lambda = R \quad \text{and} \quad \alpha = 8n/3 \quad (2.32)$$

where R is the size and n the number of extra dimensions. As is seen in the ADD model, for Planck scale of the order of a TeV scale, the possibility of $n = 1$ corresponds to a length scale of the order of 10^{12}m which has been ruled out. For $n = 2$, the radius of the extra dimension is $R \sim 10^{-1}\text{mm}$, a length scale which is of the current interest for the experiments that probe the ISL of gravity.

2. *Exchange of radions:*

In string theories, the radion is a hypothetical scalar particle that appears as a component of the metric tensor or gravitational field in higher dimensions. It is also called as *graviscalar*. Consequently the spacetime is somewhat dynamical with the radii of the new dimensions whose volume must be stabilized with radions. If there is more than one extra dimension, then there could exist several such particles. This radion exchange is expected to produce a force that

corresponds to a strength and the range given as

$$\alpha = \frac{n}{n+2} \quad ; \quad \lambda \sim \sqrt{\frac{1}{G M_*^4}} \approx 2.4 \left[\frac{1 \text{ TeV}}{M_*} \right]^2 \text{ mm}.$$

In general the radion mediated force is the long range effect of new dimensions and, unlike the large extra dimension case, does not fall with the number of extra dimensions.

3. Exchange of moduli:

In quantum field theories, the moduli fields refer to the scalar fields whose potential energy has a continuous global minima. The vacuum expectation values of these scalar fields are used to represent the respective vacua, consequently these expectation values are used as the parameters of the effective theory. This type of potential energy functions often occur in supersymmetric theories. The moduli couple weakly to the supersymmetric-breaking sector and these couplings are computable in any given vacuum, so that ISL tests are the best way to search for these particles. The best known particles of this type are *dilatons*.

4. Exchange of axions:

Axion is an elementary particle postulated to explain the strong CP problem in QCD. The force resulting from the exchange of boson with parity either 0^- or 1^+ is purely spin-dependent and vanishes between unpolarized objects. In the case where the CP violating term Θ_{strong} will not go down to zero, the axions can be accounted for as to acquire a small CP-violating scalar admixture. This results in a spin-dependent Yukawa potential between Nucleons with

$$\alpha = \left[\left(\frac{\Theta_{strong}}{10^{-10}} \right) \left(\frac{m_a}{1 \text{ meV}} \right) \right]^2 1.3 \times 10^{-6}; \quad \lambda = \frac{1}{m_a} \approx \left(\frac{1 \text{ meV}}{m_a} \right) 0.2 \text{ mm}$$

2.4.2 Experimental results

In what follows we outline two types of experiments carried out to test the inverse square law at length scales smaller than $100 \mu\text{m}$ and present the bounds obtained in these experiments on the parameters α and λ .

1. Torsion pendulum experiments

The torsion pendulum based experiments are in general used to measure the weak forces like gravitational force. In a recent experimental set-up [14, 15] for testing the ISL, a new type of torsion-balance has been developed where the test masses are the "missing masses" of holes bored into cylindrically symmetrical plates. The torsion pendulum is a thin ring containing 10 equally spaced cylindrical holes and is suspended above a uniformly rotating circular attractor disk containing 10 similar holes. Due to the gravitational field $V(\phi)$ of the disk the pendulum experiences a torque $\tau(\phi) = \partial V(\phi)/\partial\phi$ for a displacement ϕ of the disk, and undergoes oscillations. This torque, however, will be zero in the absence of these holes. Attaching to the first disk another thicker circular disk containing the holes, leads to almost *null measurements* of the torque experienced by the pendulum. The dimensions of the holes in the second disk and the orientation of this disk with respect to the first one are so chosen that the torque produced in the pendulum because of the first disk is canceled by that of the second one. The cancellation of the forces due to the Newtonian gravity is very much dependent on the distance of the pendulum from the circular disk. On the other hand, the Yukawa type of potential monotonically decreases with this distance. As a result, the location of the exact cancellation will be very sensitive to the deviations from the ISL and any deviation from the characteristic of Newtonian gravity can be used to keep the bounds on the parameters α and λ .

2. Cantilever based experiments

Another recent attempt to probe the Newtonian ISL is made by the Stanford group [16], using their cantilever based experiments. In these experiments, a single-crystal silicon bar for the cantilever and the test masses, made up of gold and of the size comparable to the distance between them, are used. A drive mass which has an alternating pattern of gold and silicon is used to create a varying gravitational field and is mounted on a piezoelectric bimorph for its horizontal movement. The test

mass is mounted on the free end of the cantilever and is subjected to experience the varying gravitational force due to the drive mass placed below it at a distance. The test mass and the drive mass are separated by a shield made up of metalized silicon nitride to minimize the non-gravitational backgrounds. Then, the drive mass is put to oscillations at the subharmonic of the resonance frequency of the cantilever. Any coupling between the test mass and the drive mass would then create a force on the cantilever at harmonics of this drive frequency, including the cantilever's resonant frequency. The motion of the cantilever can be measured using a fiber interferometer and from that the force between the masses can be deduced. The forces are measured as a function of the horizontal distance from the equilibrium position of the drive mass, maintaining a fixed vertical separation between the test mass and the drive mass. By comparing these measurements with the predictions of the finite element analysis (FEA), the bounds on the Yukawa type corrections can be obtained.

The results obtained from these ISL testing experiments conducted by various collaborations are summarized in fig.(2.2). They are presented as bounds at 95% confidence level on the Yukawa coupling strength α as a function of the range λ . Implications of these results on some of the theoretical speculations discussed above are very much informative and are useful in constraining the parameters of different models. In specific we will concentrate on the large extra dimension case. The bounds on the Yukawa range λ will give an upper limit on the size of the extra dimensions. The possibility of only one extra dimension is ruled out as no deviations from the ISL are observed at the Solar length scales. Then the other possibility that will be of interesting is the case with two extra dimensions corresponding to a scale $M_s = 1$ TeV. According to eqn.(2.32), if one of the extra dimensions is very large, which can see deviations from the ISL, then it would correspond to $\alpha = 8/3$. Corresponding to this α value, the 95% confidence limit on the size of the extra dimension will be $R \leq 160 \mu m$. For two extra dimensions of equal size the possibility of $M_s = 1$ TeV corresponds to $R \sim 380 \mu m$ and $\alpha = 16/3$ (see eqn.(2.32) and is ruled out from the above bounds. Instead, the 95% confidence limit on the size i.e. $R \leq 130 \mu m$ for

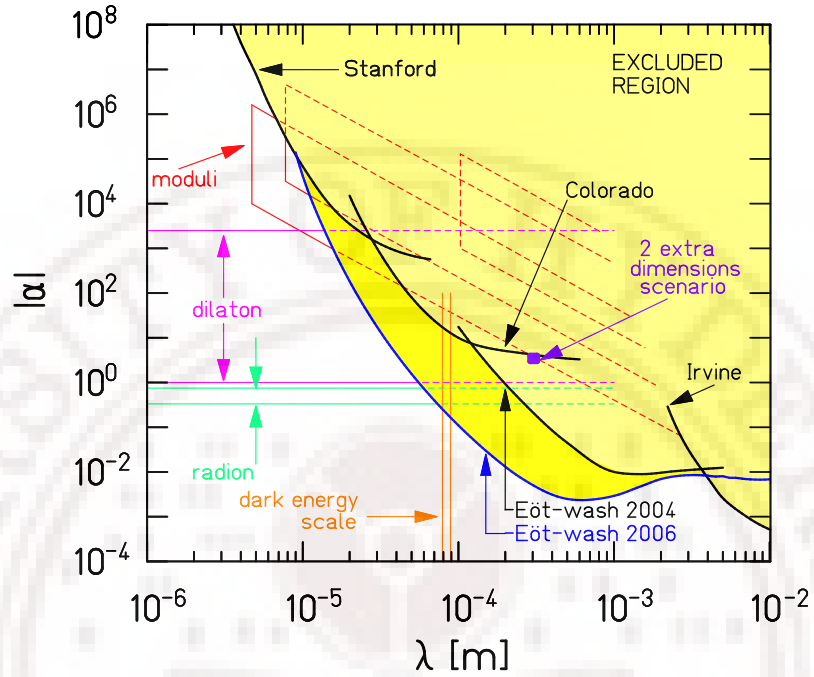


Figure 2.2: Constraints on Yukawa violations of the gravitational inverse square law [15]. The shaded region is excluded at the 95% confidence level. Heavy lines labeled Eot-Wash 2006, Eot-Wash 2004, Irvine, Colorado and Stanford show experimental constraints from the works in Refs. [14, 15], [17], [18], and [19], [16], respectively. Lighter lines show various theoretical expectations summarized in Ref. [20].

two equal extra dimensions case is used to obtain a bound on the corresponding scale of the new physics, which turned out to be $M_s \geq 1.7$ TeV. Implications on other theoretical scenarios are discussed in [14].

2.4.3 RS type corrections to ISL

Recently, there has been a proposal for an experiment to search for the Randall-Sundrum type of corrections to the Newton's ISL [21]. The RS type of correction to the ISL is given by

$$V(r) = -\frac{G_N m}{r} \left(1 + \frac{l_s^2}{r^2} \right) \quad (2.33)$$

where the RS parameter $l_s^2 = \frac{2}{3} l^2$, l is the curvature scale of 5-dimensional anti-deSitter space-time, G_N is the Newton's gravitational constant, m is the mass and r is the distance in the three dimensional space. The experimental set up is based on the torsion pendulum and the expected sensitivity of the experiment is to probe the RS parameter up to 10 microns.

2.5 Unparticle scenario

Banks and Zaks (\mathcal{BZ}) [22] studied non-abelian gauge theories by considering the number of fermions to be a continuous parameter such that the two loop beta function vanishes at an infra-red fixed point. Below this fixed point the theory becomes scale invariant. In any scale invariant sector the fields correspond to either massless particles or particles with a continuous mass distribution. Consequently in such scale invariant sector with a non-integer number of fermions, the conventional particle interpretation is lost.

Following this idea, Georgi [23] has proposed that the theory at high energies can have both the SM fields as well as the \mathcal{BZ} fields. These two sectors interact through the exchange of particles with a very large mass scale M_U . Below this scale M_U the couplings of the interaction have a generic form

$$\frac{1}{M^{d_{SM}+d_{BZ}-4}} \mathcal{O}_{SM} \mathcal{O}_{BZ}, \quad (2.34)$$

where \mathcal{O}_{SM} and \mathcal{O}_{BZ} are operators constructed out of SM and BZ fields with mass dimension d_{SM} and d_{BZ} respectively. This hidden \mathcal{BZ} sector can have an infra-red (IR) fixed point Λ_U below which the scale invariance emerges in the theory. As the couplings in the \mathcal{BZ} sector need not be zero (trivial) at the fixed point, it corresponds to a non-trivial IR fixed point. The scale invariant sector below this fixed point Λ_U can not be described in terms of well defined particles but with "unparticles". In this effective theory valid below Λ_U , the above interaction of the SM fields with the \mathcal{BZ}

sector matches onto the form

$$C_{\mathcal{U}} \frac{\Lambda_{\mathcal{U}}^{d_{\mathcal{BZ}} - d_{\mathcal{U}}}}{M_{\mathcal{U}}^{d_{\mathcal{SM}} + d_{\mathcal{BZ}} - 4}} O_{\mathcal{SM}} O_{\mathcal{U}} , \quad (2.35)$$

where $d_{\mathcal{U}}$ ¹ is the scaling dimension of unparticle operator $O_{\mathcal{U}}$. In principle, unparticle operators can have different tensor structures, such as scalar, vector or tensor. The effective interaction for scalar unparticle consistent with the SM gauge symmetries are:

$$\mathcal{L}_{int} \supset \frac{\lambda_s}{4\Lambda_u^{d_s}} F_{\mu\nu}^a F^{a\mu\nu} \mathcal{O}_u + \frac{\lambda_s}{\Lambda_u^{d_s-1}} \bar{\psi}\psi \mathcal{O}_u . \quad (2.36)$$

The coupling of the vector unparticles can be given as

$$\mathcal{L}_{int} \supset \frac{\lambda_v}{\Lambda_u^{d_v}} \bar{\psi} \gamma_{\mu} \psi O_u^{\mu} , \quad (2.37)$$

For the tensor unparticle, we assume that the SM fields couple to the unparticle operator $O_u^{\mu\nu}$ via SM energy momentum tensor $T_{\mu\nu}$:

$$\mathcal{L}_{int} \supset \frac{\lambda_t}{\Lambda_u^{d_t}} T_{\mu\nu} O_u^{\mu\nu} , \quad (2.38)$$

where d_s , d_v and d_t are the scaling dimensions of scalar, vector and tensor unparticle operators respectively, and λ_s , λ_v and λ_t are dimensionless coupling constants given by

$$\lambda_u = C_{\mathcal{U}} \frac{\Lambda_{\mathcal{U}}^{d_{\mathcal{BZ}}}}{M_{\mathcal{U}}^{d_{\mathcal{SM}} + d_{\mathcal{BZ}} - 4}}$$

Unitarity imposes constraint $d_s > 1$ on the scaling dimension of scalar unparticle [25] and scale invariance restricts [26] $(d_v, d_t) \geq 3$. The scale invariance fixes the two-point functions of unparticle operators, apart from an overall normalization, without requiring any detailed knowledge of the theory at high energies. The propagators for

¹There exist no known examples of scale invariant local field theories that are not conformally invariant [24]

the scalar, vector and tensor unparticles are respectively given as [26–28]

$$\int d^4x e^{-ik \cdot x} \langle 0 | T O_u(x) O_u(0) | 0 \rangle = -i C_S \frac{\Gamma(2 - d_s)}{4^{d_s-1} \Gamma(d_s)} (-k^2)^{d_s-2} \quad (2.39)$$

$$\begin{aligned} \int d^4x e^{-ik \cdot x} \langle 0 | T O_u(x) O_u(0) | 0 \rangle &= -i C_V \frac{(d_v - 1) \Gamma(2 - d_v)}{4^{d_s-1} \Gamma(d_v + 1)} (-k^2)^{d_v-2} \\ &\times \left[g_{\mu\nu} - \frac{2(d_v - 2)}{d_v - 1} \right] \end{aligned} \quad (2.40)$$

$$\begin{aligned} \int d^4x e^{-ik \cdot x} \langle 0 | T O_u^{\mu\nu}(x) O_u^{\alpha\beta}(0) | 0 \rangle &= -i C_T \frac{\Gamma(2 - d_t)}{4^{d_t-1} \Gamma(d_t + 2)} (-k^2)^{d_t-2} \\ &\times [d_t(d_t - 1)(g_{\mu\alpha}g_{\nu\beta} + \mu \leftrightarrow \nu) + \dots] , \end{aligned} \quad (2.41)$$

where C_S , C_V , C_T are overall normalization constants, in practice are set equal to unity. The terms given by ellipses in general do not contribute owing to the conservation of the vertex factors in the case of tensor unparticles.

The phase space for the real emission of unparticles is the same as that of d_u (scaling dimension) number of massless particles as given by [23, 28]

$$dP_{d_u} = \frac{16\pi^2 \sqrt{\pi}}{(2\pi)^{2d_u}} \frac{\Gamma(d_u + 2)}{\Gamma(d_u - 1) \Gamma(2d_u)} q^{d_u-2} \quad (2.42)$$

where $q = (p_1 + p_2 + \dots p_{d_u})$

Recently unparticle phenomenology, in the context of present and future colliders have been explored in great detail [29].

Chapter 3

Two cut-off phase space slicing method

3.1 Introduction

The phase space slicing method is a simple and useful technique for the computation of Next-to-Leading Order (NLO) QCD cross sections to various processes and is based on a semi-analytical approach. In the SM this method has been used to compute the NLO QCD corrections to various processes. [30–32]. In the case of beyond standard model (BSM) scenarios like extra dimensional models, at the leading order itself, there will be more number of subprocess contributions than in the SM. The computation of NLO cross sections in such cases becomes very complex. In order to make a reliable predictions of the cross sections that can be compared with the experimental data one has to impose various cuts that are used by the experimental collaborations on the final state particles. In addition in the processes like di-photon production, one implements isolation algorithm on the final state photons. To compute the NLO QCD corrections to such processes in BSM scenarios imposing a certain kinematic cuts on the final state particles and using fully analytical methods is extremely difficult. In these cases, this semi-analytical phase space slicing method is very useful to compute the NLO QCD corrections with relative ease. In what follows we describe the two cut-off phase space slicing method [33].

3.2 The method

In a typical NLO (QCD) computation one often encounters both infra-red (IR) (soft and collinear) and ultra-violet (UV) divergences. The soft and collinear divergences occur in both the real and the virtual (loop) diagrams. The soft singularities appear in the region where the momentum of the particle goes to zero whereas the collinear divergences arise because of the collinearity between two particles in the massless limit. The UV divergences will appear in the loop diagrams when the loop momentum goes to infinity. After renormalization, the UV divergences will disappear leaving renormalized coupling constants. The important point to be noted is that each of the above mentioned IR divergences comes from a particular region of the phase space of the real diagrams. Naively, one can slice that part of the phase space which is responsible for the divergences from the three body phase space. In the two cut-off phase space slicing method, one separates the soft and collinear regions from the three body phase space using two small cut-off parameters, namely δ_s and δ_c , that define the boundaries of these soft and collinear regions. The soft and collinear cross sections are computed using analytical methods in the dimensional regularization scheme ($n = 4 + \epsilon$). The IR divergences coming from the loop diagrams are also computed analytically in n -dimensions. The soft singularities will cancel between the real and virtual diagrams whereas the final state collinear singularities will cancel after summing over all the degenerate diagrams (KLN theorem). However the initial state collinear singularities will remain uncanceled and are factored out from the perturbatively calculable partonic cross sections in a universal way and then are absorbed into the bare parton distribution functions (PDFs). These PDFs are later extracted from the global fits to the available data from the experiments that probe the processes like Deep-Inelastic Scattering (DIS) and Drell-Yan production processes. Thus all the divergences will disappear leaving the total cross section a finite quantity. The remaining three body phase space is free of all the singularities and hence can be computed in 4 dimensions using some standard Monte-Carlo techniques. In what

follows we describe the method in detail, with the aim of calculating the NLO QCD corrections to the processes like Drell-Yan and di-photon productions at the hadron colliders. These processes do contain only initial state QCD singularities and no final state QCD singularities will arise. As an example we will consider the Drell-Yan process (in SM) in which two hadrons collide to give a pair of leptons.

3.3 Real emission processes

At the leading order in perturbation theory, the DY process takes place at order $\alpha_s^{(0)}$ via simple quark anti-quark annihilations. The process at NLO involves QCD corrections to the order α_s . A parton level process to NLO in QCD is given by

$$p_1 + p_2 \rightarrow p_3 + p_4 + p_5$$

where p_1, p_2 are the momenta of the incoming partons, p_3, p_4 are the momenta of the pair of leptons and p_5 is the momentum of the quark/gluon. In general the final state particles, denoted by p_3 and p_4 , could be any of the leptons (l^\pm), quarks ($q(\bar{q})$) or gauge bosons (both massive W^\pm, Z as well as massless g, γ).

3.3.1 Soft

In the first step, the three body cross section is decomposed into two regions as follows:

$$\sigma = \frac{1}{2\Phi} \int \bar{\Sigma} |M_3|^2 dR_3 = \frac{1}{2\Phi} \int_{soft} \bar{\Sigma} |M_3|^2 dR_3 + \frac{1}{2\Phi} \int_{hard} \bar{\Sigma} |M_3|^2 dR_3$$

where Φ is the usual flux factor, with s_{12} being the center of mass energy of the incoming partons. In the very high energy limit, one can work in the massless limit of the light particles involved. The partitioning of the phase space into *soft* and *hard* regions depends on a small cut-off parameter δ_s . Within *soft* region double pole (eikonal) approximation is made to the matrix elements and then analytically integrated over the

unobserved degrees of freedom in $n = 4 + \epsilon$ dimensions. The result can contain double and single poles in ϵ , and double or single logarithms in the soft cut off δ_s .

The energy E_5 of the gluon in the center of mass frame of the incoming partons is given by

$$E_5 = \frac{s_{12} - s_{34}}{2\sqrt{s_{12}}}$$

where $s_{ij} = (p_i + p_j)^2$ and $t_{ij} = (p_i - p_j)^2$. The soft range of the gluon momentum is defined as $0 \leq E_5 \leq \delta_s \sqrt{s_{12}}/2$. In this soft limit, one can approximate $p_5^\mu = 0$ in the momentum conserving delta function of the three body phase space to get

$$\begin{aligned} dR_3|_{soft} &= \left[\frac{d^{n-1}p_3}{2p_3^0(2\pi)^{n-1}} \frac{d^{n-1}p_4}{2p_4^0(2\pi)^{n-1}} (2\pi)^n \delta^n(p_1 + p_2 - p_3 - p_4) \right] \frac{d^{n-1}p_5}{2p_5^0(2\pi)^{n-1}} \\ &= dR_2 \frac{d^{n-1}p_5}{2p_5^0(2\pi)^{n-1}} \end{aligned}$$

Now parametrizing p_5 as $p_5 = E_5(1, \dots, \sin\theta_1 \sin\theta_2, \sin\theta_1 \cos\theta_2, \cos\theta_1)$, we can write the soft region of the phase space as

$$dR_3|_{soft} = dR_2 \left[\left(\frac{4\pi}{s_{12}} \right)^\epsilon \frac{\Gamma(1-\epsilon)}{\Gamma(1-2\epsilon)} \frac{1}{2(2\pi)^2} \right] dS$$

with

$$dS = \frac{1}{\pi} \left(\frac{4}{s_{12}} \right)^{\epsilon/2} \int_0^{\delta_s \sqrt{s_{12}}/2} dE_5 E_5^{1+\epsilon} \sin^{1+\epsilon}\theta_1 d\theta_1 \sin^\epsilon\theta_2 d\theta_2$$

In the soft limit, the $2 \rightarrow 3$ matrix element can be written as

$$M_3^a|_{soft} \simeq g\mu_r^{-\epsilon/2}(p_5) J_\mu^a(p_5) M_2; \quad \text{where} \quad J_\mu^a(p_5) = \sum_{i=1}^2 T_i^a \frac{p_i^\mu}{p_i \cdot p_5}$$

is the non-abelian **eikonal** current, M_2 being the matrix element for $2 \rightarrow 2$ leading order process and p_i being the momentum of the parton emitting this soft gluon. In the case where the final state particles, denoted by p_3 and p_4 , are partons, then they also can emit gluons. The above summation then runs from 1 to 4 instead of from 1 to 2. *It should be noted here that if the parton p_5 corresponds to a quark, then there will be no soft divergence associated with it owing to the fermion dynamics*

($\sum_s u(p)\bar{u}(p) = \not{p} + m$) of the theory. Finally, the soft part of the cross section can be written as

$$d\sigma_S = \left[\frac{\alpha_s}{2\pi} \frac{\Gamma(1+\epsilon/2)}{\Gamma(1+\epsilon)} \left(\frac{4\pi\mu_r^2}{s_{12}} \right)^{-\epsilon/2} \right] \sum_{i,j=1}^2 d\sigma_{ij}^0 \int \frac{-p_i \cdot p_j}{p_i \cdot p_5 p_j \cdot p_5} dS$$

where $d\sigma_{ij}^0$ is the $2 \rightarrow 2$ Born cross section.

3.3.2 Collinear

The *hard* region is further divided into two parts, hard collinear *hc* and non-collinear *nc*.

$$\frac{1}{2\Phi} \int_{hard} \bar{\Sigma} |M_3|^2 dR_3 = \frac{1}{2\Phi} \int_{hc} \bar{\Sigma} |M_3|^2 dR_3 + \frac{1}{2\Phi} \int_{nc} \bar{\Sigma} |M_3|^2 dR_3$$

This separation depends on another cut-off called δ_c . The collinear singularities arise when two partons become collinear to each other. If the partons p_1 and p_5 are collinear to each other, then the collinear region is defined as $0 \leq t_{15} \leq \delta_c s_{12}$. Within *hc*, the leading collinear pole approximation to the matrix element squared is made. Integration domain of *hc* is exactly defined when δ_c is much smaller than δ_s . The integration over the unobserved degrees of freedom is performed in n -dimensions, giving a factorized result with single poles in ϵ and logarithms of both cut-off parameters δ_c and δ_s .

The leading order differential cross section for the $2 \rightarrow 2$ process is given by

$$d\sigma_0^{P_A+P_B \rightarrow 3+4} = f_{1/P_A}(x_1) dx_1 f_{2/P_B}(x_2) dx_2 d\sigma_0^{1+2 \rightarrow 3+4}$$

where $f_{1/P_A}(x_1)$ is the bare parton distribution function which gives the probability of finding a parton- i from the hadron P_A with a momentum fraction between x and $x+dx$. At NLO, there will be only one gluon that can be collinear to the parton emitting it. So we can safely ignore the double collinearity due to the partons from both the hadrons. Let us consider the collinearity coming from the various possibilities parton-1 (quark/gluon) is collinear to the parton-5 (quark/gluon). The square of the matrix

element after applying the collinear approximation in terms of the unregulated splitting function P_{15} is given by

$$\overline{\Sigma}|M_3(1+2 \rightarrow 3+4+5)|^2 \simeq \overline{\Sigma}|M_2(1'+2 \rightarrow 3+4)|^2 P_{1'1}(z, \epsilon) g^2 \mu_r^{-\epsilon} \frac{-2}{zt_{15}}$$

where z is fraction of parton 1's momentum carried by parton 1' with parton 5 taking a fraction of $(1-z)$ and y is the fraction of momentum of the parent hadron P_A carried by the parton 1. Using the approximation $p'_1 = p_1 - p_5 \simeq zp_1$, we can write the three body phase space corresponding to the region of the collinearity as

$$\begin{aligned} dR_3|_{hc} &= \left[\frac{d^{n-1}p_3}{2p_3^0(2\pi)^{n-1}} \frac{d^{n-1}p_4}{2p_4^0(2\pi)^{n-1}} (2\pi)^n \delta^n(zp_1 + p_2 - p_3 - p_4) \right] \frac{d^{n-1}p_5}{2p_5^0(2\pi)^{n-1}} \\ &= dR_2 \frac{d^{n-1}p_5}{2p_5^0(2\pi)^{n-1}} \end{aligned}$$

where

$$\frac{d^{n-1}p_5}{2p_5^0(2\pi)^{n-1}} = \frac{(4\pi)^{-\epsilon/2}}{16\pi^2\Gamma(1+\epsilon/2)} dz dt_{15} [-t_{15}(1-z)]^{\epsilon/2}.$$

The hard condition $\delta_s \sqrt{s_{12}} \leq E_5 \leq \sqrt{s_{12}}$ sets the z integration limits while the collinear condition $0 \leq t_{15} \leq \delta_c s_{12}$ sets the t_{15} integration limits. The z integration limits also depend on the AP splitting kernels. For the massless case, the limits of z for each of the splittings are found to be

$$q \rightarrow qg \quad 0 \leq z \leq 1 - \delta_s$$

$$g \rightarrow q\bar{q} \quad 0 \leq z \leq 1$$

$$g \rightarrow gg \quad \delta_s \leq z \leq 1 - \delta_s$$

After performing the integration over t_{15} in the range $0 \leq t_{15} \leq \delta_c s_{12}$, the $2 \rightarrow 3$ differ-

ential hadronic cross section can be approximated by

$$d\sigma_{hc}^{P_A+P_B \rightarrow 3+4+5} = d\sigma_0^{1'+2 \rightarrow 3+4}(zs_{12}) \left[\frac{\alpha_s}{4\pi} \frac{\Gamma(1+\epsilon)/2}{\Gamma(1+\epsilon)} \left(\frac{4\pi\mu_r^2}{s_{12}} \right)^{-\epsilon/2} \right] \left(\frac{1}{\epsilon} \right) \delta_c^{\epsilon/2} \\ \times \int dz [z(1-z)]^{\epsilon/2} P_{1'1}(z, \epsilon) f_{a/P_A}(y) dy f_{2/P_B}(x_2) \delta(yz - x_1) dx_1 dx_2.$$

which on integration over y gives

$$d\sigma_{hc}^{B_1+B_2 \rightarrow 3+4+5} = d\sigma_0^{1'+2 \rightarrow 3+4}(s_{12}) \left[\frac{\alpha_s}{4\pi} \frac{\Gamma(1+\epsilon/2)}{\Gamma(1+\epsilon)} \left(\frac{4\pi\mu_r^2}{s_{12}} \right)^{-\epsilon/2} \right] \left(\frac{1}{\epsilon} \right) \delta_c^{\epsilon/2} \\ \times \int \frac{dz}{z} \left[\frac{(1-z)}{z} \right]^{\epsilon/2} P_{1'1}(z, \epsilon) f_{1/P_A}(x_1/z) f_{2/P_B}(x_2) dx_1 dx_2.$$

The factorization of collinear singularity (seen as pole in ϵ) into the parton distribution function is done with the introduction of a scale dependent parton distribution function using the \overline{MS} scheme convention.

$$f_{a/P_A}(x, \mu_f) = f_{a/P_A}(x) + \left(\frac{1}{\epsilon} \right) \left[\frac{\alpha_s}{4\pi} \frac{\Gamma(1+\epsilon/2)}{\Gamma(1+\epsilon)} \left(\frac{4\pi\mu_r^2}{s_{12}} \right)^{-\epsilon/2} \right] \int_x^1 \frac{dz}{z} P_{aa'} f_{a'/P_A}(x/z)$$

Using this definition of the scale dependent PDF in the leading order differential cross section and adding it with the hard collinear differential cross section results in the cancellation of the hard collinear singularities leaving the soft collinear divergences as given below

$$d\sigma_{hc}^{P_A+P_B \rightarrow 3+4+5} = d\sigma_0^{1'+2 \rightarrow 3+4}(s_{12}) \left[\frac{\alpha_s}{4\pi} \frac{\Gamma(1+\epsilon/2)}{\Gamma(1+\epsilon)} \left(\frac{4\pi\mu_r^2}{s_{12}} \right)^{-\epsilon/2} \right] \\ \times \left\{ \tilde{f}_{1'/P_A}(z, \mu_f) + \left[\frac{-A_1^{sc}(1 \rightarrow 1' + 5)}{2\epsilon} + A_0^{sc}(1 \rightarrow 1' + 5) \right] f_{1/P_A}(z, \mu_f) \right\}$$

where

$$\tilde{f}_{c/P_A}(x, \mu_f) = \sum_{c'} \int_x^{1-\delta_s \delta_{cc'}} \frac{dy}{y} f_{c'/P_A}(x/y, \mu_f) \tilde{P}_{cc'}(y) \\ \text{and } \tilde{P}_{ij} = P_{ij} \ln \left(\delta_c \frac{1-y}{y} \frac{s_{12}}{\mu_f^2} \right) - P'_{ij}(y)$$

The unregulated splitting functions P and P' are given in [78] and [33].

The coefficients A^{sc} correspond to soft collinear contributions and are given below :

$$\begin{aligned} A_1^{q \rightarrow qq} &= C_F(3/2 + 2 \ln \delta_s) \\ A_0^{q \rightarrow qq} &= A_1^{q \rightarrow qq} \log \frac{s_{12}}{\mu_f^2} \\ A^{g \rightarrow gg} &= N(11/6 + 2 \ln \delta_s) \\ A_0^{g \rightarrow gg} &= A_1^{g \rightarrow gg} \log \frac{s_{12}}{\mu_f^2} \end{aligned}$$

There will be no soft collinear divergences in the case of $g \rightarrow q\bar{q}$ splittings, whereas the $g \rightarrow gg$ splittings won't arise in the DY in SM at NLO.

In addition to the initial state collinear singularities, final state collinear singularities also can arise in certain processes. In such a case the summation over the experimentally degenerate final states leaves the cross sections finite (KLN theorem). However for the tagged final states, the associated collinear singularities will remain uncanceled and have to be absorbed into the bare fragmentation functions, similar to the case of initial state collinear divergences where the singularities are absorbed into the bare parton distribution functions. This procedure also involves the factorization of singularities in a universal way at an arbitrary scale μ_F , called factorization scale.

3.4 Virtual processes

The one loop diagrams in the NLO calculation are computed using the analytical methods and are not affected by the phase space slicing method at all. The collinear and soft singularities coming from the loop integration are regularized in n -dimensions. These singularities appear as poles in ϵ . The soft singularities will cancel with those coming from the real diagrams. The collinear singularities in the virtual and real diagrams are absorbed into the bare parton distribution functions. This finally results in the cross sections that are free of all kind of singularities.

3.5 Stability with slicing parameters

The two small cut-off parameters δ_s and δ_c are introduced in the intermediate stages of the calculation of NLO QCD corrections just to define the soft and collinear regions, and the final results are expected not to depend on the choice of these parameters. However, defining the soft and collinear regions for arbitrary values of these parameters is meaningless which necessitates the need to find a region of these parameters in which the cross sections are stable or least sensitive to the choice of these parameters. Hence, in any NLO computation using this slicing method, it is required first to find out these stable regions of δ_s and δ_c before proceeding to the numerical predictions. The soft, collinear and virtual pieces in the limit in which they are defined constitute the 2-body contribution while the hard non-collinear piece corresponds to the 3-body contribution. Though each of these 2-body and 3-body contributions can vary with δ_s and δ_c , the sum of these two contributions is supposed to be independent of the choice of the slicing parameters. The percentage of uncertainty in the cross sections against the variation of δ_s and δ_c is expected to be as small as possible. The broader the region, the more reliable are the results obtained using this slicing method.

In the next chapter, we will use this slicing method to compute the NLO QCD corrections to the di-photon production process in the RS model. In this case, in addition to the $q\bar{q}$ and qg initiated subprocesses, the gg initiated subprocess also contributes. Hence the NLO calculation involves the computation of soft and the collinear contributions coming from this gg initiated subprocess. The soft divergences will arise only when the gluons are emitted from the external legs but not from the internal lines. In the collinear limit, this additional subprocess involves $g \rightarrow gg$ splitting functions. The amplitudes that contain only four point interactions do not give rise to any divergences. Finally, the stability of the cross sections against the variation of the slicing parameters verifies the successful implementation of this method.



Chapter 4

Diphoton production to $\mathcal{O}(\alpha_s)$ in the RS model at the hadron colliders

4.1 Diphoton production

The production of a pair of photons at the hadron colliders is given by

$$P_A(P_1) + P_B(P_2) \rightarrow \gamma(p_3) + \gamma(p_4) + X(P_X) \quad (4.1)$$

where P_1, P_2 are the incoming hadron momenta and p_3, p_4 are the momenta of the two photons and P_X is the momenta of the inclusive final state. At the hadron colliders this process can be used as an important probe in the search of the Higgs boson, the only fundamental scalar particle in the SM. At the LHC, where the gluon flux is very high, the pair of photons can be produced in the gluon initiated subprocess via the Higgs boson with the top-quark loop originated effective couplings between the Higgs boson and the photons/gluons. Consequently, the Higgs boson can be seen as a resonance pattern in the invariant mass distribution of the diphoton production, with larger cross sections. Hence this process is often called as a golden channel for the discovery of the Higgs boson. However the di-photon production via the Higgs boson has a huge SM background coming from the $q \bar{q}$ annihilations occurring at the lowest order in the perturbation theory. For a better prediction of the signals, the quanti-

tative estimation of the background to a very high accuracy has become inevitable, which led to the computation of higher order QCD corrections to this background process. An extensive study of this process exists in the literature [34] in the context of light Higgs-boson searches as a light Higgs Boson decays dominantly to two photons.

Besides this, the photon pair production is of interest in its own right. Experimentally, it has been studied from fixed targets [35, 36] to the colliders [37, 38] in various kinematic distributions. As per the theoretical understanding of this process is considered, it relies on the higher order radiative corrections to this process. A full NLO QCD corrections to the di-photon process have been reported in [39]. Soon after this work, the QCD corrections to the subprocess $gg \rightarrow \gamma\gamma$ were also computed in [40] as this subprocess is the largest of the higher order contributions to the di-photon production process and the results have been used in isolating the light Higgs boson from the di-photon background. In a more recent work, the resummation effects have also been incorporated in the calculation by considering the all-orders resummation of initial state gluon radiation valid at next-to-next-to-leading logarithmic accuracy [41]. In the light of above, it can be easily understood that this process has now become useful in the precision study of the SM physics.

On the other hand, this pair production process has also been used to unravel the possible beyond standard model (BSM) physics scenarios [42, 43] and is studied widely in various BSM scenarios [44]. However, the predictions are based on the leading order (LO) computation in which the couplings of the BSM scenarios enter at their lowest order in the perturbation theory. At the hadron colliders like LHC, where the QCD plays an important role, the higher order radiative corrections are often expected to be large. With this idea, in the recent past, QCD radiative corrections to the Drell-Yan process have been computed for the first time by considering the gravity effects in the extra dimension models [45–48], and it was found that the QCD corrections enhanced the cross sections significantly. Subsequently, they were used [13, 49] to constrain the model parameters. Motivated by this, recently the NLO QCD corrections to the di-photon process are computed in the context of theories with

large extra-dimension and unparticle model [50]. The present work aims at a full next-to-leading order computation for the production of isolated direct photon pairs in the warped extra dimension (RS) model at the LHC ($\sqrt{s} = 14$ TeV), and to obtain various kinematical distributions by imposing the relevant experimental cuts on the photons. The estimate of enhancement over the LO results and the improvement in scale uncertainties in going from LO results to the NLO ones are the main motivations for this work.

The NLO calculation presented here uses both analytical and Monte Carlo integration methods. It is easy to implement experimental cuts in a Monte Carlo program than in a fully analytical computation. Our code is based on the method of *two cutoff phase space slicing* to deal with various singularities appearing in the NLO computation and to perform numerical integrations over the phase space. This method has been applied to the diphoton production process for the computation of NLO QCD corrections in the SM in [51]. This method is nicely reviewed in [33]. All the analytical results presented in this work were evaluated using the algebraic manipulation program FORM [52].

In the SM, at the lowest order in α_s ie., at α_s^0 , the di-photon production takes place via quark anti-quark annihilation subprocess $q\bar{q} \rightarrow \gamma\gamma$. For low invariant mass of the di-photon the subprocess $gg \rightarrow \gamma\gamma$, although of order α_s^2 , has a significant contribution, comparable to that of $q\bar{q} \rightarrow \gamma\gamma$. This is due to the large gluon flux in the small x region at the LHC. In light Higgs boson search studies this subprocess plays an important role, and it is treated formally as a leading order contribution although it is of order α_s^2 [34, 53] and is indeed a next-to-next-to leading order contribution. However, it falls off rapidly with increasing invariant mass and in the mass range of interest for the TeV scale gravity models, it need not be included at LO. It is demonstrated in [54] that this subprocess in the SM is few orders of magnitude smaller than that of $q\bar{q}$ for $Q > 500$ GeV. This subprocess amplitude can interfere with the gluon initiated LO subprocess in the BSM case, giving order α_s contribution which is included in our study. In addition order κ^2 gravity mediated Feynman diagrams fig.(4.2) $qq \rightarrow \gamma\gamma$ and

$gg \rightarrow \gamma\gamma$ also appear at the leading order. The NLO computation involves two kinds of matrix elements.

- Virtual diagrams with loops which contribute through their interference with the LO diagrams (see fig.(4.3)).
- Real emission diagrams with an additional parton in the final state (see fig.(4.4)).

Both the virtual and real corrections have been evaluated with 5 quark flavors and in the limit of vanishing of quark masses. The n -point tensor integrals coming from the integration over loop-momenta were simplified using Passarino-Veltman reduction and the computation was carried with dimensional regularization using $n = 4 + \epsilon$. The initial state QCD divergences were factorized in the \overline{MS} scheme and are absorbed into the parton distribution functions (PDFs).

4.1.1 Frixione isolation algorithm

Photons not only arise directly in a parton subprocess but also through fragmentation of a parton into a photon and a jet of hadrons collinear to it. This fragmentation is a non-perturbative phenomenon. A parton level computation involving only direct photons without including fragmentation photons is plagued with QED collinear singularities between the photons and the quarks in the final state. It is evident from the SM qg subprocess. This final state singularities can be absorbed into fragmentation functions describing the probability of a parton fragmenting into a photon in much the same way as the initial state collinear singularities are absorbed into parton distribution functions. However, fragmentation functions are poorly known to date. Hence an alternative to avoid these fragmentation functions and simultaneously suppress the QED singularities is to use the *smooth cone isolation* criterion advocated by Frixione [55]. The aim of this isolation criterion is to suppress the final state QED collinear singularities and at the same time to remove the fragmentation photons in an infrared safe manner. Let the z -axis coincide with the proton-proton collision line

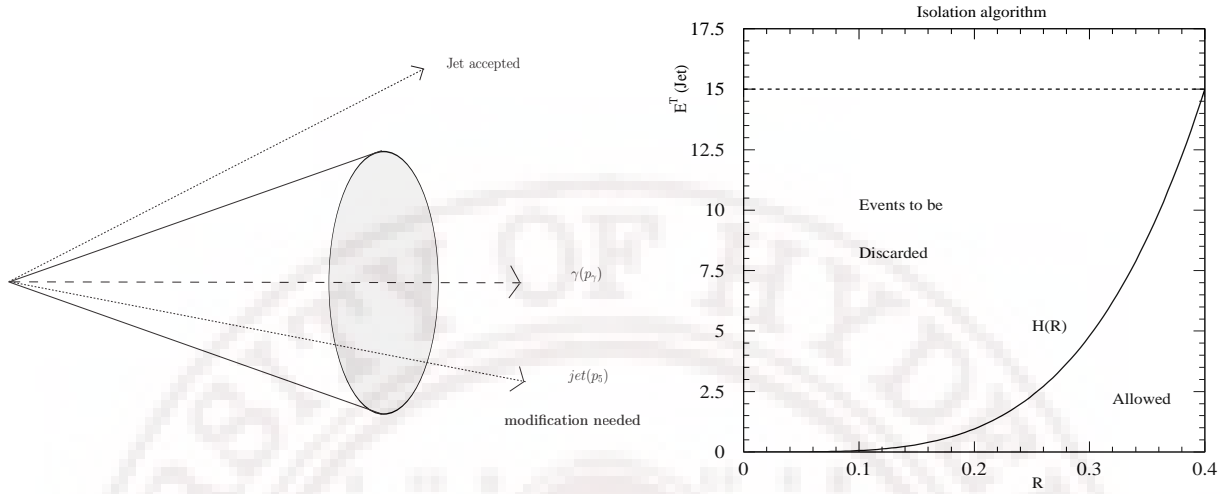


Figure 4.1: The schematic diagram of the Frixione's algorithm for the isolation of photons from the jets (left) and the choice of the function $H(R)$ (right) we have chosen in this algorithm.

and θ and ϕ denote the polar and azimuthal angles respectively. It is more convenient to use the pseudo-rapidity in the context of hadron colliders, as they are additive under boosts. The fragmentation photons are embedded in hadronic jets and the prescription to isolate a photon from hadronic activity is to draw a cone around the photon as shown in the fig.(4.1) with the axis of the cone pointing along the direction of the photon momentum. The radius of the cone can be defined in a boost invariant way as given by

$$R = \sqrt{(\eta_\gamma - \eta_j)^2 + (\phi_\gamma - \phi_j)^2}$$

where η_γ (η_j) and ϕ_γ (ϕ_j) are the pseudo-rapidity and azimuthal angle of the photon (jet) respectively. Then draw concentric circles around the direction of the photon in the $\eta - \phi$ plane with the largest circle having a fixed radius R_0 . For the jet of hadrons outside the cone i.e. for $R > R_0$, the photons are well isolated from the hadronic activity and need not require any isolation algorithm. For the jets lying inside the cone, the isolation criterion is to demand that the total hadronic transverse energy in any circle of radius $R < R_0$ be less than some specified amount $H(R)$. At the parton

level in a theoretical calculation, this hadronic transverse energy amounts to that of gluons or quarks. (i) In order to ensure the infra-red safety of the observables, the soft momentum region of the gluons must be unaffected by this algorithm through the phase space of the gluons, which includes the region inside the cone as well. This requirement implies that the choice of the function $H(R)$ must be such that for any radius of the circle $R < R_0$, the hadronic activity must not vanish inside the cone. (ii) On the other hand, for the isolation of the photons, the hadronic activity should decrease as we move closer to the photon direction and in the limit $R \rightarrow 0$, the hadronic activity should almost be zero. A choice of the function that satisfies these two requirements (i) and (ii) is given by

$$H(R) = E_T^{iso} \left(\frac{1 - \cos R}{1 - \cos R_0} \right)^n, \quad (4.2)$$

where E_T^{iso} is a fixed energy. In our analysis, $n = 2$, $R_0 = 0.4$ and $E_T^{iso} = 15$ GeV would be the default values. For this choice of the parameters, the variation of the function $H(R)$ is depicted in the right panel of fig.(4.1). Thus as we move closer to the photon direction lesser hadronic energy is allowed in its neighborhood, ensuring both the isolation of the photons and the infra-red safety of the observables.

It should be noted here that as the photons in the final state are subject to experimental cuts like $p_T > 40$ GeV, they will be away from the beam direction and a cone that is constructed around such photons can not have final state partons inside it which are collinear to the initial partons, as the initial state partons are approximated not to have any transverse momenta along the beam direction, implying that the mass factorization of the initial state collinear singularities are unaffected by this isolation algorithm.

In view of the above points, it is implicit that the slicing method and the smooth cone isolation algorithm do not conflict with each other when implemented in an NLO computation. However, in an NLO calculation using the slicing method, it will be very easy to adopt the slicing method first as it involves some analytical computation and then, after ensuring the infra-red safety of the observables with respect to QCD, to

implement the smooth cone isolation algorithm using a monte-carlo program on the final state photons to suppress the QED singularities.

4.2 Leading order cross sections

A parton level $2 \rightarrow 2$ process at the leading order is of the generic form

$$a(p_1) + b(p_2) \rightarrow \gamma(p_3) + \gamma(p_4). \quad (4.3)$$

where a and b are either quark and anti-quark or gluons. The exact matrix elements in $n = 4 + \epsilon$ dimensions for $q\bar{q}$ and gg initiated subprocesses are

$$\overline{|M^{(0)}|^2}_{q\bar{q},sm} = \frac{e_q^4}{N} \left[\frac{u}{t} + \frac{t}{u} + \epsilon \left(1 + \frac{u}{t} + \frac{t}{u} \right) + \frac{\epsilon^2}{4} \left(2 + \frac{u}{t} + \frac{t}{u} \right) \right] \quad (4.4)$$

$$\overline{|M^{(0)}|^2}_{q\bar{q},int} = -\kappa^2 \mathcal{R}e\mathcal{D}(s) \frac{e_q^2}{8N} \left[4(t^2 + u^2) + \epsilon(3t^2 + 3u^2 + 2ut) \right] \quad (4.5)$$

$$\overline{|M^{(0)}|^2}_{q\bar{q},gr} = \frac{\kappa^4 |\mathcal{D}(s)|^2}{16N} \left[ut^3 + tu^3 + \frac{\epsilon}{4} (3tu^3 + 3t^3u + 2u^2t^2) \right], \quad (4.6)$$

$$\begin{aligned} \overline{|M^{(0)}|^2}_{gg,gr} = & \frac{\kappa^4 |\mathcal{D}(s)|^2}{N^2 - 1} \left[\frac{81}{128(3 + \epsilon)^2} s^4 + \frac{27}{64(3 + \epsilon)} s^2 (u^2 + 14tu + t^2) \right. \\ & + \frac{5}{2(2 + \epsilon)^2} s^2 tu - \frac{1}{16(2 + \epsilon)} s^2 (7u^2 + 94tu + 7t^2) \\ & \left. + \frac{1}{128} (9t^4 + 28t^3u + 54t^2u^2 + 28tu^3 + 9u^4) \right] \end{aligned} \quad (4.7)$$

where sm , gr , int represent contributions from SM, gravity, and interference of SM with gravity induced process respectively, s, t, u are the usual Mandelstam invariants, e_q is the charge of a quark or anti-quark and κ is the coupling of gravity to SM fields. The bar over the symbol M represents that the matrix elements have been averaged over initial helicities and color, and summed over the final ones. A factor of 1/2 has been included for identical final state photons. This expression has been evaluated for quarks with N and gluons with $N^2 - 1$ color degrees of freedom.

4.3 Next-to-leading order cross sections

The order α_s corrections to leading order process come from interference between Born graphs and virtual graphs. It is to be noted that the virtual contribution here does not contain UV singularities. The reason lies in the facts that (i) electromagnetic coupling α does not receive any QCD corrections, (ii) and that the gravitons couple to the energy momentum tensor of SM fields which is a conserved quantity and does not get renormalized. The Feynman diagrams with external leg corrections are not shown as these vanish in the dimensional regularization in the massless limit. We give below the order α_s squared matrix element coming from virtual processes. The SM contribution is found to be

$$\begin{aligned} \overline{|M^V|^2}_{q\bar{q},sm} &= a_s(\mu_R^2) f(\epsilon, \mu_R^2, s) C_F \left[\Upsilon(\epsilon) \overline{|M^{(0)}|^2}_{q\bar{q},sm} + 2 \frac{e_q^4}{N} \left\{ (4\zeta(2) - 7) \frac{u}{t} \right. \right. \\ &\quad \left. \left. + \left(2 + 3\frac{u}{t}\right) \ln \frac{-t}{s} + \left(2 + \frac{u}{t} + 2\frac{t}{u}\right) \ln^2 \frac{-t}{s} + t \leftrightarrow u \right\} \right], \end{aligned} \quad (4.8)$$

the interference of SM with the gravity mediated processes are

$$\begin{aligned} \overline{|M^V|^2}_{q\bar{q},int} &= a_s(\mu_R^2) f(\epsilon, \mu_R^2, s) C_F \left[\Upsilon(\epsilon) \overline{|M^{(0)}|^2}_{q\bar{q},int} + \kappa^2 \mathcal{ReD}(s) \frac{e_q^2}{2N} \left\{ (17 - 8\zeta(2)) t^2 \right. \right. \\ &\quad \left. \left. - (2tu + 3u^2) \ln \frac{-t}{s} - (2tu + 2t^2 + u^2) \ln^2 \frac{-t}{s} + t \leftrightarrow u \right\} \right. \\ &\quad \left. - \kappa^2 \pi \mathcal{ImD}(s) \frac{e_q^2}{2N} \left\{ 3t^2 + 2tu + 2(t^2 + 2tu + 2u^2) \ln \frac{-u}{s} + t \leftrightarrow u \right\} \right] \end{aligned} \quad (4.9)$$

$$\begin{aligned} \overline{|M^V|^2}_{gg,int} &= a_s(\mu_R^2) e_q^2 \kappa^2 \frac{1}{N^2 - 1} \left[s \mathcal{ReD}(s) \left\{ u^2 + (2tu + t^2) \ln \frac{-u}{s} \right. \right. \\ &\quad \left. \left. + \left(u^2 + \frac{1}{2}t^2 + tu\right) \ln^2 \frac{-u}{s} \right\} + s \pi \mathcal{ImD}(s) \left\{ u^2 + 2tu \right. \right. \\ &\quad \left. \left. + (2u^2 + 2tu + t^2) \ln \frac{-u}{s} \right\} + t \leftrightarrow u \right], \end{aligned} \quad (4.10)$$

and the pure gravity contributions are

$$|\overline{M^V}|_{q\bar{q},gr}^2 = a_s(\mu_R^2) f(\epsilon, \mu_R^2, s) C_F \left[\Upsilon(\epsilon) |\overline{M^{(0)}}|_{q\bar{q},gr}^2 + 4(2\zeta(2) - 5) |\overline{M^{(0)}}|_{q\bar{q},gr}^2 \right] \quad (4.11)$$

$$\begin{aligned} |\overline{M^V}|_{gg,gr}^2 &= a_s(\mu_R^2) f(\epsilon, \mu_R^2, s) C_A \left[\left\{ -\frac{16}{\epsilon^2} + \frac{4}{C_A \epsilon} \left(\frac{11}{3} C_A - \frac{4}{3} n_f T_f \right) \right\} |\overline{M^{(0)}}|_{gg,gr}^2 \right. \\ &\quad \left. + \frac{1}{9} \left(72\zeta(2) + 70 \frac{n_f T_f}{C_A} - 203 \right) |\overline{M^{(0)}}|_{gg,gr}^2 \right] \end{aligned} \quad (4.12)$$

where

$$\Upsilon(\epsilon) = -\frac{16}{\epsilon^2} + \frac{12}{\epsilon}, \quad f(\epsilon, \mu_R^2, s) = \frac{\Gamma\left(1 + \frac{\epsilon}{2}\right)}{\Gamma(1 + \epsilon)} \left(\frac{s}{4\pi\mu_R^2} \right)^{\frac{\epsilon}{2}} \quad (4.13)$$

Here μ_R^2 is the scale at which the theory is renormalized ; $a_s(\mu_R^2) = g_s(\mu_R^2)^2/16\pi^2$ is the strong running coupling constant. Our results for the SM are in agreement with the literature [51]. The poles in ϵ arise from loop integrals and correspond to the soft and collinear divergences. Configurations in which a virtual gluon momentum goes to zero give soft singularities while collinear singularities arise when two massless partons become collinear to each other. As the soft divergences cancel completely in any observable, the ϵ poles of order-2, get canceled when real emission contributions are included. This cancellation will be shown in what follows. A next-to-leading order $2 \rightarrow 3$ parton level process for production of photon pairs is of the following generic form

$$a(p_1) + b(p_2) \rightarrow \gamma(p_3) + \gamma(p_4) + c(p_5). \quad (4.14)$$

where a,b and c are massless partons. In fig.(4.4) all gravity mediated $2 \rightarrow 3$ Feynman diagrams are given. Depending on the initial state partons, the final state may have a quark or anti-quark or a gluon. To obtain an inclusive cross-section the final state parton will be integrated over the phase-space. The $2 \rightarrow 3$ matrix elements when integrated over the phase-space give soft and collinear singularities. These singularities are regulated using dimensional regularization with $n = 4 + \epsilon$ and appear as poles in ϵ . These singularities arise when the final state gluon becomes soft (a soft

fermion does not give any soft divergences) or when the final state massless parton becomes collinear to an initial state massless parton. As was mentioned in the introduction a Monte Carlo approach allows for an easy implementation of experimental cuts on the final state photons and smooth-cone isolation criterion. This is achieved by using the semi-numerical two cutoff phase space slicing method. This method introduces two small dimensionless parameters δ_s and δ_c to deal with soft and collinear QCD singularities. δ_s divides the phase-space into *soft* and *hard* regions. The part of phase-space where the energy of the gluon in the centre of mass frame of incoming parton is less than $\delta_s\sqrt{s}/2$ is defined as *soft* and the region complementary to it is *hard*. For small values of δ_s the matrix elements can be simplified and integrated over the soft region to give a δ_s dependent, order α_s , 2-body contribution $d\sigma_S(\delta_s, \epsilon)$. This contains the poles in ϵ arising from the soft singularities. The hard region can be further divided into collinear and non-collinear regions using another small dimensionless slicing parameter δ_c . The part of phase-space in which the final state parton is collinear to the incoming parton is defined as collinear region and gives an order α_s contribution $d\sigma_{HC}(\delta_s, \delta_c, \epsilon)$. This contains the collinear singularities. The hard non-collinear 3-body contribution denoted by $d\sigma_{\overline{HC}}(\delta_s, \delta_s)$ is free of any singularities and can be evaluated numerically using Monte Carlo integration. The collinear singularities appearing in $d\sigma_{HC}(\delta_s, \delta_c, \epsilon)$ will be removed by mass factorization in \overline{MS} scheme by adding counter terms to give $d\sigma_{HC+CT}(\delta_s, \delta_c, \epsilon)$. In the following subsections it will be shown that the 2-body contribution $d\sigma_V(\epsilon) + d\sigma_S(\delta_s, \delta_c, \epsilon) + d\sigma_{HC+CT}(\delta_s, \delta_c, \epsilon)$ is free of poles in ϵ . Although individually the 2-body and 3-body contributions depend on the slicing parameters which were introduced artificially in the problem, the sum should be independent of these parameters. In what follows we will show that this sum is independent of δ_s and δ_c for a fairly wide range of these parameters.

Soft

In the soft gluon limit the $2 \rightarrow 3$ amplitude factorizes into Born matrix element and a term containing eikonal currents. These eikonal currents reveal the singularities when integrated over the soft part of phase space.

$$d\hat{\sigma}_S = a_s(\mu_R^2) f(\epsilon, \mu_R^2, s) \left(C_F d\hat{\sigma}_{q\bar{q}}^0(\epsilon) + C_A d\hat{\sigma}_{gg}^0(\epsilon) \right) \left[\frac{16}{\epsilon^2} + \frac{16}{\epsilon} \ln \delta_s + 8 \ln^2 \delta_s \right] \quad (4.15)$$

The symbol $\hat{\sigma}$ is used to indicate that the cross-section is at parton level. The terms linear and higher order in δ_s have been dropped. Note that the $1/\epsilon^2$ pole cancels with the virtual contribution. However the pole $1/\epsilon$ with coefficient $\ln \delta_s$ still remains uncanceled and later it will be seen that this pole also cancels.

Collinear

Complementary to the soft region discussed above is the hard region. In this region collinear singularities arise when the final state massless parton (quark, anti-quark or gluon) is collinear to the initial state parton. Let z denote the momentum fraction of the incoming parton carried by the parton entering into hard scattering. An initial state quark can split into a quark (and a gluon) or into a gluon (and a quark) which enter into the hard scattering and involve P_{qq} and P_{gq} splitting functions. Similarly an initial state gluon gives P_{gg} and P_{qg} splitting functions. If the energy of a final state gluon is greater than $\delta_s \sqrt{s}/2$ in the rest frame of incoming partons it is defined as a hard gluon. Thus a gluon is hard if $0 \leq z \leq 1 - \delta_s$ for P_{qq} and P_{gg} splittings. As a soft quark does not give any soft singularities, $0 \leq z \leq 1$ for P_{gq} and P_{qg} splittings. As already discussed above, in the collinear limit matrix elements simplify and can be integrated easily in $n = 4 + \epsilon$ dimensions over the collinear region. For photon pair

production the hard collinear contribution takes the following form

$$\begin{aligned}
d\sigma_{HC} = & \frac{a_s(\mu_R^2)}{\epsilon} dx_1 dx_2 f(\epsilon, \mu_R^2, s) \\
& \times \left[d\hat{\sigma}_0^{q\bar{q}}(x_1, x_2, \epsilon) \left\{ \int_{x_2}^{1-\delta_s} \frac{dz}{z} \mathcal{H}(z, \epsilon, \delta_c) P_{qq}(z, \epsilon) \sum_i f_{q_i}(x_1) f_{\bar{q}_i}(x_2/z) \right. \right. \\
& + \int_{x_1}^{1-\delta_s} \frac{dz}{z} \mathcal{H}(z, \epsilon, \delta_c) P_{qq}(z, \epsilon) \sum_i f_{q_i}(x_1/z) f_{\bar{q}_i}(x_2) + x_1 \leftrightarrow x_2 \Big\}_{q\bar{q}} \\
& + d\hat{\sigma}_0^{g\bar{q}}(x_1, x_2, \epsilon) \left\{ \int_{x_2}^1 \frac{dz}{z} \mathcal{H}(z, \epsilon, \delta_c) P_{qg}(z, \epsilon) \sum_i f_{q_i}(x_1) f_g(x_2/z) \right. \\
& + \int_{x_2}^1 \frac{dz}{z} \mathcal{H}(z, \epsilon, \delta_c) P_{gq}(z, \epsilon) \sum_i f_{\bar{q}_i}(x_1) f_g(x_2/z) + x_1 \leftrightarrow x_2 \Big\}_{qg} \\
& + d\hat{\sigma}_0^{gg}(x_1, x_2, \epsilon) \left\{ \int_{x_2}^{1-\delta_s} \frac{dz}{z} \mathcal{H}(z, \epsilon, \delta_c) P_{gg}(z, \epsilon) \sum_i f_g(x_1) f_g(x_2/z) + x_1 \leftrightarrow x_2 \Big\}_{gg} \right. \\
& + d\hat{\sigma}_0^{gq}(x_1, x_2, \epsilon) \left\{ \int_{x_2}^{1-\delta_s} \frac{dz}{z} \mathcal{H}(z, \epsilon, \delta_c) P_{gq}(z, \epsilon) \sum_i f_g(x_1) f_{q_i}(x_2/z) \right. \\
& + \int_{x_2}^{1-\delta_s} \frac{dz}{z} \mathcal{H}(z, \epsilon, \delta_c) P_{qg}(z, \epsilon) \sum_i f_g(x_1) f_{\bar{q}_i}(x_2/z) + x_1 \leftrightarrow x_2 \Big\}_{gq} \Big] \quad (4.16)
\end{aligned}$$

where x_1, x_2 are momentum fraction of incoming parton momenta $P_{ij}(z, \epsilon)$ are splitting functions in $4 + \epsilon$ dimensions, and

$$\mathcal{H}(z, \epsilon, \delta_c) = \left(\delta_c \frac{1-z}{z} \right)^{\epsilon/2}. \quad (4.17)$$

The collinear singularities can be removed by the method of mass factorization. To this effect, counter terms to cancel these singularities in \overline{MS} scheme are obtained by introducing in the leading order cross-section

$$\begin{aligned}
d\sigma_0 = & dx_1 dx_2 \left(d\hat{\sigma}_0^{q\bar{q}}(x_1, x_2, \epsilon) \sum_i \left[f_{q_i}(x_1) f_{\bar{q}_i}(x_2) + f_{\bar{q}_i}(x_1) f_{q_i}(x_2) \right] \right. \\
& \left. + d\hat{\sigma}_0^{gg}(x_1, x_2, \epsilon) f_g(x_1) f_g(x_2) \right) \quad (4.18)
\end{aligned}$$

the following factorization scale dependent parton distribution functions in the \overline{MS} scheme.

$$\begin{aligned}
f_q(x) &= f_q(x, \mu_F) - \frac{a_s(\mu_R^2)}{\epsilon} \left(\frac{\mu_F^2}{\mu_R^2} \right)^{\frac{\epsilon}{2}} \int_x^1 \frac{dz}{z} \left[P_{qq}(z) f_q(x/z) + P_{qg}(z) f_g(x/z) \right] \\
f_g(x) &= f_g(x, \mu_F) - \frac{a_s(\mu_R^2)}{\epsilon} \left(\frac{\mu_F^2}{\mu_R^2} \right)^{\frac{\epsilon}{2}} \int_x^1 \frac{dz}{z} \left[P_{gg}(z) f_g(x/z) + P_{gq}(z) (f_q(x/z) + f_{\bar{q}}(x/z)) \right]
\end{aligned} \tag{4.19}$$

Note that the upper limits on the integrals are 1 for all the splittings. Substituting these distribution functions in $d\sigma_0$ an adding to σ_{HC} the following order a_s term is obtained.

$$\begin{aligned}
d\sigma_{HC+CT} &= a_s(\mu_R^2) dx_1 dx_2 f(\epsilon, \mu_R^2, s) \left[d\sigma_0^{q\bar{q}}(\epsilon) \sum_i f_{\bar{q}_i}(x_1, \mu_F) \left\{ \frac{1}{2} \tilde{f}_{q_i}(x_2, \mu_F) \right. \right. \\
&\quad \left. \left. + \left(f_{q_i}(x_2, \mu_F) A_{q \rightarrow q+g} + f_g(x_2, \mu_F) A_{g \rightarrow q+\bar{q}} \right) \left(-\frac{1}{\epsilon} + \frac{1}{2} \ln \frac{s}{\mu_F^2} \right) \right\} \right. \\
&\quad \left. + d\sigma_0^{gg}(\epsilon) f_g(x_1, \mu_F) \left\{ \frac{1}{2} \tilde{f}_g(x_2, \mu_F) + \left(f_g(x_2, \mu_F) A_{g \rightarrow g+g} \right. \right. \right. \\
&\quad \left. \left. \left. + \sum_i f_{q_i}(x_2, \mu_F) A_{q \rightarrow g+q} \right) \left(-\frac{1}{\epsilon} + \frac{1}{2} \ln \frac{s}{\mu_F^2} \right) \right\} \right] + (q \leftrightarrow \bar{q}, x_1 \leftrightarrow x_2) \tag{4.20}
\end{aligned}$$

The function $A_{a \rightarrow b+c}$ result from the mismatch in the integral limits on z -integrals in $d\sigma_{HC}$ and counter term and can be easily evaluated using the definition of *plus*-prescription.

$$\begin{aligned}
A_{q \rightarrow q+g} &= 4C_F \left(2 \ln \delta_s + \frac{3}{2} \right), & A_{q \rightarrow g+q} &= 0. \\
A_{g \rightarrow g+g} &= \frac{22}{3} C_A - \frac{4}{3} n_f + 8C_A \ln \delta_s, & A_{g \rightarrow q+\bar{q}} &= 0,
\end{aligned} \tag{4.21}$$

The function $\tilde{f}_{q,g}$ are defined by

$$\begin{aligned}\tilde{f}_q(x, \mu_F) &= \int_x^{1-\delta_s} \frac{dz}{z} f_q\left(\frac{x}{z}, \mu_F\right) \tilde{P}_{qq}(z) + \int_x^1 \frac{dz}{z} f_g\left(\frac{x}{z}, \mu_F\right) \tilde{P}_{qg}(z) \\ \tilde{f}_g(x, \mu_F) &= \int_x^{1-\delta_s} \frac{dz}{z} f_q\left(\frac{x}{z}, \mu_F\right) \tilde{P}_{gq}(z) + \int_x^1 \frac{dz}{z} f_g\left(\frac{x}{z}, \mu_F\right) \tilde{P}_{gg}(z)\end{aligned}\quad (4.22)$$

with

$$\tilde{P}_{ij}(z) = P_{ij}(z) \ln \left(\delta_c \frac{1-z}{z} \frac{s}{\mu_F^2} \right) - P'_{ij}(z) \quad (4.23)$$

The P' is the order ϵ part of $P_{ij}(z, \epsilon)$.

After mass factorization the poles still remain and do not cancel completely in $d\sigma_{HC+CT}$ and these cancel with the uncanceled simple poles in virtual and soft contributions. The contribution $d\sigma_{HC+CT} + d\sigma_S + d\sigma_V$ is an order a_s 2-body contribution free of any singularities and can be evaluated numerically using Monte Carlo integration with the experimental cuts on the final state photons. This, however depends on the choice of arbitrary small parameters δ_s and δ_c used for slicing of phase space. The 3-body hard non collinear contribution also depends on slicing parameters and is free of any singularities and can be evaluated numerically. The sum of 2-body and 3-body contribution should be independent of the δ_s and δ_c .

4.4 Results for LHC

In this section various kinematical distributions for production of isolated direct photon pairs are presented to next-to-leading order accuracy in QCD in the RS scenario. Both for the SM background and the SM+RS signals the following distributions are presented:

1. Invariant mass (Q) distribution of the di-photon system
2. Transverse momentum (Q_T) distribution of the photon pair

3. Angular distribution $\cos\theta^*$ of the photons
4. Rapidity (Y) distribution of the di-photon system.
5. Rapidity y^γ distribution of photon

We impose the same kinematical cuts on the two photons in our study which are used by ATLAS and CMS collaborations [56, 57]: (i) $p_T^\gamma > 40$ (25) GeV for the harder (softer) photons, (ii) rapidity $|y_\gamma| < 2.5$ for each of the photons. (iii) The minimum separation between the two photons in the $y - \phi$ plane is taken to be $R_{\gamma\gamma} = 0.4$. As this study does not include poorly known fragmentation functions, the final state QED singularity is suppressed using the smooth cone isolation discussed in eqn.(4.2). In what follows $E_T^{iso} = 15$ GeV and $n = 2$ with $R_0 = 0.4$ would be our default choices. This choice allows a maximum of hadronic transverse energy equal to 15 GeV in a cone of radius 0.4 in $\eta - \phi$ plane around a photon. As parton in the final state in our NLO computation is a crude approximation to the jet of hadrons detected in the detectors, the results depend on the choice of the parameters used in the isolation criterion. This dependency has been studied in the subsequent sections. For our LO and NLO analysis we have used CTEQ6L and CTEQ6M [60] parton density sets respectively, with $n_f = 5$ light quark flavours, and the corresponding two loop strong running coupling constant $\alpha_s(M_Z) = 0.118$. The fine structure constant is taken to be $\alpha(M_W) = 1/128$. Unless mentioned otherwise we have set the renormalization and the factorization scales to $\mu_R = \mu_F = Q$ in all the distributions.

4.4.1 Stability analysis

Before proceeding further we present the stability of the sum of 2-body and 3-body contributions against the variation of the slicing parameters δ_s and δ_c . We have studied the variation of this $\mathcal{O}(\alpha_s)$ contribution in the invariant mass distribution $d\sigma/dQ$ ($Q = 1500$ GeV) of both the SM and the signal (SM+RS). First we have checked the variation of the sum with δ_s in the range $10^{-5} \leq \delta_s \leq 7.5 \times 10^{-2}$ by keeping δ_c fixed at a small

value of 10^{-5} . This variation is clearly depicted in fig.(4.5) for the SM and in fig.(4.6) for the signal (SM+RS). As can be seen from these two figures, though the 2-body and 3-body contributions depend on δ_s , their sum does not depend on it and is stable for a wider range of δ_s . Hence one can choose safely any value of δ_s in this stable region for computing various kinematic distributions. In each of the figures, the lower panel demonstrates the finer variation of the sum with δ_s , which is contrasted against the one at $\delta_s = 10^{-3}$. A similar analysis is done for the variation of the SM and the signal cross sections with δ_c in the range $10^{-6} \leq \delta_c \leq 10^{-3}$ and keeping δ_s fixed at 10^{-3} . This variation is presented in the fig.(4.7) for the SM and in the fig.(4.8) for the signal. It is clear from the figures that the cross sections are again stable for a wider range of other slicing parameter δ_c and hence a value of δ_c chosen from this stable region is fairly acceptable in our numerical prediction of various kinematic distributions in the RS model.

The general condition required for the slicing method to work efficiently is to choose δ_c to be much smaller than δ_s . Hence in the rest of our computation, we choose $\delta_c = 10^{-5}$ and $\delta_s = 10^{-3}$. This stability analysis serves as a check on the successful implementation of the phase space slicing in our numerical code. As a further test we compared our SM results with those in [61]. Our SM results are in good agreement with [61] when the isolation criterion used there is implemented in our code. This gives us a further confidence about our code.

The transverse momentum of the photon pair is defined by $Q_T = \sqrt{q_x^2 + q_y^2}$. At LO, the photon pairs will have zero Q_T as incoming partons have no transverse momentum, and hence Q_T distribution will be proportional to $\delta(Q_T)$. However, at NLO, the photon pairs will be accompanied by a quark (anti-quark) or a gluon in the final state resulting in a non-zero Q_T .

4.4.2 Kinematic distributions

In this section we present the kinematic distributions of the photon pairs in the RS model at the LHC to order α_s . Unlike the ADD model wherein the spectrum of the KK modes is uniform and almost continuous, the spectrum in the RS model is quite non-uniform and contains heavy resonances. They can be probed via their resonance decays at large values of Q . We first present various subprocess contribution to the invariant mass distribution of the diphoton in fig.(4.9) for $360 \leq Q \leq 3000$ GeV. The choice of the RS parameters is : (i) the mass of the first RS mode is $M_1 = 1.5$ TeV and (ii) the effective coupling between the RS modes and the SM fields is $c_0 = 0.01$. This choice is consistent with the latest bounds obtained from the Tevatron [13]. In the SM, both the subprocesses initiated by $q\bar{q}$ and gg have continuum background with former being dominant over the later. In the RS case, we present in each of the subprocess, the sum of the contributions coming from the direct RS gravitons and from the their interference (SM*RS) with the SM. Owing to the high gluon flux at the LHC, the gg initiated process has dominant contribution over the rest at the resonance, with the $q\bar{q}$ initiated subprocess having a negative contribution. Off the resonance, the sum of direct and interference contributions do have a pattern that can change the sign as a function of Q . On the average, for the range of Q we have considred, the $q\bar{q}$ subprocess has a lower contribution than that of the $q\bar{q}$ in magnitude. It can be noticed that the gg interference contribution which is included in the subprocess denoted by RS gg has a very negligible contribution differing by more than few orders of magnitude from the direct gg contribution.

In the left panel of fig.(4.10), we present the invariant mass distribution of the di-photon to LO and NLO in QCD, where the RS modes being heavy show up as resonances. In the right panel, we have plotted the rapidity distribution of the photon pairs (see eqn.(4.24)) after integrating over the invariant mass of the photon pairs around the first resonance i.e. in the range $1100 < Q < 1600$ GeV. The rapidity of the

photon pair is defined by

$$Y = \frac{1}{2} \ln \left(\frac{P_1 \cdot q}{P_2 \cdot q} \right) \quad (4.24)$$

where P_1, P_2 are the momenta of incoming hadrons and $q = p_3 + p_4$. We find that the signal has maximum contribution at the central rapidity ($Y=0$) and is differing from the SM background by an order of magnitude. The NLO QCD corrections enhance the signal and the background. Even though, the resonance pattern in the high Q region can point to new physics, identification of the spin of the resonance will be very important to discriminate between the various new physics scenarios. It is well known that spin information of these resonances will be reflected in the angular distribution and we study them in the following.

In fig.(4.11), rapidity y^γ of the photons is plotted $|y^\gamma| \leq 2.0$ both in the SM and in SM+RS to order α_s . The rapidity of a photon is given by

$$y^\gamma = \frac{1}{2} \ln \left(\frac{E + p_z}{E - p_z} \right), \quad (4.25)$$

where E and p_z are its energy and the longitudinal momentum respectively. This distribution is obtained after integrating over the invariant mass of the photon pairs in the range $1100 \leq Q \leq 1600$ GeV around the first RS resonance mode. The SM cross sections show very little variation with respect to y^γ while the signal peaks at the central rapidity. The cosine of the angle (eqn.(4.26)) between the final state photon and one of the incoming hadrons in the c.o.m. frame of the final state photons is defined by

$$\cos\theta^* = \frac{P_1 \cdot (p_3 - p_4)}{P_1 \cdot (p_3 + p_4)}. \quad (4.26)$$

The angular distribution is plotted in the fig.(4.11) in the range $|\cos\theta^*| \leq 0.95$. Again, we have restricted the invariant mass in the range $1100 \leq Q \leq 1600$ GeV as in the case of y^γ distribution. The distribution coming from the SM has a minimum for the photons in the transverse direction and becomes large for the photons close to the beam direction. However, in the RS model, the signal shows an oscillating behavior

and differs by more than an order of magnitude for the photons in the transverse direction. This is due to the different dynamics involved in the theory of gravity (via contact interactions) and in the SM. Mathematically speaking, the matrix elements in these two cases have different functional dependency on this angular variable $\cos\theta^*$. This is one of the unique features of new physics scenarios involving spin-2 particle decays into SM particles. We find our QCD corrections enhance the cross sections. Next, we present the Q_T distribution which is non-zero at NLO. This is also obtained after integrating over Q around the first resonance region as before. The numerical results are shown in fig.(4.12). We find that the signal has a large enhancement over the SM background for the entire range of Q_T considered i.e. from 100 GeV to 900 GeV.

4.4.3 Scale variations

In this section, we discuss the impact of NLO QCD corrections to various distributions. The uncertainty in LO computation of observables at the hadron colliders originates from two important sources, namely, the missing higher order radiative corrections and the choice of factorization and renormalization scales. The former enters through parton density sets and the latter through the renormalized parameters such as running coupling constant α_s of the theory. The radiative corrections coming from QCD in our case enhance both SM as well as the RS distributions. Hence, the K -factor ($K = \sigma^{NLO}/\sigma^{LO}$), that quantifies these effects is always positive and greater than one for the cases we have studied. It is clear from the plots that the K -factor is different for different distributions and also within a given distribution, it varies with the kinematical variable, say Q or Y etc. More importantly, the numerical value of K depends very much on the kinematical cuts imposed on the distributions. We find that the K factors of the distributions are not large and hence our NLO results are stable under perturbation and reliable for further study. Observables are expected to be independent of renormalization and factorization scales, thanks to renormaliza-

tion group invariance. However, any truncated perturbative expansion does depend on the choice of these scales. This is expected to improve if higher order corrections are included in the perturbative expansion. Indeed, our NLO results show significant improvement on the factorization scale uncertainty entering through parton density sets at LO level. In order that the perturbative expansion does not break down these scales should be chosen close to the hard scale in the problem such as Q or Q_T . We studied this variation for Y and $\cos \theta^*$ distributions and the results are shown in fig.(4.13). Here, we have integrated the invariant mass around the first resonance region $1100 \leq Q \leq 1600$ GeV. In the case Q_T distribution, as mentioned before, it comes only at NLO and there is no distribution at LO. The factorization scale dependency in this distribution is shown in the right panel of fig.(4.12).

4.4.4 Cone variations

Here we address few points concerning the uncertainty coming from the arbitrariness of the parameters used at the parton level calculation *viz.* E_T^{iso} and the radius of the cone, and that coming from the choice of the function $H(R)$ in the smooth cone isolation algorithm.

1. In an NLO calculation the total hadronic energy corresponds to that of a single parton in the final state. The E_T^{iso} at the parton level is a crude estimate of that at the hadron level which gives rise to the dependency of the cross sections on the value chosen in the calculation. In our NLO calculation of the RS model distributions, we present numerically this uncertainty in the invariant mass distribution of the di-photon for a variation of E_T^{iso} in the range $15 \leq E_T^{iso} \leq 30$ GeV (4.1).
2. Similarly, in the isolation of the photons, the radius of the cone that one uses is based on the rapidity and azimuthal angle of the parton, approximating it to that at the hadron level used in the experimental analysis. A quantitative information of the uncertainty that might arise due to the choice of the R_0 value will be

useful for a better prediction of the results. In the table (4.1), we present this uncertainty in the cross sections for a variation of R_0 in the range $0.4 \leq R_0 \leq 1.0$.

3. In the experimental analysis, the isolation of photons would involve hadronic activity which corresponds to an all-ordered effect in a theoretical calculation. Hence the isolation of photons in an NLO calculation with a single parton as to correspond to that of the total hadronic activity, can give uncertainty due to the potential higher order radiative corrections. In this point of view, we have studied the dependency of the cross sections on the choice of the function $H(R)$ used in the calculation by varying n , used to define this function, from 1 to 2 and presented our results numerically in the table (4.1).

Q (GeV)	$E_T^{iso} = 15\text{GeV}, n=2$			$E_T^{iso} = 30\text{GeV}$	$E_T^{iso} = 15\text{GeV}$
	$R_0 = 0.4$	$R_0 = 0.5$	$R_0 = 1.0$	$n=2$	$n=1$
1440	0.2507E-04	0.2430E-04	0.1882E-04	0.2532E-04	0.2537E-04
1500	0.6348E-02	0.6115E-02	0.4509E-02	0.6446E-02	0.6441E-02
1560	0.2181E-04	0.2108E-04	0.1503E-04	0.2207E-04	0.2205E-04

Table 4.1: Cone variations

Table 4.2: Variation of the RS model signals to NLO in the invariant mass distribution of the di-photon production at the LHC, with the isolation parameters R_0 , E_T^{iso} and the choice of n in $H(R)$ ($E-n = 10^{-n}$).

As can be seen from the table that the uncertainties in the cross sections due to the variation in E_T^{iso} and n in $H(R)$ are not very large around the first RS mode (1.5 TeV). By varying the cone radius R_0 from its default value of 0.4 to a value of 0.5, there is no significant uncertainty noticed in the cross sections. However by taking R_0 to a large value say 1.0 the cross sections dropped significantly, showing a non-trivial dependency on large variations of R_0 .

4.5 Results for Tevatron

In this section we present the numerical results for the di-photon production to NLO in QCD in the RS model at the Tevatron where the centre of mass energy of the colliding beams is $\sqrt{s} = 1.96$ TeV. In our computation, on the final state photons, We have used the following kinematical cuts: (a) transverse momentum $p_T^\gamma > 14$ (13) GeV for the harder (softer) photons, (b) rapidity $|y_\gamma| < 0.9$ for each photon, and (c) $r_0 = 0.4$ and $r_{\gamma\gamma} = 0.3$. In addition, for the smooth-cone-isolation we use $E_T^{iso} = 1$ GeV and $n = 2$. For our analysis, we have chosen the first RS mode to be $M_1 = 850$ GeV and the effective coupling $c_0 = k/M_{Pl} = 0.01$. The latest bounds on the RS model parameters [13], obtained using 1 fb^{-1} of data from $p\bar{p}$ collisions at Tevatron are presented in the fig.(2.1). Our choice of the RS parameters mentioned above is consistent with these bounds obtained from the D0 collaboration. In fig.(4.14), we present the invariant mass distribution of the di-photon in the range $300 \leq Q \leq 1000$ GeV. At $Q = 850$ GeV, the peak shown is due to the narrow resonance of the first RS mode. After the peak, there is a steep fall in the signal due to the destructive interference (SM*RS) contributions. At Tevatron, for higher Q values, the $q\bar{q}$ flux is dominant over that of gg . Hence, the dominant contribution to this destructive interference comes from the $q\bar{q}$ (SM*RS) subprocess. Our results also show that the NLO QCD corrections to the di-photon production at the Tevatron are not significant as can be seen from the left panel of fig.(4.14).

However at NLO in QCD the additional information available, which is absent at LO, is the transverse momentum distributions of the di-photons. In the right panel of fig.(4.14), this transverse momentum distribution of the di-photon is presented in the range $50 \leq Q_T \leq 500$ GeV. For this transverse momentum distribution, we have integrated over the invariant mass distribution around the first RS mode i.e. in the region $750 \leq Q \leq 950$ GeV. It can be seen from the figure that throughout the range of Q_T considered, the signal is dominant over the SM back ground by more than an order of magnitude.

4.6 Conclusions

In this work, we have presented full next to leading order QCD corrections to production of direct photon pairs at hadron colliders in the context of warped extra-dimension model (RS model). In this model, photon pairs can be produced in collisions of partons through virtual exchange of RS gravitons. These gravitons can be seen as a resonance pattern over the SM continuum background. Due to the warp factor, the effective coupling between the gravitons and the SM particles can have only TeV scale suppression instead of Planck scale suppression. Only the spin-2 gravitons are included in our analysis and they show distinct features in the angular distributions of photon pairs. Photon pairs at hadron colliders often provide a clean channel to probe the physics beyond the SM. In this study, only direct photons have been considered and the fragmentation photons are removed by the method of smooth cone isolation. The isolation used also removes final state QED singularities. The leading order contributions to the diphoton production rates resulting from quark as well as gluon initiated processes depend very much on the factorisation scale through the parton distribution functions giving significant theory uncertainty. In order to bring down this uncertainty, we have systematically included all order α_s contributions to the process. This includes all virtual and real emission processes to order α_s both in SM as well as in the RS model. To obtain various kinematic distributions of the final state photons, we have used phase space slicing method to deal with all the soft and collinear singularities and the resulting finite pieces are integrated with the appropriate kinematical cuts using a Monte Carlo program. We have made several tests on our NLO code by showing the independence of the results on the slicing parameters and also comparing with the known NLO corrected SM results available in the literature. Our numerical results including the NLO corrections show significant enhancements over the LO predictions in all the distributions presented. The enhancement varies with the distributions. We have estimated them through the K-factor which quantifies the reliability of the perturbative expansion. We find the K-factor is moderate for

all the distributions and hence the results present here are stable under perturbation. We have also shown the impact of α_s corrected results on the scale uncertainty. We find that the factorisation scale dependence gets reduced considerably when α_s contributions are included.

Besides the predictions for the LHC, we have considered the diphoton production cross sections at the Tevatron as well. The predictions are obtained with that choice of the model parameters that is consistent with the latest bounds obtained from the Tevatron data. We have used the same cut-off parameters of the slicing method as those in the case of LHC and obtained the kinematic distributions. From the cross sections presented here, we conclude that at the LHC the NLO QCD corrections to the diphoton production process are more pronounced in probing new physics scenarios such as RS model than at the Tevatron. We also emphasize that the entire analysis based on this QCD corrections is model independent and a similar significance of the QCD corrections can be expected in other models as well such as the ADD model, where the new gauge bosons at the virtual level can mediate this diphoton production process.

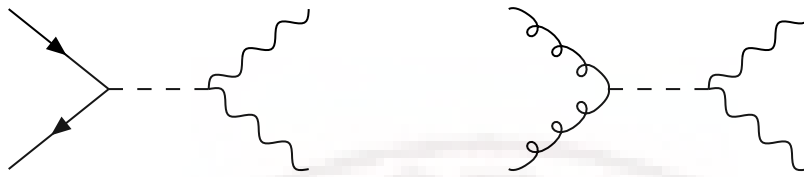


Figure 4.2: Born contributions

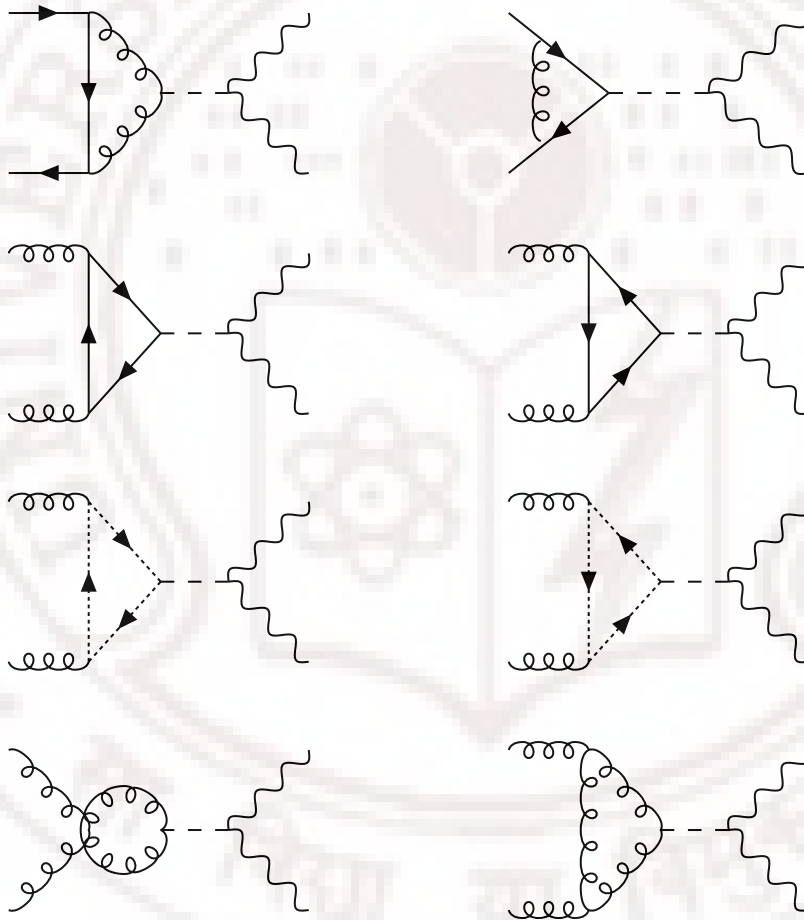


Figure 4.3: Virtual contributions

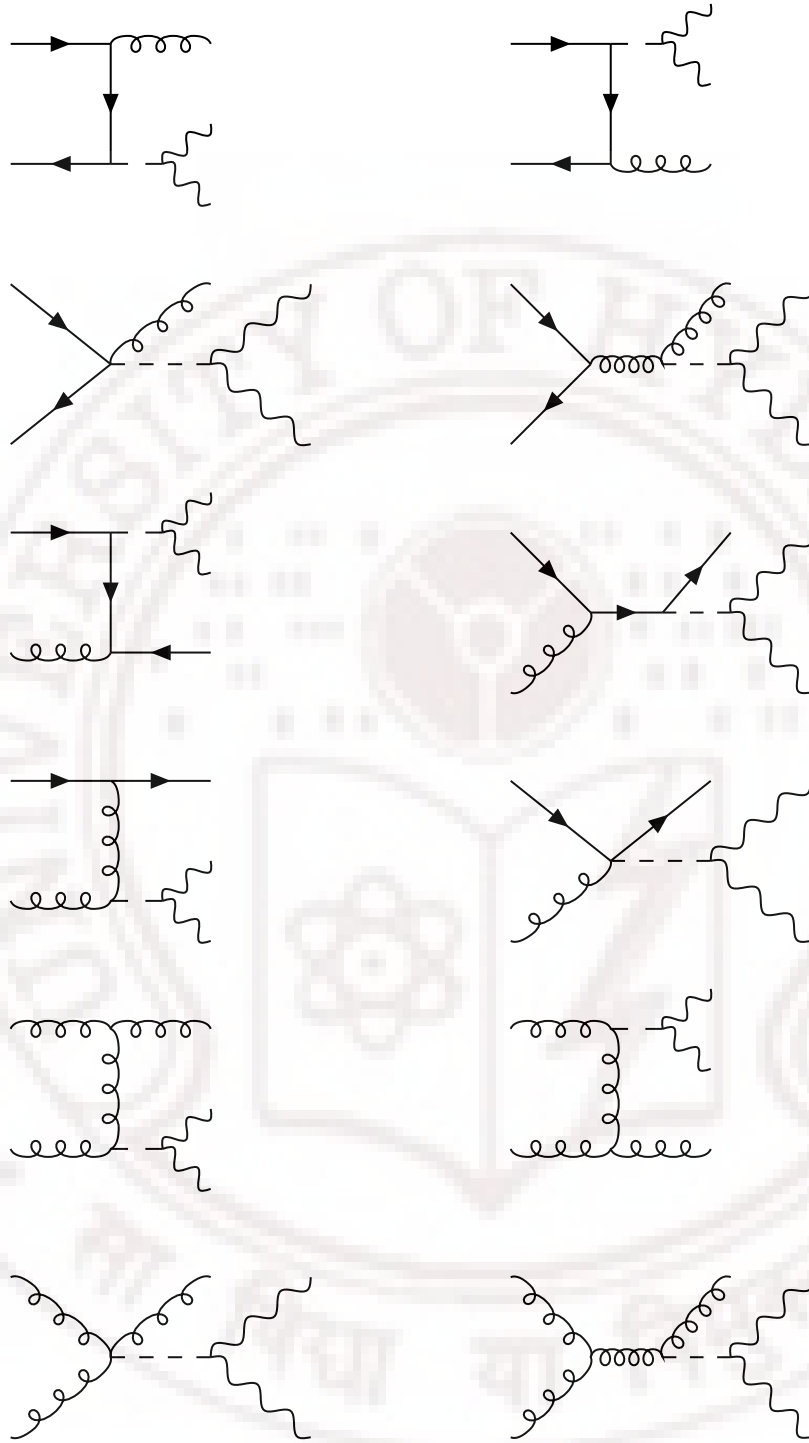


Figure 4.4: Real emission contributions

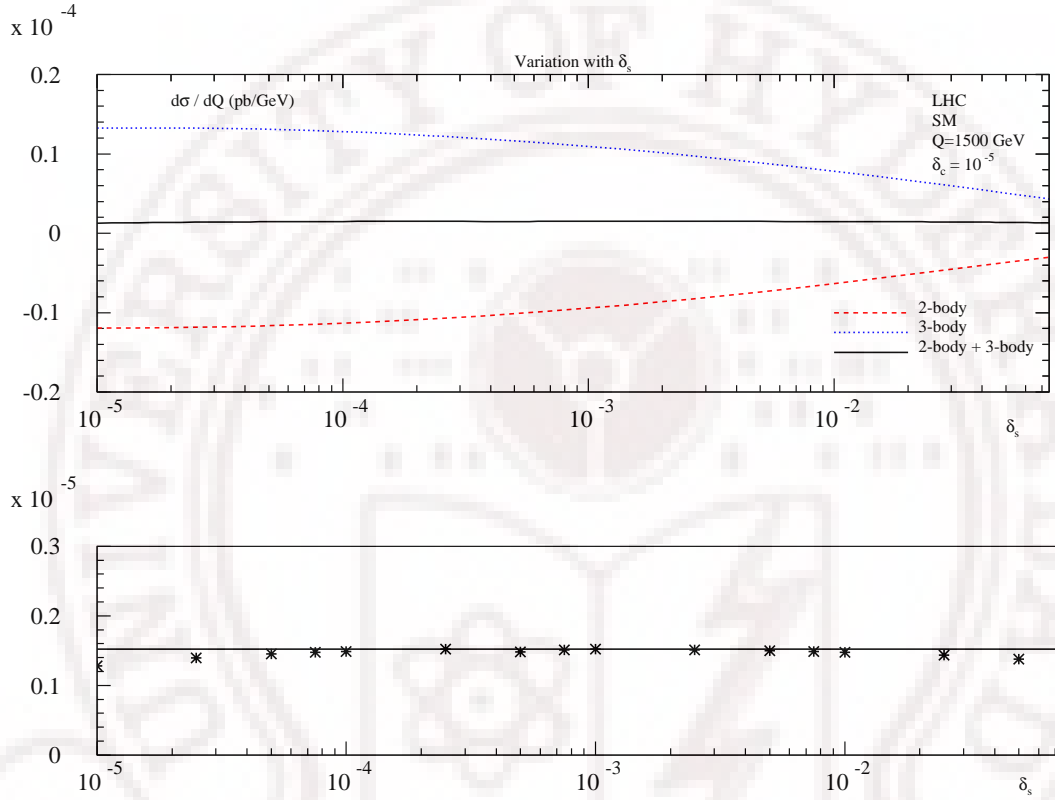


Figure 4.5: Stability of the order α_s contribution to the SM cross section against the variation of the slicing parameter δ_s (top), with $\delta_c = 10^{-5}$ fixed, in the invariant mass distribution of the di-photon. Below is shown the variation of the sum of 2-body and 3-body contributions over the range of δ_s considered and contrasted against the one at $\delta_s = 10^{-3}$.

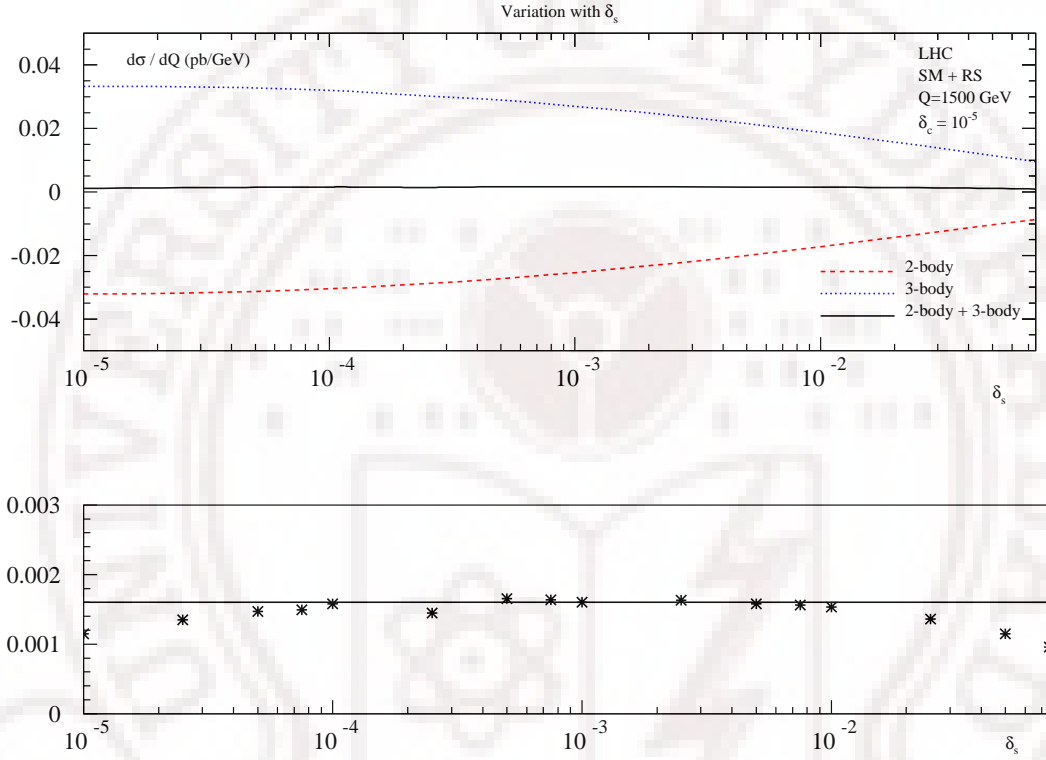


Figure 4.6: Stability of the order α_s contribution to the SM+RS cross section against the variation of the slicing parameter δ_s (top), with $\delta_c = 10^{-5}$ fixed, in the invariant mass distribution of the di-photon with $M_1 = 1.5$ TeV and $c_0 = 0.01$. Below is shown the variation of the sum of 2-body and 3-body contributions over the range of δ_s considered and contrasted against the one at $\delta_s = 10^{-3}$.

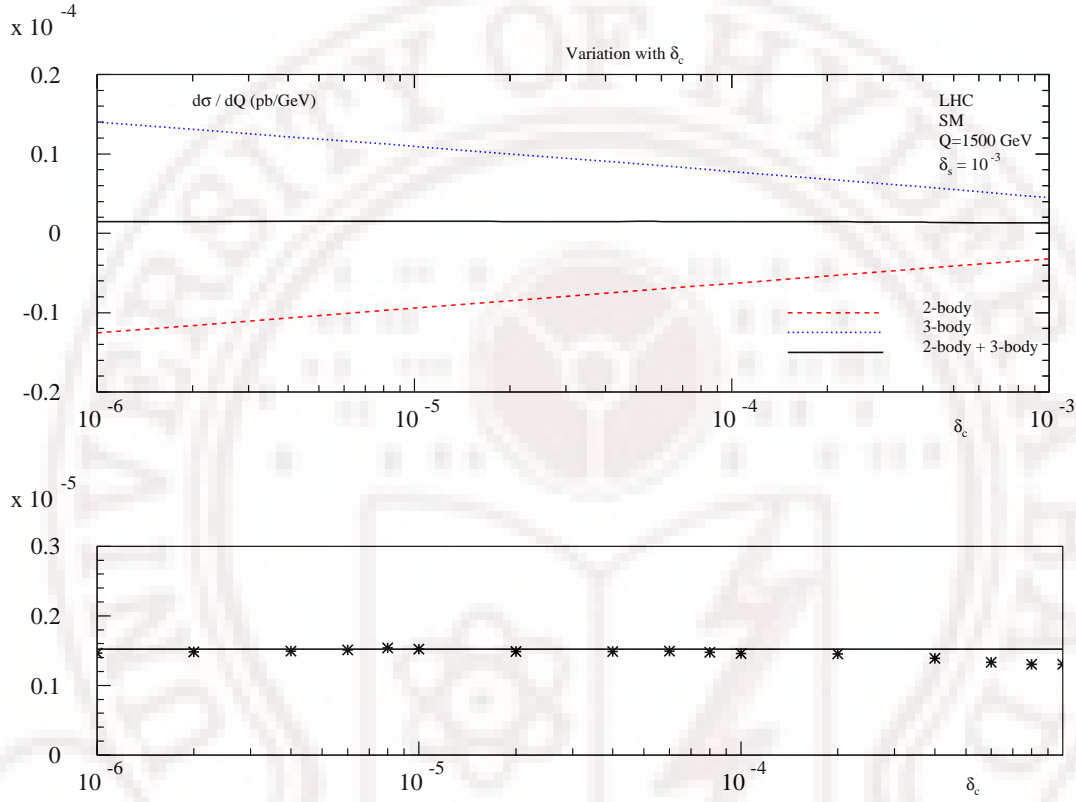


Figure 4.7: Stability of the order α_s contribution to the SM cross section against the variation of the slicing parameter δ_c (top), with $\delta_s = 10^{-3}$ fixed, in the invariant mass distribution of the di-photon. Below is shown the variation of the sum of 2-body and 3-body contributions over the range of δ_c considered and contrasted against the one at $\delta_c = 10^{-5}$.

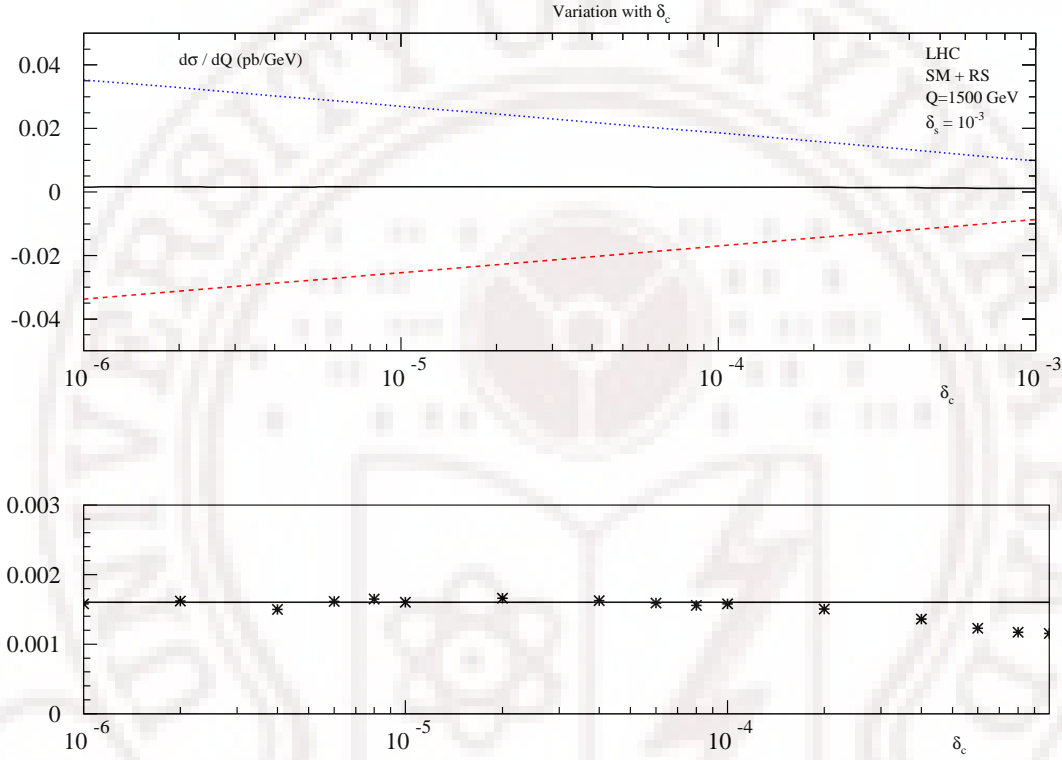


Figure 4.8: Stability of the order α_s contribution to the SM+RS cross section against the variation of the slicing parameter δ_c (top), with $\delta_s = 10^{-3}$ fixed, in the invariant mass distribution of the di-photon with $M_1 = 1.5$ TeV and $c_0 = 0.01$. Below is shown the variation of the sum of 2-body and 3-body contributions over the range of δ_c considered and contrasted against the one at $\delta_c = 10^{-5}$.

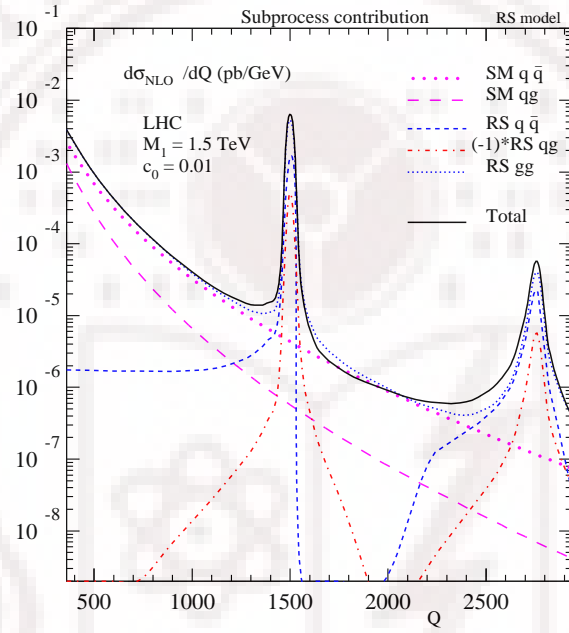


Figure 4.9: Subprocess contribution to the invariant mass distribution $d\sigma/dQ$ of the di-photon production in the RS model with $M_1 = 1.5$ TeV and $c_0 = 0.01$ at the LHC. The RS contribution includes the interference effects (SM*RS).

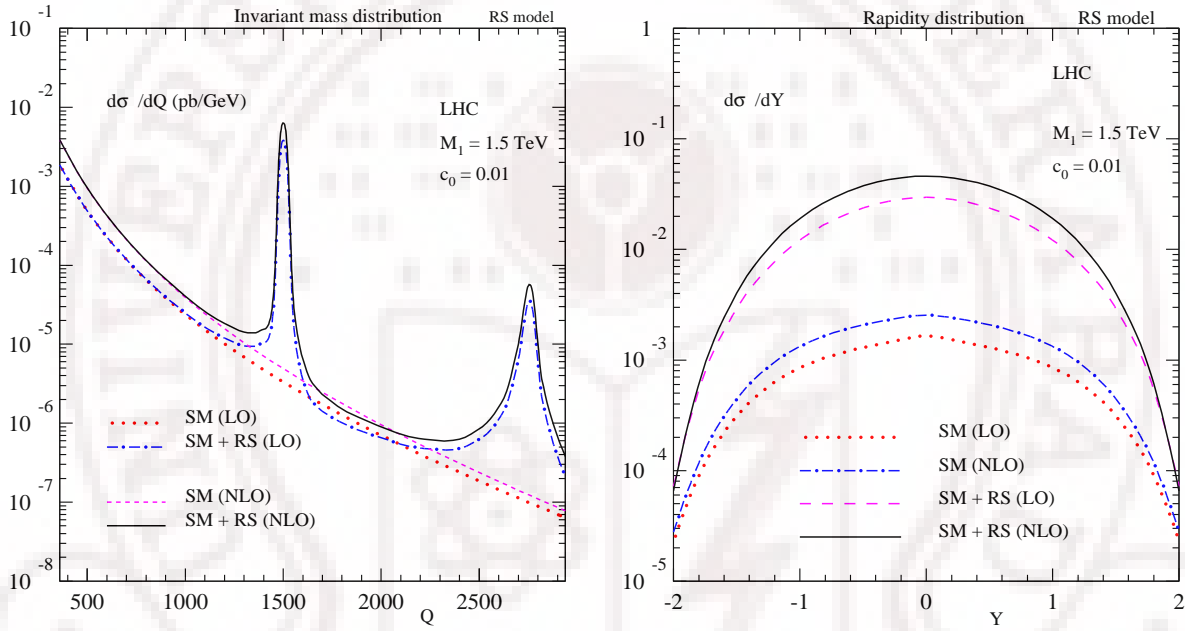


Figure 4.10: Invariant mass $d\sigma/dQ$ (left) and rapidity $d\sigma/dY$ (right) distributions of the di-photon production in the RS model with $M_1 = 1.5$ TeV and $c_0 = 0.01$ at the LHC.

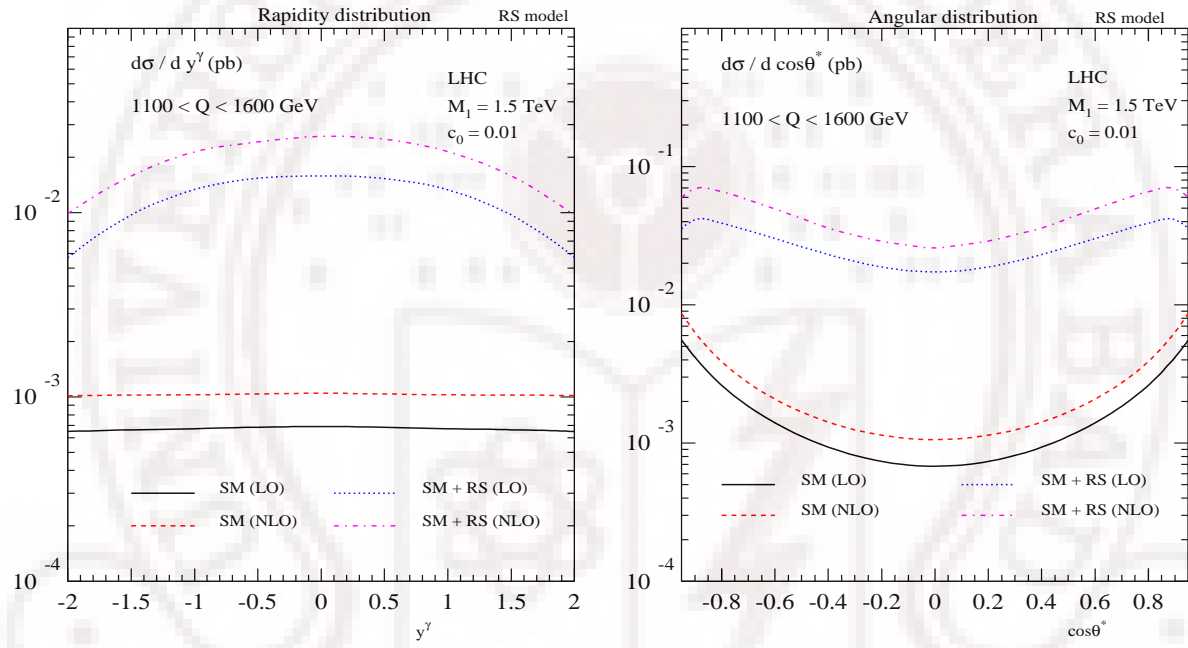


Figure 4.11: Rapidity $d\sigma/dy^\gamma$ (left) and angular $d\sigma/d \cos \theta^*$ (right) distributions of the photons in the RS model with $M_1 = 1.5$ TeV and $c_0 = 0.01$ at the LHC.

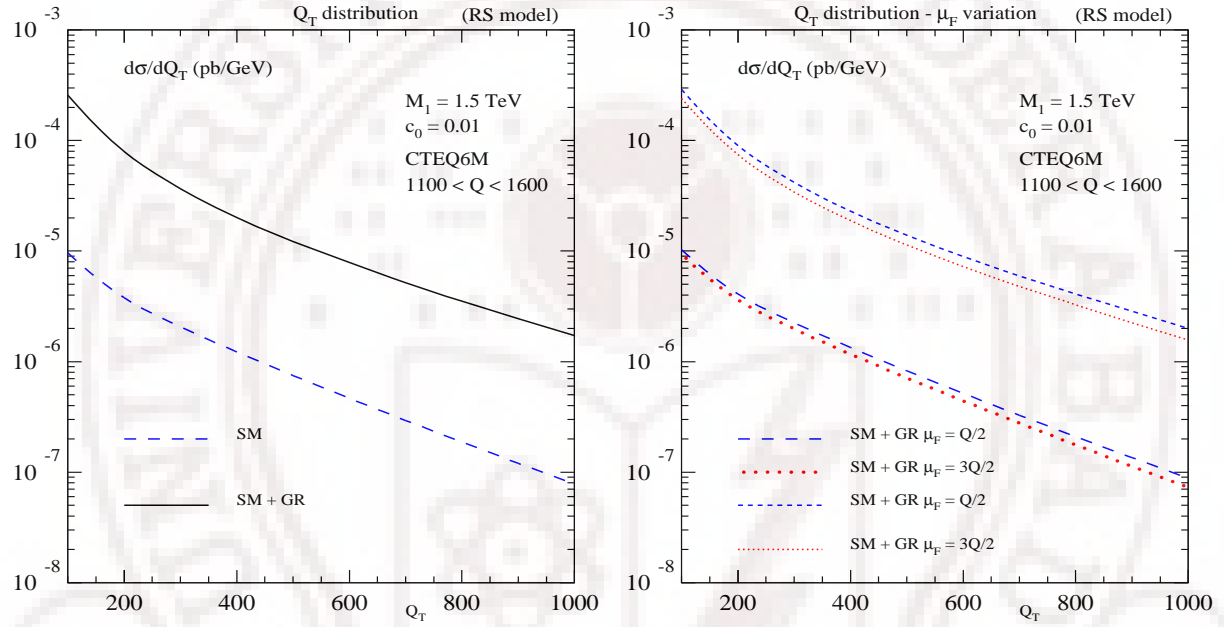


Figure 4.12: Transverse momentum distribution (left) of the di-photon production in the RS model with $M_1 = 1.5$ TeV and $c_0 = 0.01$. Here we have integrated over Q around the first resonance region $1100 \leq Q \leq 1600$ GeV. The factorization scale dependency (right) is also shown for the scale variation of $Q/2 \leq \mu_F \leq 3Q/2$.

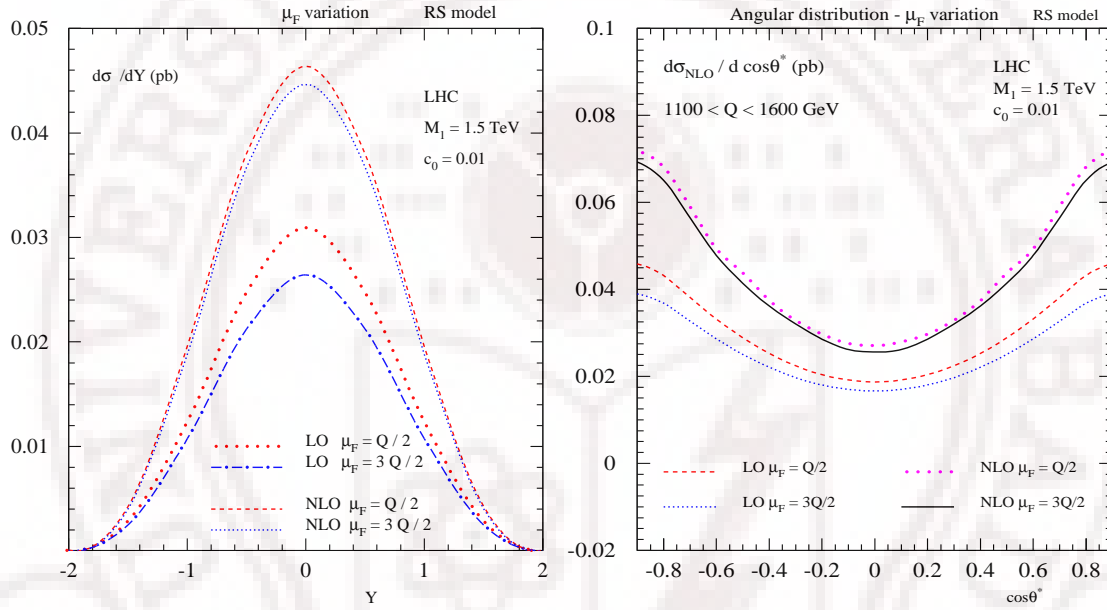


Figure 4.13: The factorization scale dependency is shown in the rapidity distribution $d\sigma/dY$ (left) of the di-photon and the angular distribution $d\sigma/d\cos\theta^*$ (right) of the photons for a scale variation of $Q/2 \leq \mu_F \leq 3Q/2$. For these distributions we have integrated over the invariant mass of the di-photon in the range $1100 \leq Q \leq 1600$ GeV.

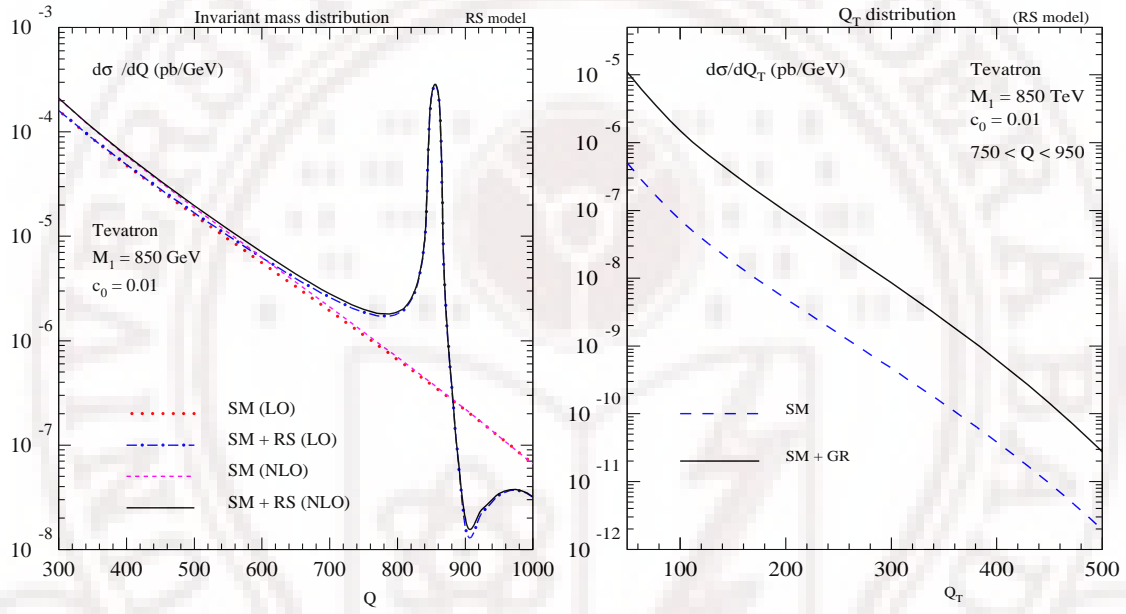


Figure 4.14: Invariant mass (left) and transverse momentum (right) distributions of the di-photon production at the Tevatron with $\sqrt{S} = 1.96$ TeV. The mass of the first RS mode is chosen to be $M_1 = 850$ GeV and the effective coupling is $c_0 = 0.01$. For the transverse momentum distribution we have integrated over the invariant mass of the di-photon around the first RS mode resonance in the region $750 \leq Q \leq 950$ GeV.

Chapter 5

Drell-Yan uncertainties to NLO in QCD in the extra dimension searches

5.1 Introduction

In the previous chapter, we have studied the di-photon production to Next-to-Leading Order (NLO) in QCD in the warped extra dimension model at the hadron colliders. Therein, the higher order QCD corrections are found to have enhanced the cross sections significantly as well as decreased one of the theoretical uncertainties considerably, namely the factorization scale uncertainty. In the case of Drell-Yan (DY) process, recently, for the first time the NLO QCD corrections have been reported considering the gravity effects in both the large and warped extra dimension models at the LHC [45]. Though the higher order QCD corrections have quantitative enhancements and qualitative improvements in the cross sections, various issues concerning the uncertainties coming from the QCD at NLO level in various kinematic distributions useful for the extra dimension searches at the hadron colliders are yet to be addressed. A quantitative information of these uncertainties will be very much useful for the experimental data analysis and consequently in obtaining a relatively more stringent bounds on the model dependent parameters. In this chapter, in view of the above, we will study various aspects of the Drell-Yan process to NLO in QCD in the

context of both large and warped extra dimension searches at the Tevatron as well as at the LHC.

5.2 Drell-Yan process

The production of lepton pairs at hadron colliders is known as Drell-Yan process [62] and is given by

$$P_a(p_1) + P_b(p_2) \rightarrow l^+(k_1) + l^-(k_2) + X(p_x)$$

where p_1, p_2 are the incoming hadron momenta, k_1, k_2 are the outgoing lepton momenta and X is the inclusive final state with momenta p_x . After the deep inelastic scattering process, this process stands as another application of the parton model as in this model the production of the lepton pairs has a simple theoretical interpretation in terms of the quark anti-quark annihilations into a vector boson. This process has another major advantage of providing the necessary data for generating the global fits that are useful in the extraction of the universal and non-perturbative parton distribution functions; in that sense this process is almost indispensable and stands next to the deep inelastic scattering process. Technically speaking, the detection of the leptons (e or μ) is precise and is easier in contrast to that of the hadrons in any collider experiment, and so these dilepton events have become vital in the study of collider physics. In the SM, the dilepton channel has been used at the Tevatron experiments (i) for extracting the limits on anomalous gauge couplings by measuring the WW production cross sections [63] and (ii) for extracting the top quark mass from $t\bar{t}$ production cross section rates [64].

In addition, this process has been used to study the precision standard model physics by computing higher order QCD corrections to it. For the first time, the NLO QCD corrections to this process in the SM were computed in [65]. It was shown that these $\mathcal{O}(\alpha_s)$ corrections have enhanced the cross sections significantly inferring that neglecting these radiative corrections would not be justifiable for any reasonable

parametrization of the parton densities. In going one step ahead, the second order QCD corrections to this process are taken up in [66–68] and a complete $\mathcal{O}(\alpha_s^2)$ QCD corrections are presented in [69], wherein these NNLO corrections not only have improved the quantitative predictions but also stabilized the total cross sections against the factorization scale variations. Further, this stability of the cross sections with respect to the factorization scale variations is also shown in the differential distributions, such as the rapidity of the di-lepton [70], as the differential distributions in general are very useful in the experimental analysis.

On the other hand, this process has also been used in the search of beyond standard model (BSM) physics scenarios. In the BSM scenarios, the production of di-lepton can take place via the quark anti-quark annihilations into the gauge bosons corresponding to this new physics, in very much the same way as the quark anti-quark annihilations into the Z or γ^* in the SM, and followed by their decay into a pair of leptons. Some of these gauge bosons of the new physics can also be produced via gluon fusion processes. The gravitons appearing in the large extra dimension model and warped extra dimension model, and Z' bosons being the examples of such gauge bosons. If the gauge bosons are very heavy, then they can be seen as a resonance pattern in the invariant mass distribution of these di-leptons. Consequently, both theoretical speculations [12, 43] as well as the experimental searches have gained lot of interest towards the BSM scenarios that can be probed by this process. At the Tevatron experiments this process has already been used in the search of large extra dimensions [10] and warped extra dimensions [13] to constrain the parameters of these models.

However, all these theoretical predictions are based on a leading order (LO) computation (α_s^0) in perturbation theory. These leading order cross sections obtained from the Monte-Carlo methods are then approximated to NLO predictions by scaling them with roughly the SM K factor (which is around 1.3) and then compared with the experimental data in order to extract the limits on the unknown parameters at 95% C.L. At the LHC, where the gluon flux is very large, the QCD corrections often play

a significant role. Hence the contribution coming from the higher order QCD corrections is often expected to be large. In the work on NLO QCD corrections to DY process in the ADD and RS models [45–47], it is found that the $\mathcal{O}(\alpha_s)$ QCD corrections have significantly enhanced the cross sections by contributing an average of 60% of the leading order predictions to the total cross sections. Thus the K factor is estimated to be around 1.6 as opposed to the SM K factor which is around 1.3. However, the impact of these QCD corrections are subject to various QCD inputs *viz.* the choice of the parton distribution functions and the arbitrary scales involved in the calculation. Hence a detailed study of the QCD uncertainties has become crucial in presenting various DY distributions at the LHC energies, not only in the search of beyond SM physics scenarios but also in the study of precision SM physics itself. With this motivation, in what follows we concentrate on such QCD uncertainties coming at NLO in the DY process both in the SM as well as in the extra dimension models. For completeness, we also study the variation of the signals with the parameters of the underlying model.

At hadron colliders, it is important to have a precise knowledge of the parton distributions functions (PDFs) to predict production cross sections of both signals and backgrounds. These universal PDFs are non-perturbative inputs that are extracted from global fits to available data on deep-inelastic scattering (DIS), Drell-Yan (DY) and other hadronic processes. They describe the momentum distribution of the partons in a proton and various groups have parametrized the PDFs for a wide range of proton momentum fraction x carried by the parton and for the center-of-mass energy Q^2 at which the process takes place. Parametrization of PDFs to a particular order in QCD would involve various theoretical and experimental uncertainties. In [45], NLO-QCD corrections to dilepton production at hadron colliders in the ADD model were presented first and then this was extended to the RS model in [46]. Further in [47] the double differential cross section, $d^2\sigma/dQ^2/d\cos\theta^*$ is considered, for dilepton production in these extra dimension models. This angular distribution is the one that is actually used by experiments and hence is of particular importance. These NLO results would certainly reduce one aspect of the theoretical uncertainties as results

prior to this calculation were only at leading order (LO) in QCD for process involving gravity.

Unlike the standard model contribution to DY, the extra-dimensional models bring in more processes even at the LO level. For example, in these models, the gluon initiated process enter at the LO level in addition to quark anti-quark initiated process. At LHC, the gluon initiated process is more sensitive to factorization scale compared to quark initiated process that necessitated the relevance of NLO computation. This entire analysis is model independent because the QCD corrections factor out from the model dependent quantities. In [45], the MRST parton density sets were used. It is well known that different PDF sets themselves can affect the theoretical predictions and it is important to quantify these effects in the observable that could probe new physics. With this in mind we have performed a model independent analysis on uncertainties coming from the choice of PDF sets in order to make our predictions more reliable. We have looked at the dependence of DY cross section on various PDFs at the LHC and Tevatron including gravity effects in the ADD and RS models incorporating the NLO QCD corrections. The PDF sets used in this study are CTEQ [60], Alekhin [71], and MRST [72]. Dependence on PDF sets is also compared with experimental errors that enter the parametrization of the PDF, which are now available to NLO QCD [73,74]. For this purpose we used the MRST distribution [74] as a typical case. The dependence of factorization scale μ_F and renormalization scale μ_R in going from LO to NLO is also studied.

Next, we will discuss both the large and warped extra dimension models in relevance to the present work, they are presented in detail in previous chapters.

5.3 Extra Dimension Models

Extra dimension models that allow gravity to propagate the extra dimensions would in 4-dimensions have KK modes which couple to SM particles through the energy momentum tensor. The Feynman rules of the KK mode interactions with the SM

fields are given in [6, 7]. Due to the different methods of compactification of the extra dimensions in ADD and RS models, their KK spectrum are very distinct. Experimental signature of extra dimensions would correspond to deviation from SM predictions due to the virtual exchange of KK modes or direct production of KK modes at a collider.

In the ADD case, there is a tower of KK modes which are almost degenerate in energy and a sum over these KK modes gives an observable effect. In the case of dilepton production, in addition to the SM photon and Z production modes, one has to take into account virtual KK modes. Performing the sum over the virtual KK modes leads to an integral which has to be regulated by an UV cutoff. The propagator after the KK mode summation becomes

$$\kappa^2 \mathcal{D}(Q^2) \equiv \kappa^2 \sum_n \frac{1}{Q^2 - m_n^2 + i\epsilon} = \frac{8\pi}{M_S^4} \left(\frac{Q}{M_S} \right)^{d-2} \left[-i\pi + 2I\left(\frac{\Lambda_c}{Q}\right) \right], \quad (5.1)$$

where $\kappa = \sqrt{16\pi}/M_P$ is the strength of the gravitational coupling to the SM particles, m_n the mass of KK modes, d is the number of extra dimensions and M_S is the scale of the $4 + d$ dimensional theory. The summation over the non-resonant KK modes yields $I(\Lambda_c/Q)$ [6]. Conventionally the UV cutoff Λ_c is identified with the scale of the extra dimension theory M_S , which simplifies the expression giving a mild dependence on the number of extra dimensions [6, 7].

In this analysis, we have kept the cutoff Λ_c different from M_S ¹. Note that the summation of KK modes in Eq. (5.1), modifies the M_P suppression to M_S suppression. The ADD model is a effective low energy theory valid below the scale M_S , for consistency it is essential to satisfy the condition $Q < \Lambda_c < M_S$. The parameters of the ADD model are M_S the scale of the $4 + d$ dimensional theory and d the number of extra spatial dimensions. If $\Lambda_c \neq M_S$ then there is an additional parameter. We have studied the dependence of the cross section on the cutoff $\Lambda_c = \alpha M_S$ and varied $\alpha = 0.7 - 1$. In Fig. 5.1a we see that the cross section decreases as we lower the cutoff Λ_c . The corresponding K-factor also decreases for lower cutoff Fig. 5.1b. Dependence

¹Effects of various UV cutoff methods on the low scale quantum gravity model have been discussed in [92].

of the cross section on the number of extra dimensions d is shown in Fig. 5.1c for $\Lambda_c = M_S$, the cross section decreases as d increases. Reducing Λ_c decreases the cross sections and if d is increased it brings down the cross section much faster Fig. 5.1d.

In the RS model, the gravity propagate one extra dimension which is warped by an exponential factor $\exp(-\pi kL)$, where L is the compactification length and k is the curvature of the AdS_5 space-time. The parameters of the RS model are $m_0 = k \exp(-\pi kL)$ which sets the mass scale of the KK modes and $c_0 = k/M_P$ the effective coupling. The higher KK modes have enhanced coupling to SM particles due to the warp factor and decouple from the zero mode, which is as usual M_P suppressed. RS KK spectrum is distinct from the ADD case and hence the summation of the KK modes that contribute to the virtual process would also be different. The function $\mathcal{D}(Q^2)$ in the KK mode propagator results from summing over the resonant KK modes and is given by

$$\mathcal{D}(Q^2) = \sum_{n=1}^{\infty} \frac{1}{Q^2 - M_n^2 + iM_n\Gamma_n} \equiv \frac{\lambda}{m_0^2}, \quad (5.2)$$

where M_n are the masses of the individual resonances and Γ_n are the corresponding decay widths. The graviton widths are obtained by calculating their decays into final states involving SM particles. λ is defined as

$$\lambda(x_s) = \sum_{n=1}^{\infty} \frac{x_s^2 - x_n^2 - i\frac{\Gamma_n}{m_0}x_n}{x_s^2 - x_n^2 + i\frac{\Gamma_n}{m_0}x_n}, \quad (5.3)$$

where $x_s = Q/m_0$. We have to sum over all the resonances to get the value of $\lambda(x_s)$, which is done numerically for a given value of x_s . Searches for the RS KK modes at Tevatron in the dielectron, dimuon and digamma channel [76] have yielded a lower limit between 250 - 785 GeV depending on the coupling to the SM particles. In this analysis for the RS model, we follow these limits.

5.4 Theoretical uncertainties

In the QCD improved parton model the hadronic cross section can be expressed in terms of perturbatively calculable partonic cross sections denoted by

$\hat{\sigma}^{ab}(\tau, Q^2, \mu_F)$ convoluted with appropriate non perturbative partonic flux $\Phi_{ab}(\tau, \mu_F)$ at a factorization scale μ_F . The subprocess cross section is a perturbative expansion in the strong coupling constant $\alpha_s(\mu_R)$ and is calculated order by order in α_s . Here μ_R is the renormalization scale and $\tau = Q^2/S$ is the DY scaling variable. In perturbative QCD, the unknown higher order corrections and the scale uncertainties are strongly correlated. The factorization of mass singularities from the perturbatively calculable partonic cross sections leads to the introduction of factorization scale μ_F in both non-perturbative partonic flux $\Phi_{ab}(\mu_F)$ as well as the finite partonic cross sections $d\hat{\sigma}_{ab}(x, \mu_F)$. Even though the choice of the scale is guided by the hard scale of the problem, the exact value does not come from the theory. The PDFs and partonic cross sections satisfy renormalization group equations such that the hadronic cross section is independent of the factorization scale μ_F . In addition to the factorization scale, the partonic cross sections are dependent on the renormalization scale μ_R . The choice of the scale is again arbitrary. Even though this is an advantage to choose appropriately to do perturbative calculations, it also introduces theoretical uncertainties through the size of unknown higher order corrections. Usually, one chooses this scale such that the perturbative methods can be applied and then computes higher order corrections sufficiently such that the exact choice of this scale becomes almost immaterial. Gravity couples to the SM fields via its energy momentum tensor, and the calculations are done in the high energy limits where masses of the SM particles are ignored. Only parameter that requires UV renormalization is the strong coupling constant, because of this we have the following expansion for the mass factorized partonic cross section:

$$d\hat{\sigma}_{ab}(z, \mu_F^2) = \sum_{i=0}^{\infty} a_s^i(\mu_R^2) d\hat{\sigma}_{ab}^{(i)}(z, \mu_F^2, \mu_R^2) , \quad (5.4)$$

where the coupling constant satisfies standard renormalization group equation. Since we are only interested in the NLO order corrections, the Altarelli-Parisi kernels $P^{(0)}(z)$, $P^{(1)}(z)$ and the coefficients β_0, β_1 are sufficient for our analysis. The scale uncertainties come about from the truncation of the perturbative series. Unlike the perturbatively calculable partonic cross sections, the PDFs being non-perturbative in nature

are extracted from various experiments. These are fitted at a scale of the experiments and then evolved according to the AP evolution equations to any other relevant scale. They are not only sensitive to experimental errors but also to theoretical uncertainties that enter through the partonic cross section calculations and the splitting functions that are known only to certain orders in strong coupling constant in perturbative QCD. Here, we mainly concentrate on the uncertainties coming from PDFs in detail and quantify their impact on the new physics searches in extra dimensional models.

5.4.1 PDF uncertainty

In this section we focus on the uncertainties coming from different PDF sets. The information of the PDFs enters the hadronic cross sections through parton fluxes. The parton flux factor is given by

$$\Phi_{ab}(\tau) = \int_{\tau}^1 \frac{dx}{x} f_a(x, \mu_F) f_b\left(\frac{\tau}{x}, \mu_F\right) \quad (5.5)$$

where $\tau = Q^2/S$, Q is the invariant mass of the pair of leptons and S is the center of mass energy of the incoming hadrons. $f_a(x_a, \mu_F)$ and $f_b(x_b, \mu_F)$ are the parton distribution functions of the incoming hadrons P_a and P_b . The $q\bar{q}$, qg and gg parton fluxes at both the LHC and the Tevatron would give an idea as to which component would be dominant in the kinematical region of interest. At the LHC, owing to a very high center of mass energy of $\sqrt{S} = 14$ TeV, it is possible to probe high Q values and hence in our study we have taken a maximum of Q upto 3000 GeV, whereas at the Tevatron it is taken upto only 1100 GeV because of low center of mass energy of $\sqrt{S} = 1.96$ TeV at the Tevatron. This flux factor that enters the hadronic cross sections is computed with MRST parton density sets and is shown in fig.(5.2) for both LHC and Tevatron. The gluon flux is clearly much larger in the kinematical region of interest ($Q < 1000$ GeV) at the LHC and for the Tevatron the $q\bar{q}$ flux is the dominant contribution. Hence any uncertainty in the gluon distribution functions would have a significant impact on the physical observables used to probe the new physics.

The dilepton in the extra dimension models could also be produced from the exchange of a KK mode in addition to the usual SM gauge boson exchange. Also, at LO itself the gg subprocess could contribute in addition to the $q\bar{q}$ subprocess as the gravity couples with equal strength to both quarks and gluons. However, as the gluon flux is higher than the $q\bar{q}$ flux at the LHC, the gg initiated subprocess has the dominant contribution while at the Tevatron the $q\bar{q}$ flux is higher than gg flux and so is the $q\bar{q}$ initiated subprocess. These parton fluxes are thus crucial in predicting the cross sections and any uncertainty in them coming from the choice of the PDFs, would then translate into the uncertainties in the hadronic cross sections. In our analysis, we have used three different parton density sets parametrized by Alekhin [71], CTEQ [60] and MRST [72] groups.

These groups perform a global analysis of a wide range of DIS and other scattering data to get best fits to a particular order in QCD. Though all these parametrization satisfies the general constraints, they could differ from each other. This is expected as PDFs are not by themselves physical quantities and are extracted subject to experimental and theoretical uncertainties and various assumptions and initial conditions used by the different groups. Differences among various PDFs would translate as uncertainties on the physical observable.

To NLO in QCD for various PDFs, we now present the comparison plots for the following differential distributions

$$\frac{d\sigma}{dQ}, \quad \frac{d^2\sigma}{dQ dY}, \quad \frac{d^2\sigma}{dQ d\cos\theta^*}. \quad (5.6)$$

We would look at the invariant mass distribution Q , the double differential cross section with respect to Q and rapidity Y and the double differential cross section with respect to Q and $\cos\theta^*$. As the detailed expressions for these cross sections are available in [45–47], in the present work we restrict ourselves to the numerical results of these distributions and concentrate directly on studying the relevant uncertainties in them. The angle θ^* is the angle between the final state lepton momenta and the initial state hadron momenta in the *c.o.m* frame of the lepton pair. The corresponding

K-factor which is the ratio of NLO to LO of the above distributions are also plotted for various PDFs. For the double differential cross section we fix the invariant mass Q in the region of interest of extra dimensions and plot the cross section with respect to rapidity Y and $\cos \theta^*$. The first two distributions in Eq. (5.6) are $\cos \theta^*$ integrated distributions and hence are independent of the interference between the SM background and the low scale gravity effects [45]. The double differential with respect to Q and $\cos \theta^*$ would contain the interference terms, but numerically it is not very significant [47]. Consequently even for the $\cos \theta^*$ distributions we can express the K factor of the model involving both SM and gravity as

$$K^{(SM+GR)}(Q) = \frac{K^{SM} + K^{GR}K^{(0)}}{1 + K^{(0)}} , \quad (5.7)$$

where K^{GR} is the K factor of the pure gravity part. We have introduced a quantity $K^{(0)}$, defined as the ratio of the LO distribution of gravity to SM, given by

$$K^{(0)}(Q) = \left[\frac{d\sigma_{LO}^{SM}(Q)}{dQ} \right]^{-1} \left[\frac{d\sigma_{LO}^{GR}(Q)}{dQ} \right] . \quad (5.8)$$

The behaviour of $K^{(0)}(Q)$ is governed by the competing coupling constants of SM and gravity and the parton fluxes involved. Basically the factor $K^{(0)}$ is an indicator as to the source of the total $K^{(SM+GR)}$ -factor. $K^{(0)}(Q)$ as a function of Q rises much faster for LHC than Tevatron and reaches 1 much earlier. Since the gg subprocess contributes at LO itself for the gravity mediated process, the gravity effects are much larger at the LHC where the gluon flux is much larger. This would also result in larger K-factor for the process at the LHC at large Q where the gravity contribution dominates. At Tevatron since the gluon flux is smaller the K-factor is similar to the SM K-factor. For both ADD and RS models the signal for new physics is the excess of events in the total cross section or various distribution over the SM background. If we restrict ourselves to these extra dimensional models, the signal is due to the effect of the KK modes and can not be mimicked by the SM. We would like to emphasize that we are not analyzing the existing Tevatron data to extract bounds on the ADD and RS parameters, which would need a full hadron-level simulation, but estimate various uncertainties to NLO

in QCD by choosing typical representative values for the ADD and RS parameters. We begin with the ADD model wherein we have chosen $d = 3$ and $M_S = 2$ TeV. In Fig. 5.3a the cross section is plotted as a function of the invariant mass Q of the dilepton at the LHC for various PDFs. There is only a mild dependence on the difference in the PDFs, but when plotted for the corresponding K-factor then the PDF dependence is larger for both low and high values of Q , Fig. 5.3b. At low Q it is the SM part which contributes to the K-factor while at high Q it is the beyond SM effects that contribute. At low Q where the K-factor is due to SM part, MRST and CTEQ are similar, while Alekhin is smaller. At large Q the K-factor is due to the gravity part and here CTEQ is larger.

For the double differential cross section with respect to invariant mass distribution and rapidity Y Fig. 5.4a, we have plotted as a function of rapidity Y for a fixed $Q = 0.7$ TeV. Only in the central rapidity region do the PDFs differ, with MRST being the dominant while CTEQ is the smallest. The K-factor is quite large at the central rapidity region and would range from 1.5 - 1.6 depending on the PDF set used. The general behaviour of the K-factor is similar for MRST and Alekhin. At large rapidities $y = \pm 2$ the K-factors are quite different with Alekhin being 1.25 while CTEQ the largest is 1.45. For $Q = 0.7$ TeV the K factor is large which we can see from Fig. 5.3b, wherein the dominant contribution is from the gravity mediated gg initiated subprocess.

In Fig. 5.4c we have plotted the double differential cross section with respect to Q and $\cos \theta^*$ as a function of $\cos \theta^*$ for a fixed $Q = 0.7$ TeV. MRST gives the largest and CTEQ the least with Alekhin being a central value in the spread. The difference exists for the full range of $\cos \theta^*$. The SM background has a different $\cos \theta^*$ dependence. The interference of the SM and the gravity effect is not zero for the $\cos \theta^*$ distribution but does not contribute significantly. The K-factor for central $\cos \theta^* = 0$ region is about 1.52 but differ with PDFs as $\cos \theta^* \rightarrow \pm 1$, Fig. 5.4d. Since there is no gg initiated process in the SM background to NLO the K-factor is much smaller.

In the RS model we have chosen the mass of the first KK mode $M_1 = 1.5$ TeV and the coupling $c_0 = 0.01$. In Fig. 5.5a we have plotted invariant mass distribution of the

dilepton in the RS model. At the KK mode resonances the cross section differs from the SM cross section, but the dependence on the PDFs are very mild. In Fig. 5.5b the corresponding K-factors are plotted for various PDFs. The behaviour of the K-factor of the RS model can be understood with the help of Eq. (5.7,5.8). It is only in the RS graviton resonances region that $K^{(0)}$ is large and hence the K-factor is dominated by the K^{GR} factor. In the off resonance regions it is the K^{SM} which contributes. There is a wide difference in the K-factor more in the second peak and even off peak where the effect is mainly SM. This is due to the high Q value that is chosen in the RS case.

For the double differential with respect to rapidity and invariant mass, in Fig. 5.6a we have plotted it for the rapidity range of LHC for $Q = 1.5$ TeV, which is the region of the first RS KK mode. It is only in the resonance region that the effects of RS are visible. Here there seems to be a clustering of PDFs but for CTEQ in the central rapidity region. In the central rapidity region the K-factor varies from 1.6 - 1.75 Fig. 5.6b. In the first RS KK resonance region at $Q = 1.5$ TeV the gravity dominates and hence the K-factor is large (Eq. (5.7)). Beyond the central rapidity region $Y = 0$ the K-factor dependence on PDFs is substantial. In Fig. 5.6c we have plotted the double differential with respect to $\cos \theta^*$ for Q fixed at the first resonance. The cross section is largest for $\cos \theta^* = 0$ and MRST is the largest among the PDFs. The K-factor in Fig. 5.6d is about 1.65 for wide range of $\cos \theta^*$ for Alekhin and MRST but for CTEQ it varies between 1.7 - 1.8.

In the above we discussed the extra dimension effects at the LHC, now we look at the Tevatron. For the ADD case, in Fig. 5.7a we have plotted the invariant mass distribution for various PDFs. The spread due to various PDFs over the Q^2 range is not too large. Only at large Q there is some deviation from the SM result which is plotted in Fig. 5.7a. The K-factor for the Q distribution for various PDFs are plotted in Fig. 5.7b, which are in tune with the SM K-factor at the Tevatron. In Fig. 5.7c we have plotted the PDF comparison plot for the rapidity distribution at $Q = 0.7$ TeV. CTEQ and MRST plots are very similar while Alekhin is larger in the central rapidity region. In the $Y = 0$ region, the K-factor for CTEQ is about 1.1 while for MRST and Alekhin it

is about 1.2, which is in the range of the SM K-factor, Fig. 5.7d.

For the RS model the PDF comparison plots are given in Fig. 5.8. In Fig. 5.8a we have the invariant mass distribution and the deviation from the SM is only in the resonance region. The PDF dependence is very mild. In the first resonance region the K-factor (Fig. 5.8b) is dominated by K^{GR} at $Q = 0.7$ TeV but at Tevatron this value is not too different from the SM K-factor. In Fig. 5.8c the $\cos \theta^*$ distribution at the first resonance region is plotted, CTEQ and MRST overlap while Alekhin is larger over a wide range of $\cos \theta^*$. The K-factor Fig. 5.8d is in the range of the SM K-factor.

5.4.2 Renormalization/Factorization scale uncertainties

In Fig. 5.9a we have plotted the double differential $d^2\sigma/dQdY$ in the Y range for LHC energies for a fixed $Q = 0.7$ TeV. The dependence of cross section on μ_R comes from the strong coupling constant at NLO and so at LO there is no μ_R dependence. At NLO μ_R dependence for the Y distribution is plotted for the μ_R range $0.5 Q \leq \mu_R \leq 1.5 Q$. The μ_R spread is largest in the central rapidity region and would only reduce at the NNLO order level when the μ_R dependencies would be compensated for by the dependence coming from the coefficient functions. In Fig. 5.9b we have plotted the K-factor for SM and SM+GR and see how it dependence on μ_R . The uncertainties due to μ_R is much larger when the gravity is included. The percentage spread is of the order of 3.5 % which is comparable to the μ_F spread at NLO.

In Fig. 5.10 we have plotted Y distribution and its K-factor for ADD and RS model at a fixed $Q = \mu_R$. The μ_F variation is studied by varying μ_F in the range $0.5 Q \leq \mu_F \leq 1.5 Q$. We see that for both the ADD and RS model in going from LO to NLO in QCD, the uncertainties due to μ_F variation considerably get reduced. The spread of K-factor with μ_F is much smaller for the SM as compared to SM+GR. This certainly indicates need to go beyond NLO. Similar trends are observed for the $\cos \theta^*$ distribution plotted in Fig. 5.11.

In Table 5.1 we tabulate the percentage spread of the factorization scale μ_F depen-

	Distributions	Tevatron		LHC	
		LO	NLO	LO	NLO
ADD	$d^2\sigma/dQdY$	22.8	7.4	9.5	3.5
	$d^2\sigma/dQd\cos\theta$	24.2	8.2	10.9	3.8
RS	$d^2\sigma/dQdY$	23.2	7.7	18.7	6.9
	$d^2\sigma/dQd\cos\theta$	24.2	8.0	18.4	6.8

Table 5.1: Percentage spread as a result of factorization scale variation in the range $0.5Q \leq \mu_F \leq 1.5Q$. For the ADD case $Q = 0.7$ TeV. For the RS first resonance region $Q = 1.5$ TeV for LHC and $Q = 0.7$ TeV for Tevatron.

dence in the range $0.5Q \leq \mu_F \leq 1.5Q$ for the LHC and Tevatron. On the average at the LHC and Tevatron, the percentage spread of the scale variation get reduced by about 2.75 times in going from LO to NLO.

5.5 Experimental Uncertainties

In addition to the theoretical uncertainties that we have described in the previous section, there are uncertainties due to errors on the data. Various groups have studied the experimental errors and have estimates of the uncertainties on the PDFs within NLO QCD framework [73, 74]. Now that NLO QCD results are also available for extra dimension searches [45] for the dilepton production, we consider some of the distributions and estimate the uncertainties due to the experimental error. In Fig. 5.12a we have plotted the error band for the MRST 2001 PDF [74] in the ADD model for the dilepton invariant mass distribution at the LHC. This error band is comparable to the spread associated with the different set of PDFs as given in Fig. 5.3a. At $Q = 1$ TeV the percentage of experimental error is 7.5 % for $SM + GR$ while the pure SM error

is about 3.3 %. For the RS case at the LHC in the first resonance region at $Q = 1.5$ TeV the experimental error is about 12.8 %. At Tevatron the ADD model experimental error is 7.4 % at $Q = 1$ TeV. The experimental error for this distribution for the central rapidity region is about 3.5 % and is indicated in the Fig. 5.12b. In general the experimental error increases with the increase in Q .

5.6 Conclusions

We have studied the impact of various parton density sets at next to leading order in strong coupling constant α_s in QCD on one of the most important processes, namely Drell-Yan production of dileptons at hadron colliders such as LHC and Tevatron. This process can probe the physics beyond SM through exchange of new particles that these theories predict. At hadron colliders, the precise measurement of DY production cross sections is possible. In this context, we have studied the theories of extra dimensions such as ADD and RS which attempt to explain gauge hierarchy problem in SM. We have discussed various theoretical uncertainties that enter through renormalisation, factorisation scales and the parton density sets. We have quantified the uncertainties coming from various parton density sets using the recent results on NLO QCD corrections to parton level cross sections and recent PDF sets that take into account various theoretical and experimental errors. Our entire analysis is model independent thanks to the factorisation of QCD radiative corrections from the model dependent contributions. More precisely, our findings are independent of the finer details of the model as they factor out from the rest. We find that the K-factor for various observable depends on the choice of PDFs.

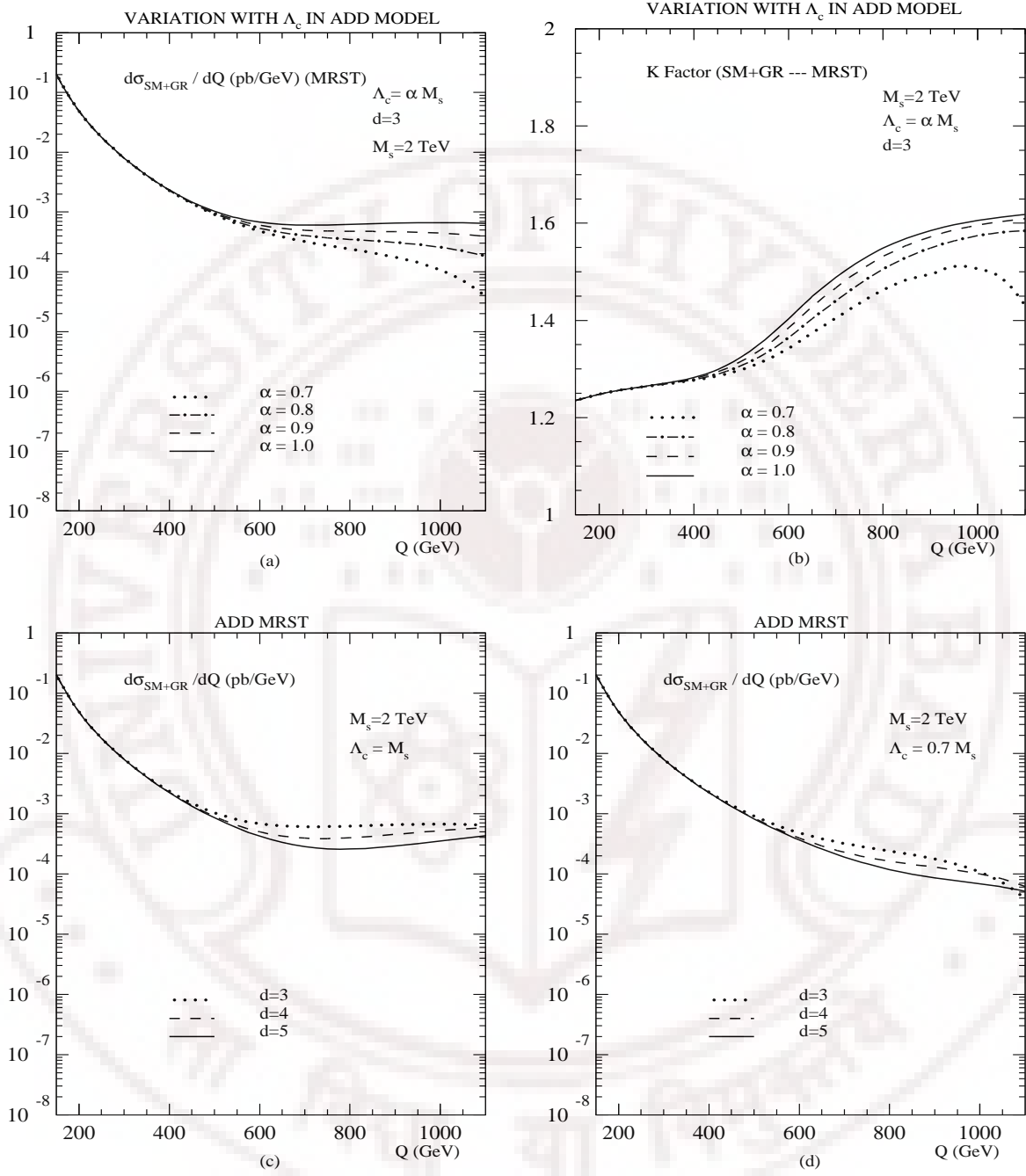


Figure 5.1: (a) Invariant mass distribution is plotted for various values of the cutoff $\Lambda_c = \alpha M_s$ in the ADD model. (b) The corresponding K-factor. (c) Invariant mass distribution as a function of the number of extra spacial dimension d for $\Lambda_c = M_s$ TeV at the LHC. (d) The same plot as (c) for $\Lambda_c = 0.7 M_s$.

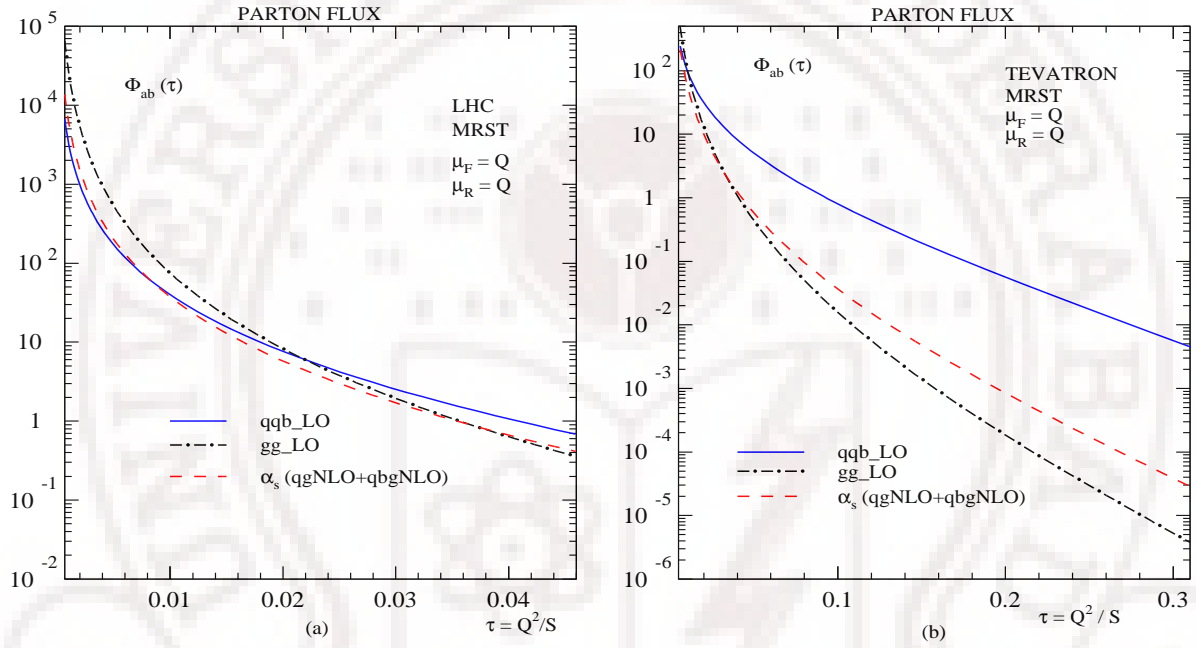


Figure 5.2: The parton fluxes as a function of $\tau = Q^2/S$ for both LHC (left) and Tevatron (right). We have considered the invariant mass $360 \leq Q \leq 3000$ GeV for the LHC, and $150 \leq Q \leq 1100$ GeV for the Tevatron. Both the factorization scale and the renormalization scales are set equal to Q .

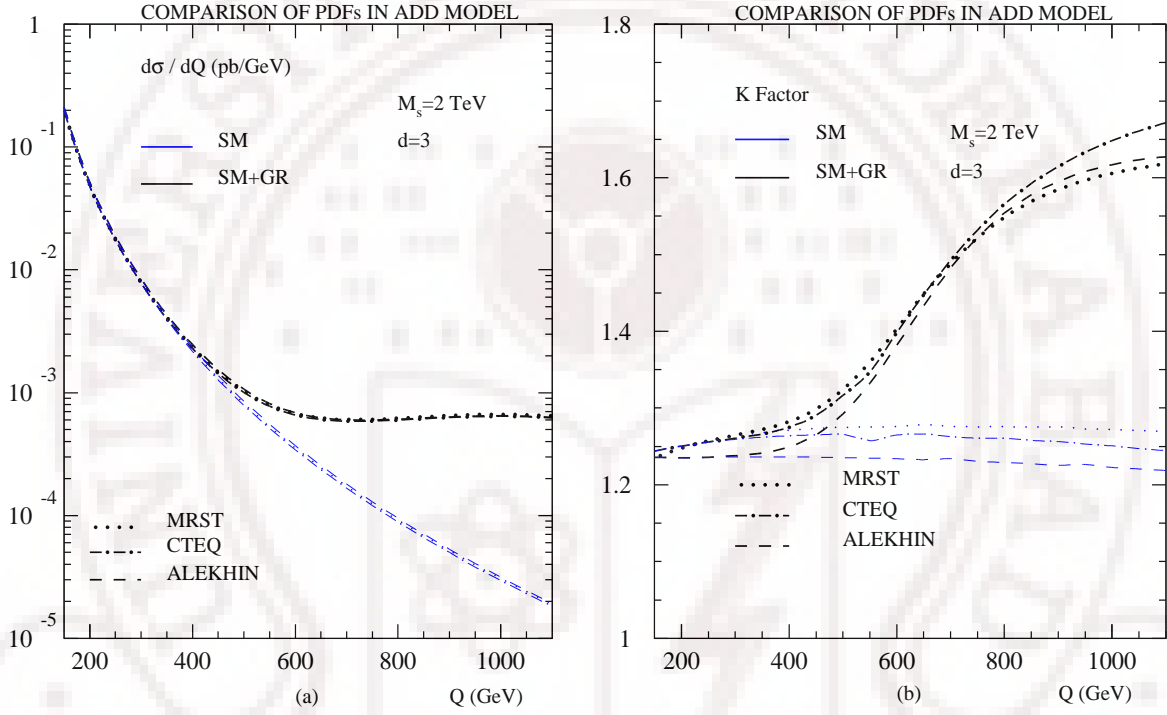


Figure 5.3: (a) Invariant mass distribution of the dilepton pair for ADD model with different PDFs to NLO in QCD. (b) The corresponding K-factor for various PDFs. In both (a) and (b) the blue (light) colour curves correspond to the SM while the black (dark) colour correspond to the signal.

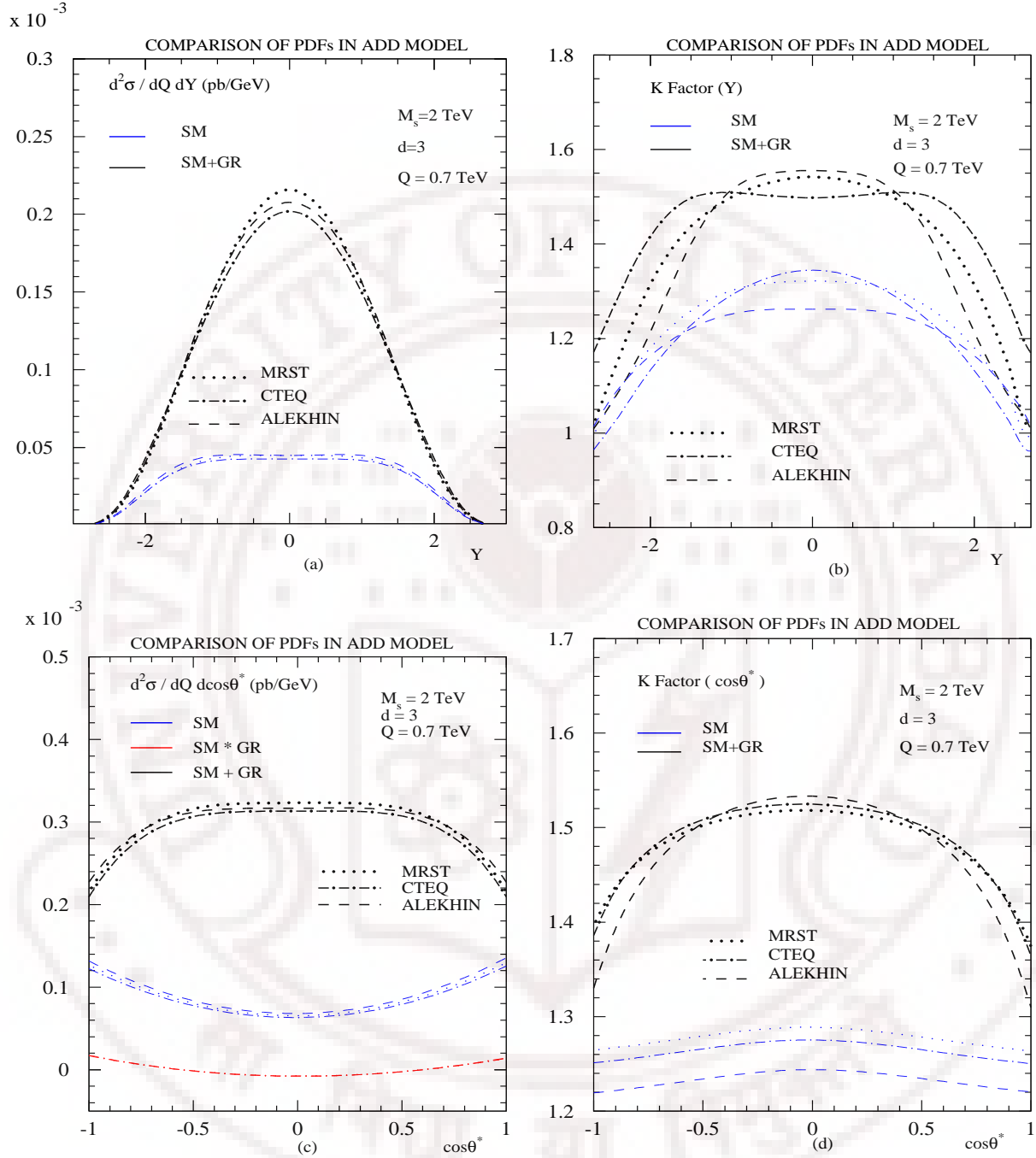


Figure 5.4: The comparison plots for various PDF sets for $Q = 0.7$ TeV at LHC. (a) The double differential cross section with respect to invariant mass and rapidity as a function of rapidity. (b) The corresponding K-factor as a function of rapidity. (c) The angular distribution of the double differential cross section with respect to invariant mass and $\cos\theta^*$. The interference of the SM background and gravity effects is also plotted. (d) The corresponding K-factor.

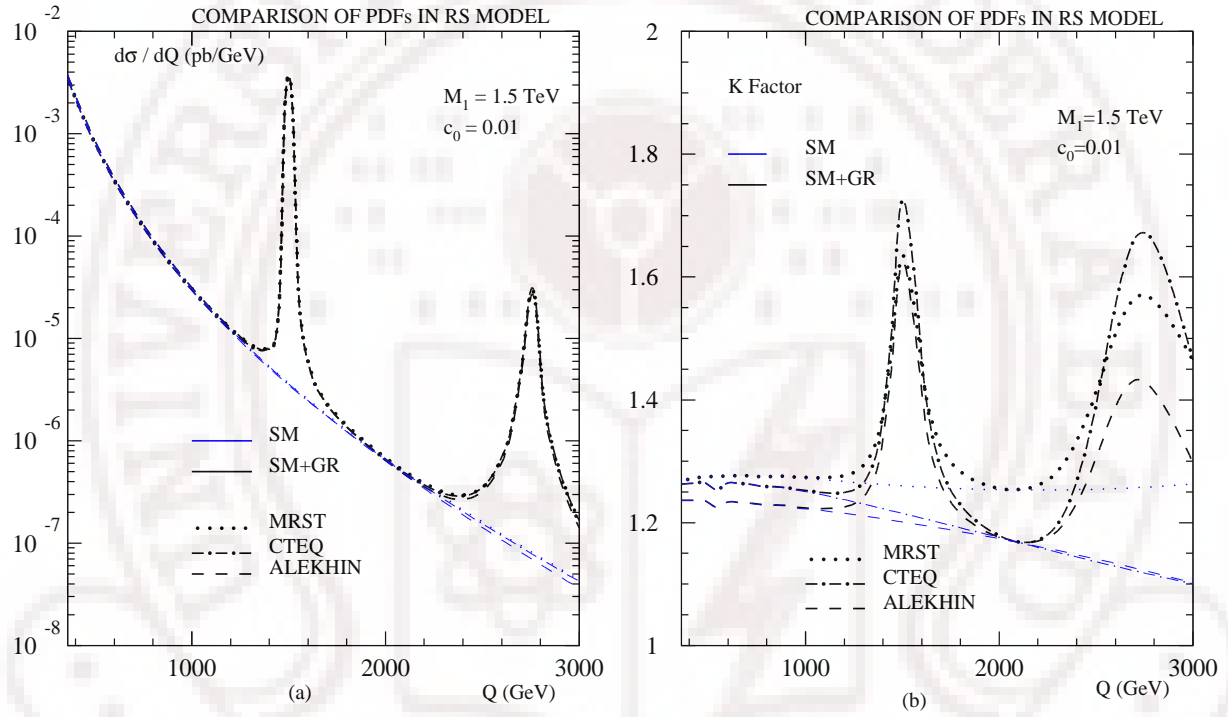


Figure 5.5: (a) The invariant mass distribution of dilepton pair production at the LHC in the RS model for various PDFs. (b) The corresponding K-factor for various PDFs.

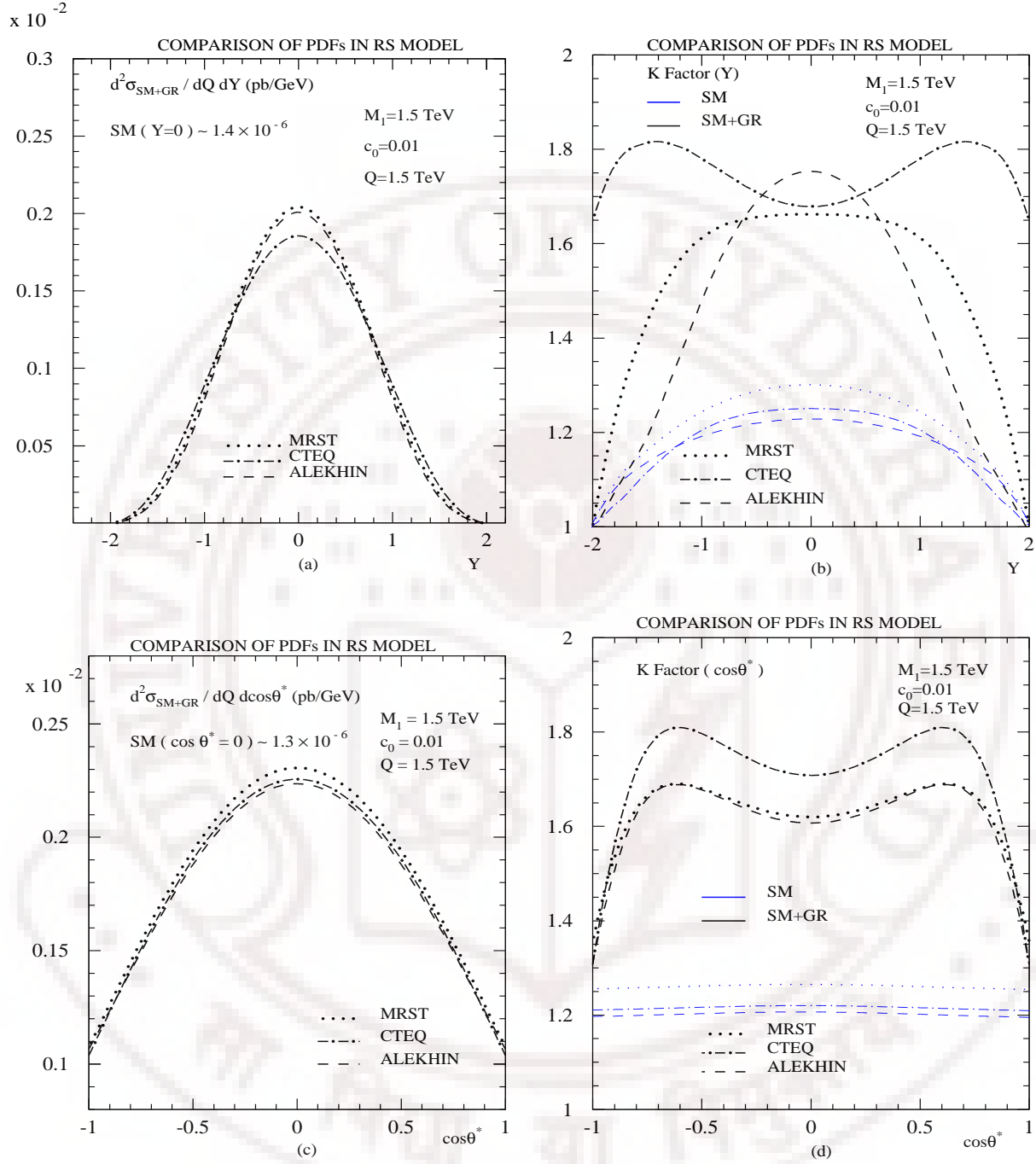


Figure 5.6: (a) The double differential cross section with respect invariant mass and rapidity for various PDFs in the RS model at $Q = 1.5 \text{ TeV}$, the region of first resonance. (b) The corresponding K-factor as function of rapidity at $Q = 1.5 \text{ TeV}$. (c) In the region of first RS resonance, the double differential with respect to invariant mass and angular distribution of the lepton is plotted for various PDFs at the LHC. (d) The corresponding K-factor for the various PDFs.

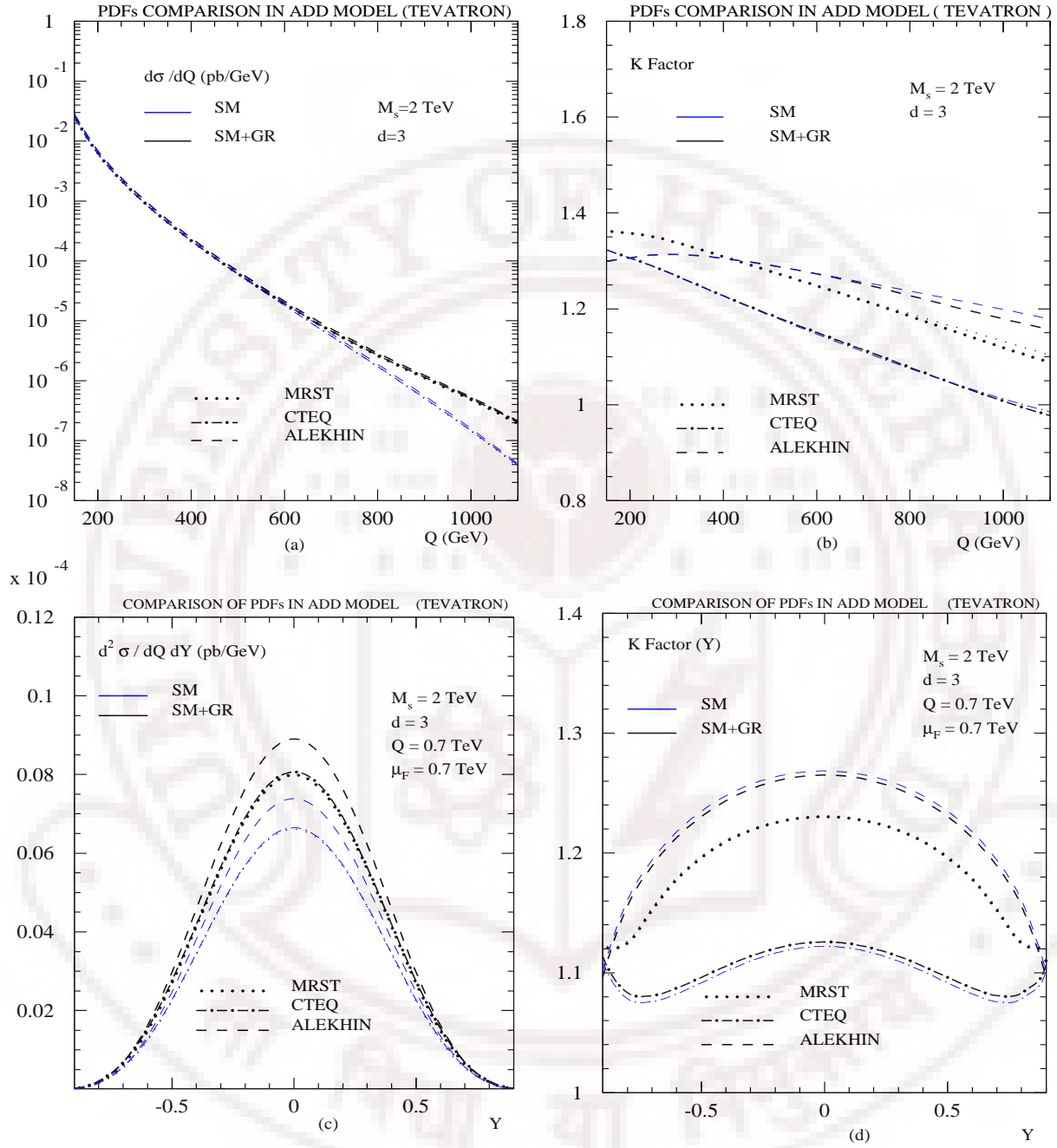


Figure 5.7: ADD model at Tevatron for various PDF sets, we plot in (a) the invariant mass distribution. In (b) the corresponding K-factor. (c) The double differential with respect to Q and Y is plotted for a fixed $Q = 0.7$ TeV and for the Y range of Tevatron. In (d) the corresponding K factor is plotted.

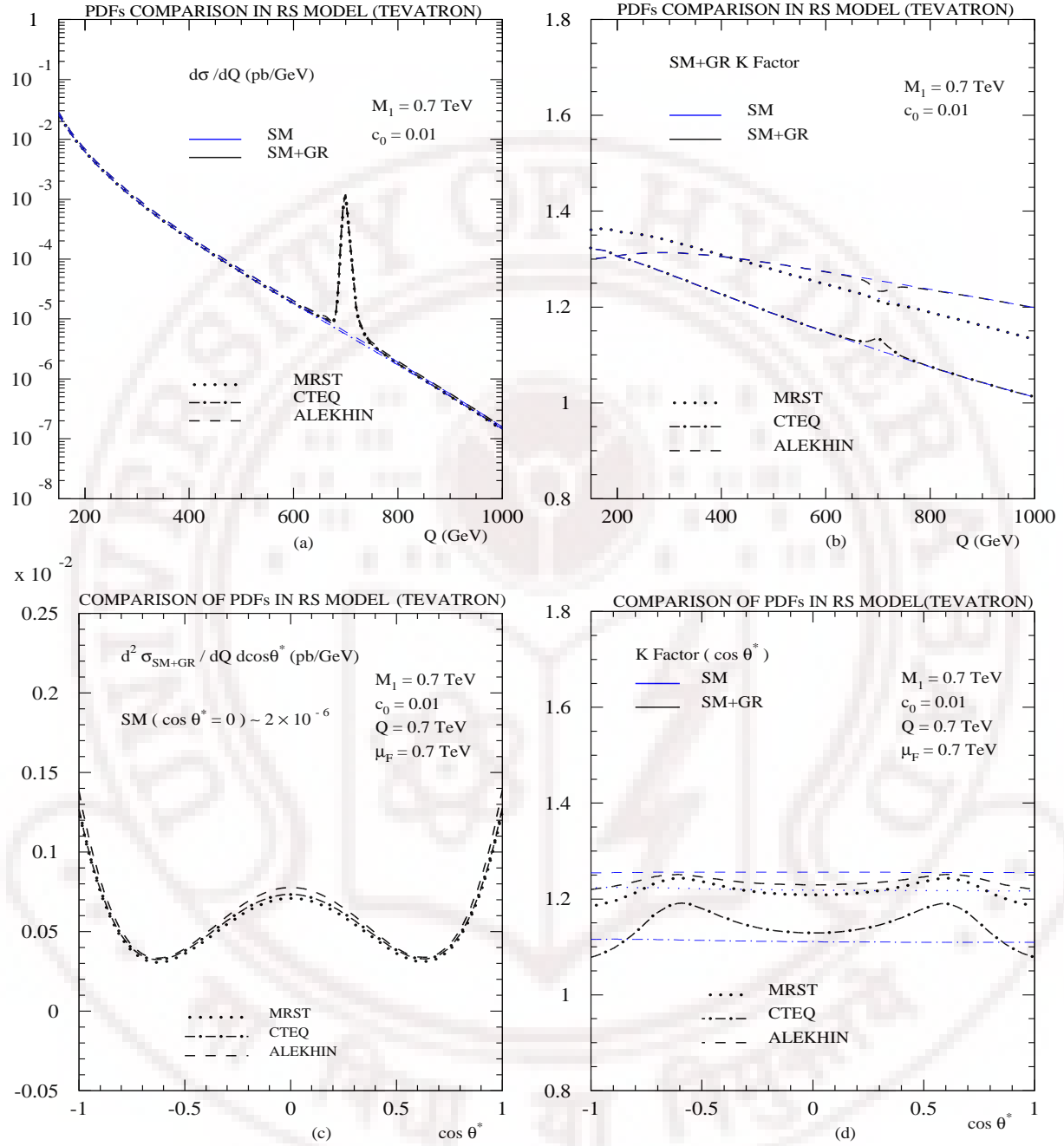


Figure 5.8: RS model at Tevatron for various PDF sets, we plot in (a) the invariant mass distribution. In (b) the corresponding K-factor. (c) The double differential with respect to Q and $\cos\theta^*$ is plotted for a fixed $Q = 0.7$ TeV and for the $\cos\theta^*$. In (d) the corresponding K factor is plotted.

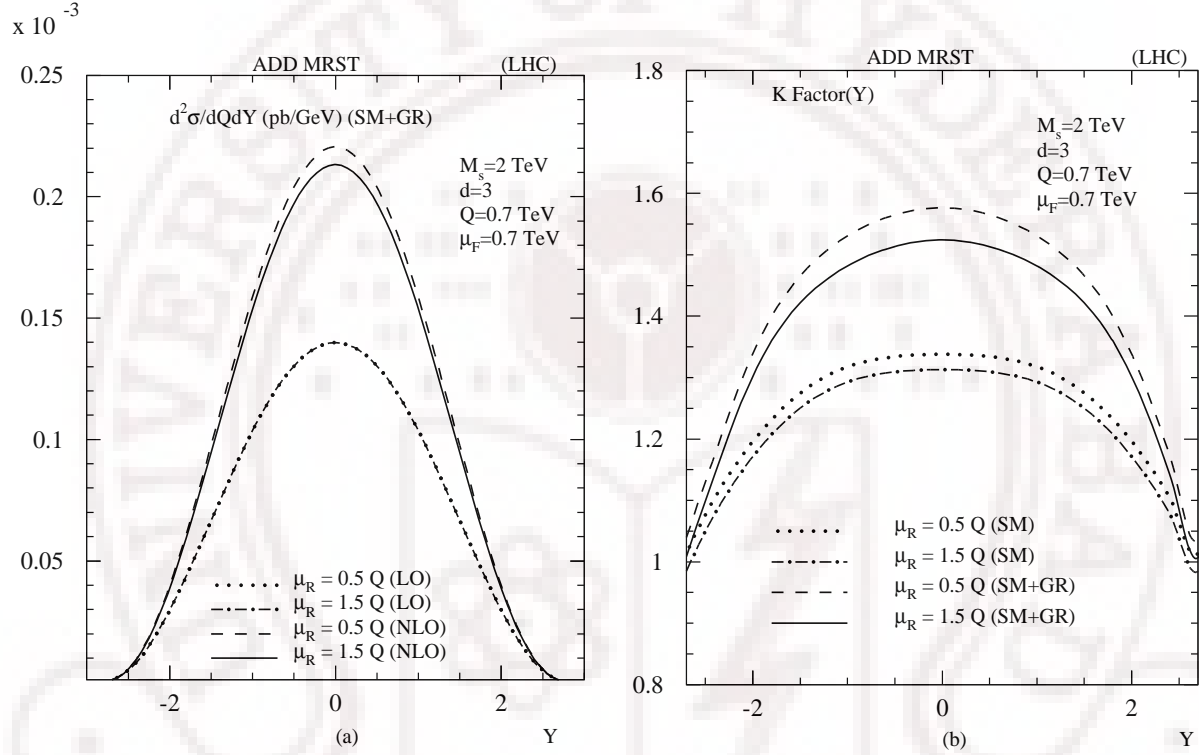


Figure 5.9: The renormalisation scale dependence for double differential cross section as a function of rapidity for $Q = 0.7 \text{ TeV}$. The PDF set used is MRST and the renormalisation scale is varied in the range $\mu_R = 0.5 Q - 1.5 Q$ for LO and NLO. (b) The K-factor dependence on μ_R for both SM and SM+GR.

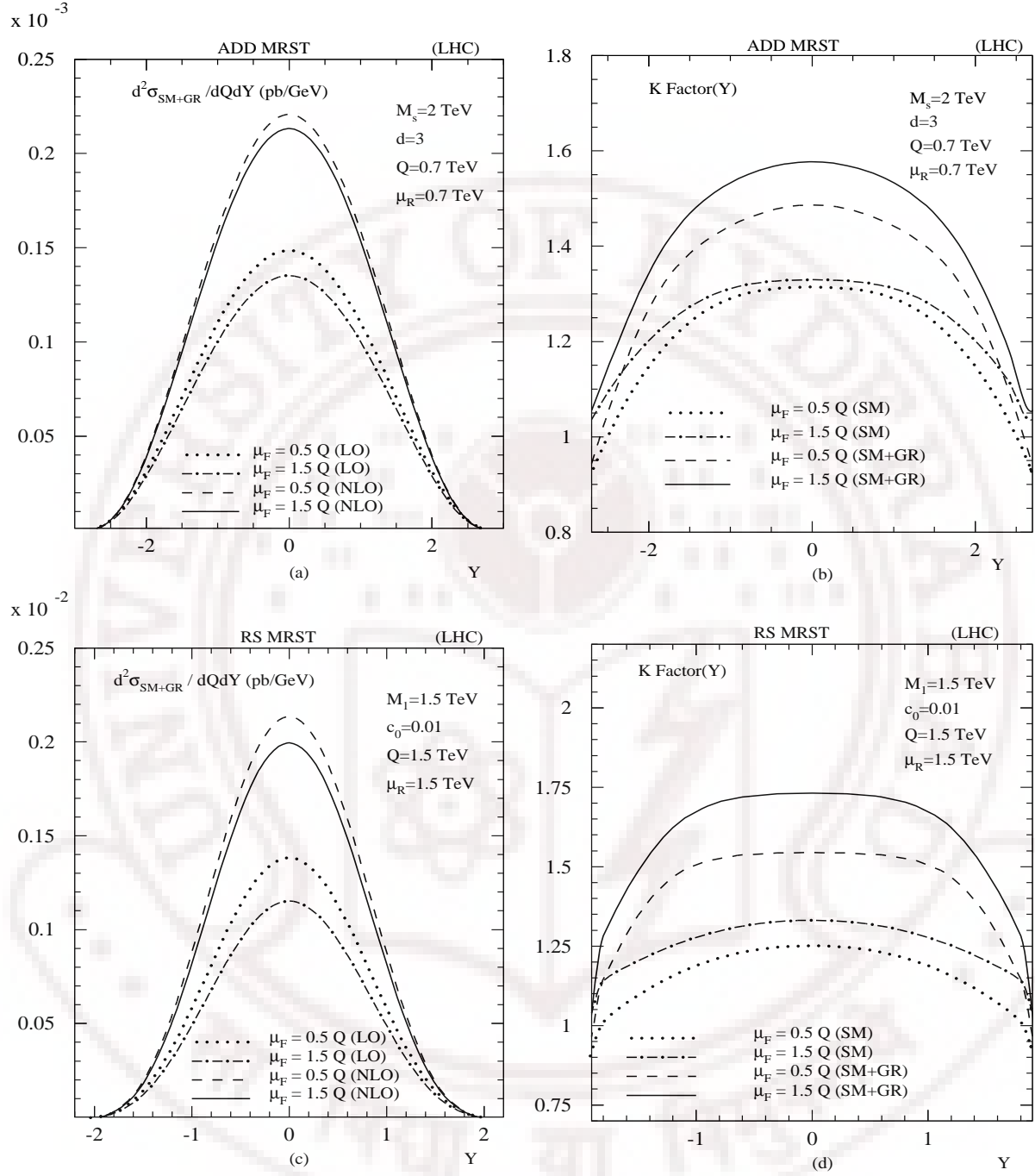


Figure 5.10: (a) Factorisation scale dependence for the double differential cross section as a function of rapidity for LO and NLO for factorisation scale in the range $\mu_F = 0.5 Q - 1.5 Q$. (b) SM and SM+GR K factor for ADD rapidity distribution in the same variation of μ_F . In (c) the RS distribution at $Q = \mu_R = 1.5$ TeV in the region of first resonance. (d) The SM and SM+GR K factor for RS rapidity distribution.

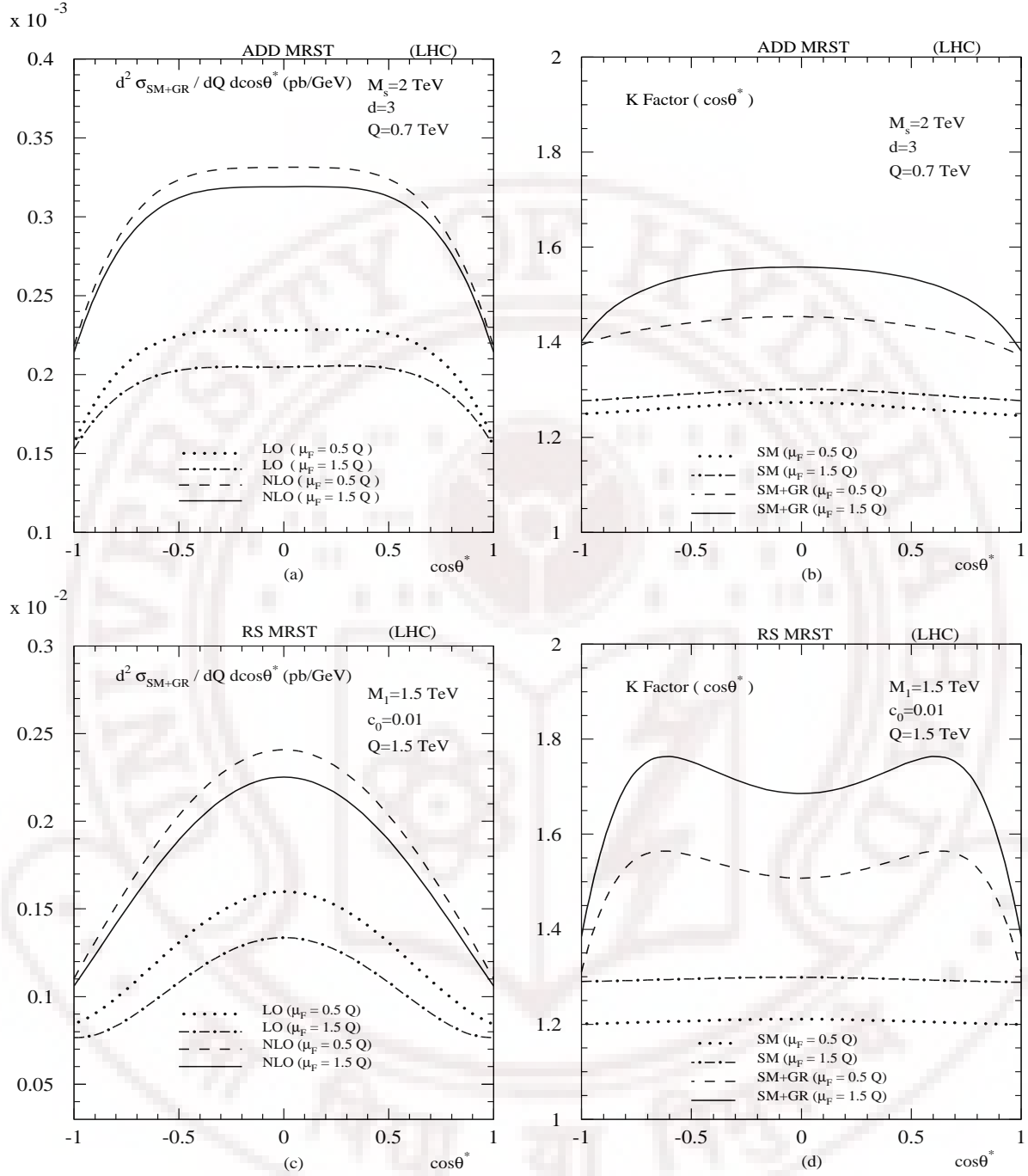


Figure 5.11: (a) Factorisation scale dependence for the double differential cross section as a function of $\cos\theta^*$ for LO and NLO for factorisation scale in the range $\mu_F = 0.5 Q - 1.5 Q$. In (b) we have plotted the SM and SM+GR K factor for ADD at $Q = \mu_R = 0.7$ TeV. In (c) the RS $\cos\theta^*$ distribution for LO and NLO in the same range of μ_F . (d) The SM and SM+GR K-factor at $Q = \mu_R = 1.5$ TeV, the region of first resonance.

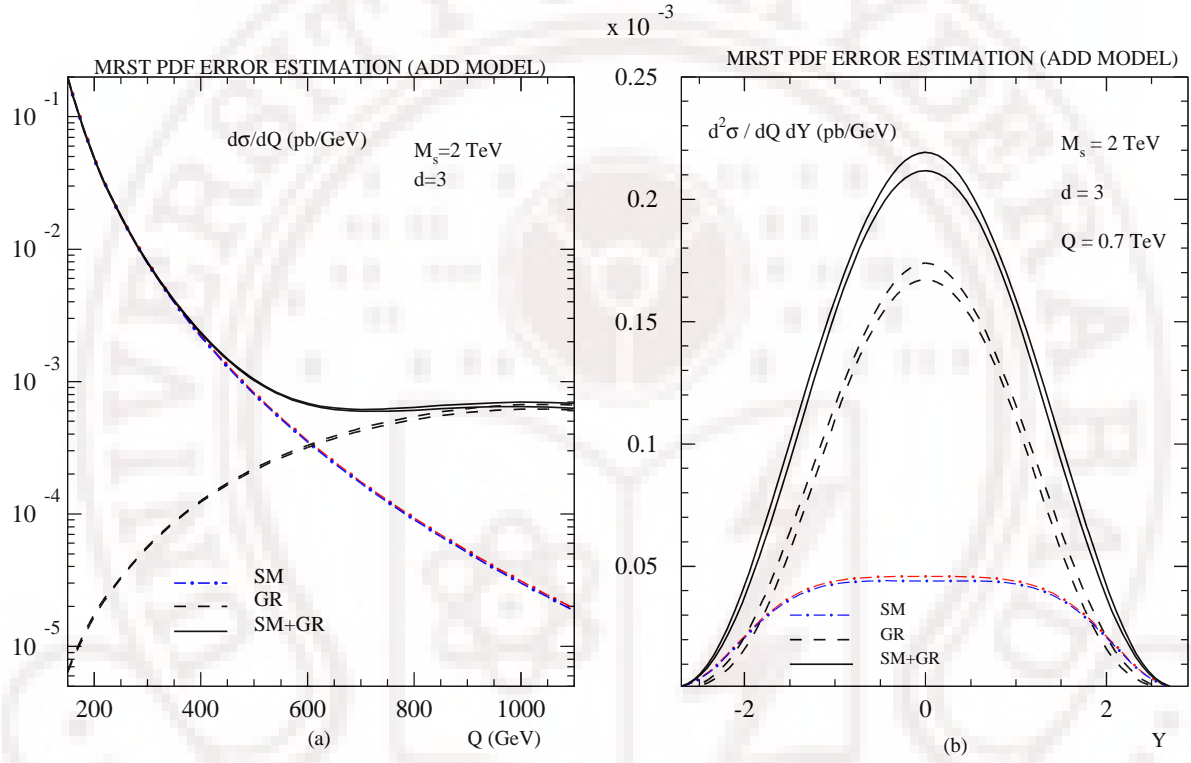


Figure 5.12: The experimental error on the MRST PDF set at the LHC in the ADD model for (a) The invariant mass distribution and (b) The rapidity distribution for a fixed $Q = 0.7$ TeV.

Chapter 6

Di-jet production at the LHC through unparticles

The LHC can provide a testing ground for physics of unparticles if Λ_u is of the order of a TeV. There are various important channels available at LHC to explore the new physics at TeV scales, namely production of di-leptons, isolated photon pairs, di-jets etc. The importance of di-lepton and di-photon production channels in the context of unparticles were already studied in detail in [81] and [82, 83] respectively. Here we will study the effects of scalar and spin-2 unparticles on the di-jet production rates at the LHC if the scale Λ_u is of the order of a TeV. Di-jet production is an important discovery mode and many studies in the context of various new physics scenarios have been carried out, namely, SUSY searches [84], searches of the low mass strings [85]. In [86–88], di-jet production has been used to probe spin-2 Kaluza-Klein gravitons appearing in the extra dimensional models.

To lowest order in strong coupling constant the di-jets arise from $2 \rightarrow 2$ scattering of partons as given by

$$a(p_1) + b(p_2) \rightarrow c(p_3) + d(p_4) \quad (6.1)$$

where p_1, p_2 are the incoming parton momenta and p_3, p_4 are momenta of the outgoing partons. The partons in the final state then hadronize to give two jets at the detector level. Signals of new physics can be discovered because of the deviations they pro-

duce over the SM contributions. The unparticles can contribute through intermediate states as well as via real emission. The former one can interfere with the SM contributions, while the later can lead to missing energy in the final state. In the present work we will restrict ourselves to the case where the spin-0 and spin-2 unparticles appear at the intermediate states.

6.1 SM contribution

The parton level $2 \rightarrow 2$ subprocesses that can contribute to the dijet production process in the SM as well as in the unparticle scenario are

$$\begin{array}{lll}
 qq' \rightarrow qq' & qq \rightarrow qq & q\bar{q} \rightarrow q\bar{q} \\
 q\bar{q} \rightarrow q'\bar{q}' & q\bar{q} \rightarrow gg & gg \rightarrow q\bar{q} \\
 qg \rightarrow qg & gg \rightarrow gg &
 \end{array}$$

Here we have used primes to distinguish quark flavours.

The leading order SM matrix elements are of order g_s^2 , where g_s is the strong coupling constant and those in the unparticle model are of order κ^2 , where $\kappa = \lambda_t/\Lambda_u^{d_t}$, $\lambda_{s1}/4\Lambda_u^{d_s}$, $\lambda_{s2}/\Lambda_u^{d_s-1}$. The matrix element square takes the following form:

$$g_s^4 |\mathcal{M}_{SM}|^2 + \kappa^4 |\mathcal{M}_u|^2 + g_s^2 \kappa^2 (\mathcal{M}_{SM} \mathcal{M}_u^* + \mathcal{M}_{SM}^* \mathcal{M}_u)$$

where the interference of SM with the unparticle mediated processes will be sensitive to phase coming from $(-k^2)^d$ in the propagators given in eqn.(2.39,2.41). In the table (6.1), we list the matrix elements square, summed (averaged) over final (initial) state colors and spins, for SU(N) gauge theory with fermions in the fundamental representation. The SM ones agree with those existing in the literature [89]. We have not listed the subprocesses such as $\bar{q}\bar{q} \rightarrow \bar{q}\bar{q}$, $\bar{q}\bar{q}' \rightarrow \bar{q}\bar{q}'$ and $\bar{q}g \rightarrow \bar{q}g$ as they can be obtained from the rest using charge conjugation. Henceforth, we do not list them in the rest of the article. In addition, the process $\bar{q}q' \rightarrow \bar{q}q'$ is obtained from $qq' \rightarrow qq'$ through crossing.

6.2 Unparticle contribution

For the scalar case, not all of the above processes contribute. The first term in (2.36) describes the coupling of gauge fields to scalar unparticles giving $gg \rightarrow gg$ process. The second term couples fermions to scalar unparticles, which allows subprocesses which have only fermions in the initial and the final states. We shall study the effects of these two terms in (2.36) separately.

The matrix elements for pure unparticle contribution and interference with SM for spin-0 coupling through first term in (2.36) are given below (see eqn.(6.3)). Here only $gg \rightarrow gg$ contributes. The factor $(-k^2)^{d-2}$ in propagators is complex for a s -channel propagator and is real for u - and t -channel propagators.

$$|\mathcal{M}_u|^2 \stackrel{gg \rightarrow gg}{=} \frac{1}{16(N^2 - 1)} \left(\mathcal{D}_u \text{Re}(\mathcal{D}_s) s^2 u^2 + \mathcal{D}_t \text{Re}(\mathcal{D}_s) s^2 t^2 + \mathcal{D}_t \mathcal{D}_u t^2 u^2 \right) + \frac{1}{16} (\mathcal{D}_u^2 u^4 + \mathcal{D}_t^2 t^4 + |\mathcal{D}_s|^2 s^4) \quad (6.2)$$

$$2\text{Re}(\mathcal{M}_{SM} \mathcal{M}_u^*) \stackrel{gg \rightarrow gg}{=} -\frac{N}{2(N^2 - 1)} \left(\text{Re}(\mathcal{D}_s) \frac{s^4}{ut} + \mathcal{D}_u \frac{u^4}{st} + \mathcal{D}_t \frac{t^4}{us} \right) \quad (6.3)$$

where

$$\mathcal{D}_s = -C_S \frac{\Gamma(2 - d_s)}{4^{d_s-1} \Gamma(d_s)} (-s)^{d_s-2}. \quad (6.4)$$

Table (6.2) contains the corresponding matrix element square for spin-0 unparticle interacting via the second term in (2.36). In table (6.3), we give the matrix element square for spin-2 unparticles with \mathcal{D}_s is defined by

$$\mathcal{D}_s = -C_T \frac{\Gamma(2 - d_t)}{4^{d_t-1} \Gamma(d_t + 2)} (-s)^{d_t-2} d_t (d_t - 1). \quad (6.5)$$

The t and u -channel propagators can be obtained by the replacement $s \rightarrow t, u$ respectively in eqns.(6.4,6.5) .

We now study invariant mass Q distribution, namely $d\sigma/dQ$, of the di-jet for the LHC with a center of mass of energy $\sqrt{S} = 14$ TeV. We have implemented all the parton level matrix element squares in a Monte Carlo based code that can accommodate all

the experimental cuts relevant for the phenomenological study. A $1/2$ factor for sub processes involving identical particles in the final state has been taken care of, when the angular integration is done over the range $-1 \leq \cos(\theta) \leq 1$. We use the leading order (LO) CTEQ 6L parton distribution functions (PDF) with the corresponding value of LO strong coupling constant $\alpha_s(M_Z) = 0.118$ and 5 light quark flavours. The factorization scale μ_F that appears in the PDFs and the renormalization scale μ_R in $\alpha_s(\mu_R^2)$ are identified to a single scale Q . In accordance with the CMS [90], we restrict the jets to satisfy rapidity cut $|\eta| < 1$ and the transverse momentum cut $p_T > 50$ GeV for each final state jet. We choose the scale Λ_u to be 2 TeV below which the scale invariance in the BZ sector sets in. The dimensionless coupling constants $\lambda_t, \lambda_{s1}, \lambda_{s2} = 0.9$ (see eqns.(2.36,2.38)) for all our phenomenology and we fix $C_T, C_S = 1$ appearing in the normalization of the propagators given in eqns.(2.39,2.41). The scaling dimension for the scalar unparticle is taken to be $d_s = 1.99$ and for the tensor unparticle, it is $d_t = 3.001$. We will also study the sensitivity of our results to these scaling dimensions, in particular for the scalar unparticle.

In the left panel of fig (6.1), we have plotted various subprocess contributions to the di-jet invariant mass distribution for spin-0 case (eqn.(2.36)) as a function of Q between 600 GeV and 1800 GeV. Interference of unparticle contribution with SM is added to those coming from pure unparticles in plotting these curves. Solid line gives the prediction in the SM. We note that $gg \rightarrow gg$ contribution resulting from the first term of eqn.(2.36) is numerically small compared to those coming from the second term. All the quark (and anti-quark) initiated subprocesses contribute almost equally for most of the Q range. In the right panel, we have shown the sensitivity of the scaling dimension d_s to $d\sigma/dQ$ distribution as a function of Q . Various curves here correspond to different values of d_s (1.91, 1.95, 1.99). It is clear from the right panel that the fermionic unparticle effects can be visible above $Q = 800$ GeV for scaling dimension closer to 1.99. As we deviate from $d_s = 1.99$ to lower values, the effects get washed away completely for a wide range of Q .

In fig (6.2) we have plotted the invariant mass distribution resulting from the spin-

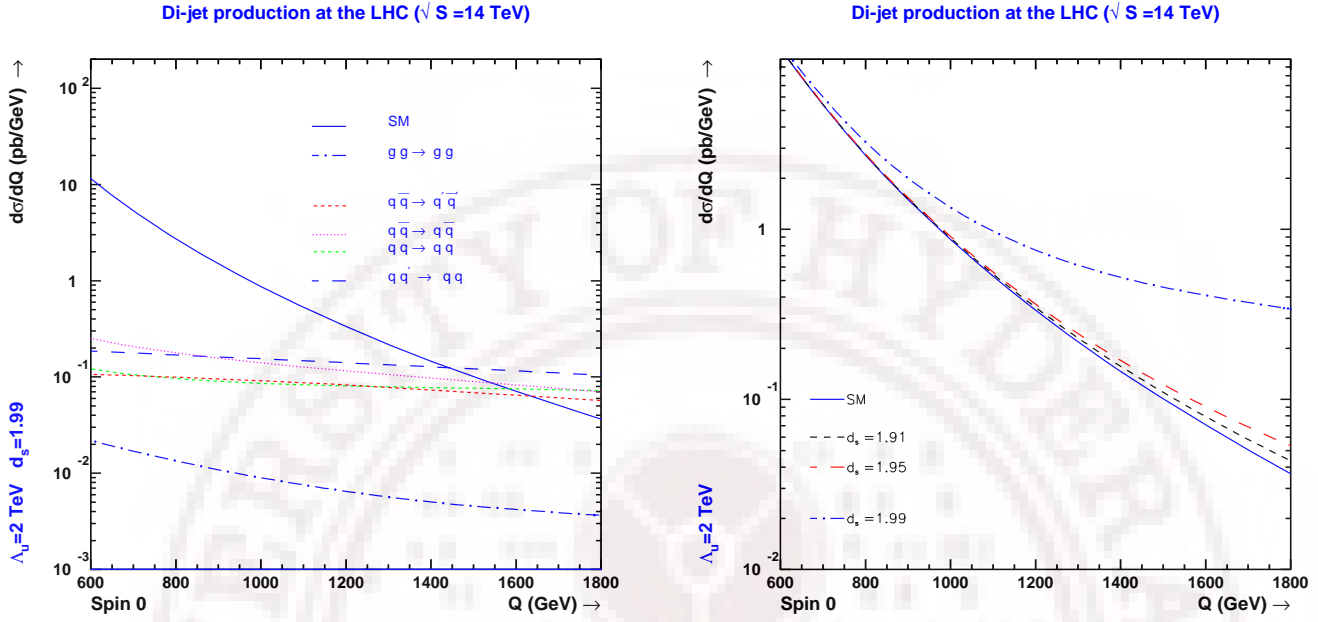


Figure 6.1: $d\sigma/dQ$ for di-jet production with spin-0 unparticles. The couplings are taken to be $\lambda_{s1,s2} = 0.9$ Left panel: Subprocess contribution. Right panel: Variation of scaling dimension.

2 unparticles (see eqn.(2.38)). Scale invariance restricts the scaling dimension to be greater than 3. We have chosen $d_u = 3.001$ for our analysis and find that the contribution of spin-2 unparticles do not give enhancement over the SM di-jet cross-section except very close to the cutoff scale Λ_u . The tensor unparticle contribution is smaller than that of the scalar unparticle due to the additional Λ_u suppression (see eqn.(2.38)) and large d_t value. Thus we conclude that the di-jet production is not much sensitive to the spin-2 unparticles and hence in what follows, only spin-0 unparticles will be considered.

In fig (6.3), we present the scalar unparticle contribution in the transverse momentum and the rapidity distributions of the jets. Because of the rapidity cut $|\eta| < 1$ on the jets, the events will be transverse in nature. In the limit where the momentum of the jet is in the transverse direction, it is easy to see that $p_T = Q/2$, where Q is the in-

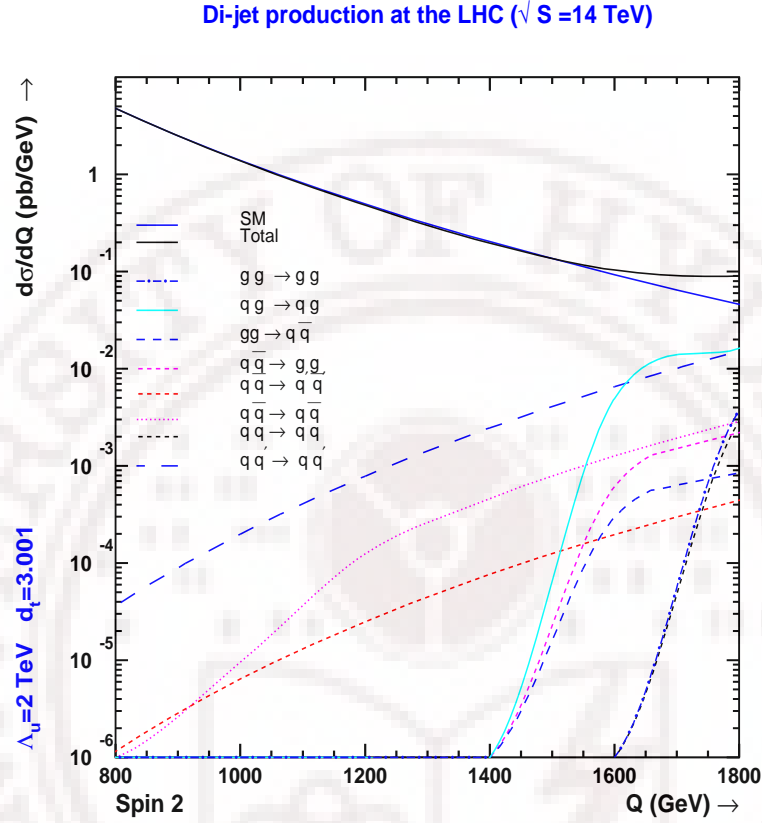


Figure 6.2: Subprocess contributions to the invariant di-jet mass distribution for $\Lambda_u=2\text{TeV}$ and $d_t = 3.001$.

variant mass of the di-jet. As Q is required to be less than Λ_u in the unparticle sector, we choose $Q^{max} = 0.9 \Lambda_u$ which translates into $p_T^{max} = Q^{max}/2$. As p_T is directly related to Q , the unparticle contribution is expected to be visible in the high p_T region as can be seen from the figure (left panel). The steep fall in the distribution close to 900 GeV is due to the limit on p_T ($< p_T^{max}$). For the rapidity distribution (right panel), we have integrated over Q in the region $1200 < Q < Q^{max}$ where the unparticle contribution is dominant over the SM background. For the rapidity distribution, as the two jets are experimentally indistinguishable, we have taken the average of the events coming from both the jets. The rapidity distributions in SM and unparticle model will then

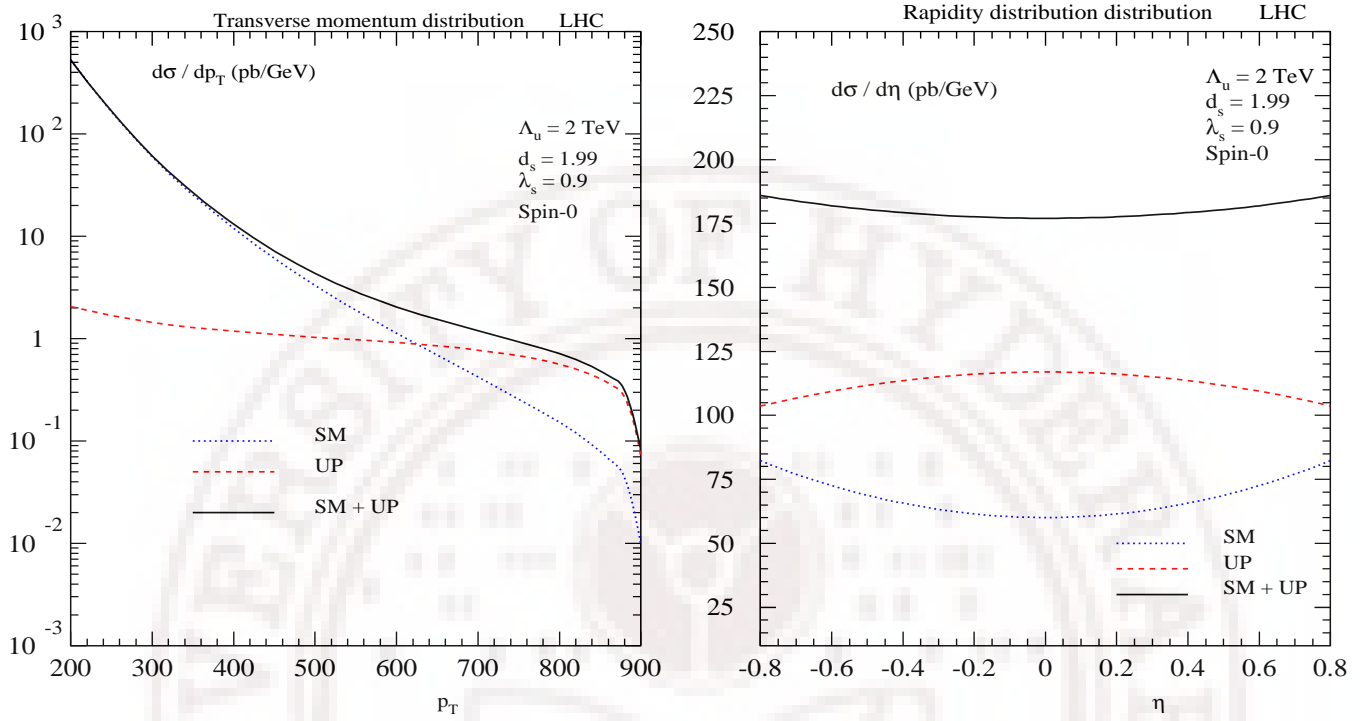


Figure 6.3: Scalar unparticle contribution to the transverse momentum and rapidity distributions of the jet in the di-jet production for $\Lambda_u = 2$ TeV and $d_s = 1.99$.

turn out to be symmetric about the central rapidity ($\eta = 0$), similar to the Drell-Yan and di-photon production cases.

If vector unparticles exist, then they also could contribute to the dijet production cross sections. This case is again similar to the tensor unparticle case, in the sense that the unitarity restricts the scaling dimension of the vector unparticles to $d_v > 3$ [26]. As the couplings of the unparticles with the SM fields are suppressed by the scale Λ_u raised to the power of scaling dimension d_v , the vector unparticle contribution is expected not to give any significant enhancements over the SM predictions. Also, in the vector unparticle case, not all of the above mentioned subprocesses will contribute, only quark initiated subprocesses can contribute.

6.3 Conclusions

We have studied the effects of scalar and tensor unparticles to di-jet production at the LHC. We have considered two SM scalar operators constructed out of quark (anti-quark) and gluon field operators that couple to the scalar unparticles. The tensor unparticles couple to a second rank SM operator which we take it to be the SM energy-momentum tensor. We have computed all the parton level cross sections and implemented in a Monte Carlo code that can easily incorporate all the experimental cuts. We have presented various subprocess contributions coming from scalar and tensor unparticles along with the SM contributions. This includes the interference of unparticle effects with the SM. We find that the scalar unparticle effects are large compared to that of tensor ones. Moreover, for a wide range of Q and d_t , the di-jet cross section is insensitive to tensor unparticles. This is in contrast to the di-photon production, for example, which gets significant enhancements from spin-2 unparticles as well. However, the scalar unparticles can give significant enhancements in the large invariant mass and p_T distributions over the SM predictions.

subprocess	$\overline{\sum} M ^2$
$qq' \rightarrow qq'$	$\frac{f_N}{2} \frac{s^2 + u^2}{t^2}$
$qq \rightarrow qq$	$\frac{f_N}{2} \left(\frac{u^2 + s^2}{t^2} + \frac{t^2 + s^2}{u^2} \right) - \frac{f_N}{N} \frac{s^2}{ut}$
$q\bar{q} \rightarrow q\bar{q}$	$\frac{f_N}{2} \left(\frac{u^2 + t^2}{s^2} + \frac{u^2 + s^2}{t^2} \right) - \frac{f_N}{N} \frac{u^2}{st}$
$q\bar{q} \rightarrow q'\bar{q}'$	$\frac{f_N}{2} \frac{u^2 + t^2}{s^2}$
$q\bar{q} \rightarrow gg$	$\frac{Nf_N}{2} \frac{(u^2 + t^2)^2}{uts^2} - \frac{f_N}{2N} \frac{u^2 + t^2}{ut}$
$gg \rightarrow q\bar{q}$	$\frac{1}{2N} \frac{(u^2 + t^2)^2}{uts^2} - \frac{1}{N^3 f_N} \frac{u^2 + t^2}{s^2}$
$qg \rightarrow qg$	$\frac{(u^2 + s^2)}{t^2} - \frac{f_N}{2} \frac{u^2 + s^2}{us}$
$gg \rightarrow gg$	$\frac{4}{f_N} \frac{(s^2 + su + u^2)^3}{s^2 u^2 t^2}$

Table 6.1: Matrix elements for the Standard Model. $s = (p_1 + p_2)^2, t = (p_1 - p_3)^2, u = (p_1 - p_4)^2$ and $f_N = (N^2 - 1)/N^2$

subprocess	$\overline{\sum} \mathcal{M}_u ^2$	$2 \operatorname{Re}(\mathcal{M}_u \mathcal{M}_{SM}^*)$
$qq' \rightarrow qq'$	$\mathcal{D}_t^2 t^2$	0
$qq \rightarrow qq$	$\frac{1}{N} \mathcal{D}_t \mathcal{D}_u tu + \mathcal{D}_t^2 t^2 + \mathcal{D}_u^2 u^2$	$\frac{N^2 - 1}{N^2} \left(\mathcal{D}_u \frac{u^2}{t} + \mathcal{D}_t \frac{t^2}{u} \right)$
$q\bar{q} \rightarrow q\bar{q}$	$\frac{1}{N} \mathcal{D}_t \operatorname{Re}(\mathcal{D}_s) st + \mathcal{D}_t^2 t^2 + \mathcal{D}_s ^2 s^2$	$\frac{N^2 - 1}{N^2} \left(\operatorname{Re}(\mathcal{D}_s) \frac{s^2}{t} + \mathcal{D}_t \frac{t^2}{s} \right)$
$q\bar{q} \rightarrow q'\bar{q}'$	$ \mathcal{D}_s ^2 s^2$	0

Table 6.2: Matrix elements for scalar unparticle in fermion initiated processes

subprocess	$\overline{\sum} \mathcal{M}_u ^2$	$2 \operatorname{Re}(\mathcal{M}_u \mathcal{M}_{SM}^*)$
$qq' \rightarrow qq'$	$\frac{1}{128} \mathcal{D}_t^2 (u^4 + s^4 - 6su[u^2 + s^2 - 3su])$	0
$qq \rightarrow qq$	$\frac{1}{128N} (N \mathcal{D}_t^2 [u^4 + s^4 - 6su(u^2 + s^2 - 3su)] + \mathcal{D}_t \mathcal{D}_u s^2 [4s^2 + 9ut]) + t \leftrightarrow u$	$-\frac{1}{8} \mathcal{D}_u f_N (3u + 4s) \frac{s^2}{t} - (u \leftrightarrow t)$
$q\bar{q} \rightarrow q\bar{q}$	$\frac{1}{128N} (N \mathcal{D}_t^2 [u^4 + s^4 - 6su(u^2 + s^2 - 3su)] + \operatorname{Re}(\mathcal{D}_t \mathcal{D}_s) u^2 [9ts + 4u^2]) + t \leftrightarrow s$	$-\frac{1}{8} f_N (\operatorname{Re}(\mathcal{D}_s) (3s + 4u) \frac{u^2}{t} - \mathcal{D}_t (3t + 4u) \frac{u^2}{s})$
$q\bar{q} \rightarrow q'\bar{q}'$	$\frac{1}{128} \mathcal{D}_s ^2 (u^4 + t^4 - 6tu[u^2 + t^2 - 3tu])$	0
$q\bar{q} \rightarrow gg$	$\frac{1}{8} N f_N \mathcal{D}_s ^2 ut(u^2 + t^2)$	$-\frac{1}{2} f_N \operatorname{Re}(\mathcal{D}_s) (u^2 + t^2)$
$gg \rightarrow q\bar{q}$	$\frac{1}{8} \frac{1}{N f_N} \mathcal{D}_s ^2 ut(u^2 + t^2)$	$-\frac{1}{2(N^2 - 1)} \operatorname{Re}(\mathcal{D}_s) (u^2 + t^2)$
$qg \rightarrow qg$	$-\frac{1}{8} \mathcal{D}_t^2 us(u^2 + s^2)$	$\frac{1}{2N} \mathcal{D}_t (u^2 + s^2)$
$gg \rightarrow gg$	$\frac{2}{8(N^2 - 1)} (\mathcal{D}_u \operatorname{Re}(\mathcal{D}_s) t^4 + \mathcal{D}_t \operatorname{Re}(\mathcal{D}_s) u^4 + \mathcal{D}_t \mathcal{D}_u s^4) + \frac{1}{8} \mathcal{D}_u^2 (t^4 + s^4) + \frac{1}{8} \mathcal{D}_t^2 (u^4 + s^4) + \frac{1}{8} \mathcal{D}_s ^2 (t^4 + u^4)$	$-\frac{1}{N f_N} (\mathcal{D}_u \frac{t^4 + s^4}{st} + \mathcal{D}_t \frac{u^4 + s^4}{su} + \operatorname{Re}(\mathcal{D}_s) \frac{t^4 + u^4}{ut})$

Table 6.3: BSM: Matrix elements for spin 2 unparticle



Chapter 7

Conclusions

At the LHC where it is very much possible to look for the collider signatures of the beyond standard model scenarios like extra dimension models, we have taken up an important task of computing the next-to-leading order QCD corrections to the pair production processes. In particular, we have computed the $\mathcal{O}(\alpha_s)$ QCD corrections to the di-photon production process in the context of warped extra dimension model (RS) at the Tevatron as well as at the LHC. For this NLO computation, we have used a semi-analytical two cut-off phase space slicing method which enables the successful implementation of various kinematic cuts on the photons and the Frixione's smooth cone isolation algorithm to suppress the final state QED singularities between the quarks and the photons. All the pieces of the NLO cross sections that are computed using this slicing method are incorporated in a Monte-Carlo based numerical code to obtain various kinematic distributions. We have checked our code first for the stability of the cross sections against the variation of the slicing parameters and found that the NLO cross sections are fairly stable for a wide range of both the cut-off parameters. Any value of the slicing parameters in this range is acceptable for the predictions of the signals. Further, we have compared our SM cross sections with those in the literature for their choice of the constraints on the final state photons and found a very good agreement. With this confidence, we have presented various kinematic distributions like invariant mass, rapidity, angular momentum distributions of the photon pairs

both for the SM and for the signal (SM+RS). The choice of the model parameters we have considered is consistent with the latest bounds obtained on them from the Tevatron data. It is found that the NLO QCD corrections have enhanced the cross sections significantly in almost all the distributions we have considered. It should be noted that the transverse momentum Q_T distribution of the di-photons come at higher orders in the perturbation theory from NLO onwards and there is no distribution of Q_T at the leading order. In this sense, the computation of the NLO corrections are advantageous in predicting the observables like Q_T which is otherwise not possible at the leading order.

One of the manifestations of the QCD is that the scale uncertainties will decrease with higher order contributions in the perturbation theory. In our analysis, we have studied the factorization scale μ_F dependency of the cross sections by varying it in the range $Q/2 < \mu_F < 3Q/2$, where ‘ Q ’ is the invariant mass of the di-photon. It is found that the scale uncertainties in the rapidity and angular distributions have reduced considerably in going from LO to NLO.

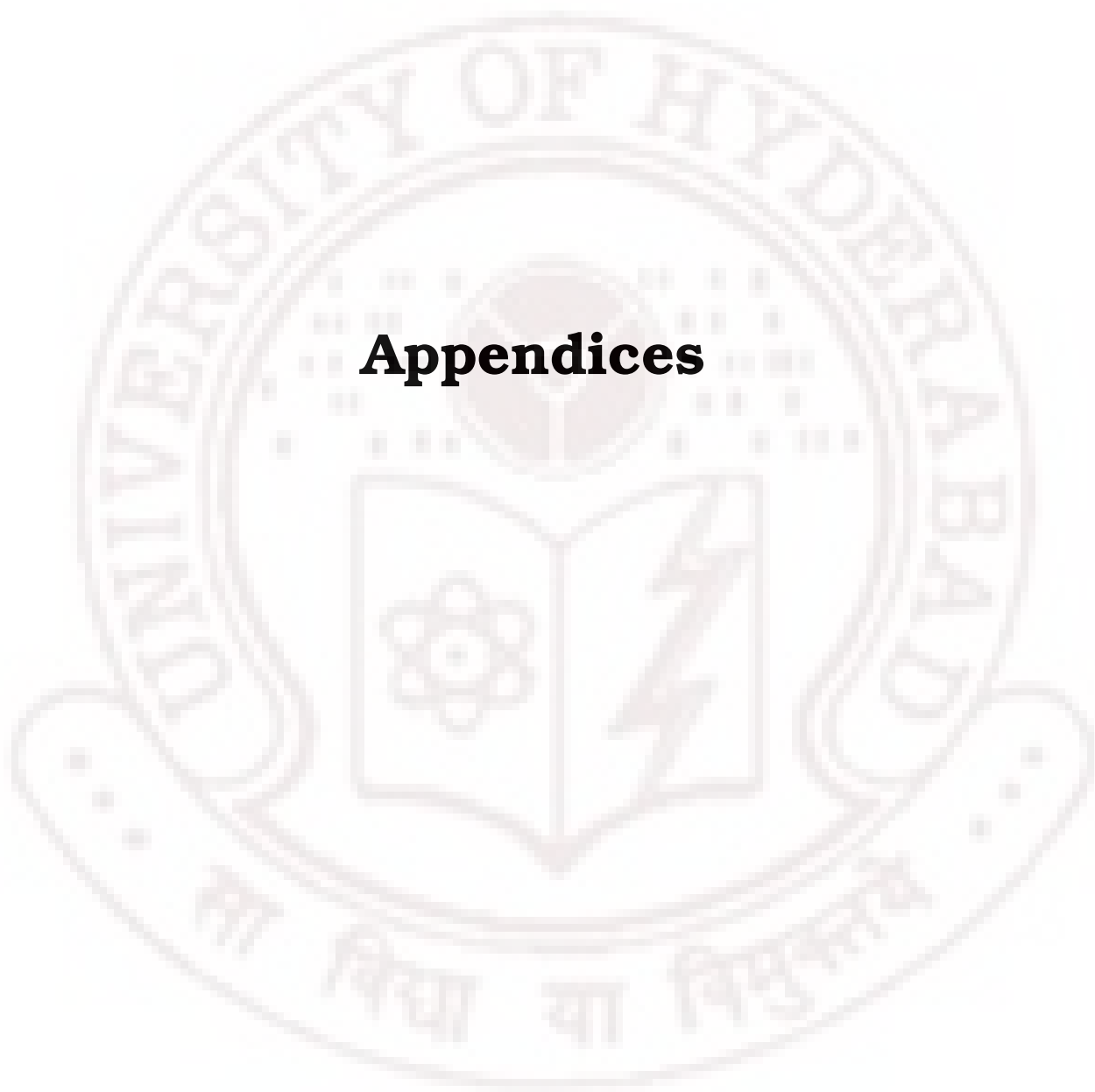
In the case of Drell-Yan (DY) process at the hadron colliders in the context of both large and warped extra dimension models, we have quantified various QCD uncertainties. For the parton distribution function (PDF) uncertainty, we have used three different parton density sets MRST2001, CTEQ6L/M and ALEKHIN and presented the dependency of the cross sections in various DY distributions both at the LHC and the Tevatron. We have also studied the scale dependency of these DY distributions by varying the factorization and renormalization scales in the range $Q/2 < (\mu_F, \mu_R) < 3Q/2$. It is found that the scale uncertainties decreased considerably by around a factor of 2.75 times in going from LO to NLO, irrespective of the model (ADD or RS) and independent of the machine (Tevatron or LHC) indicating that the QCD part factors out from the model dependent information and making this study a model independent one.

In the case of unparticle physics, we have studied the di-jet production process at the LHC by considering the effects of both spin-0 and spin-2 unparticle propagators.

It is found that the scalar unparticles can give significant contribution to the signal while the spin-2 unparticle effects are unnoticeable. We have presented the dijet cross sections in the case of scalar unparticles in different kinematic distributions like invariant mass, transverse momentum p_T and rapidity distributions of the jets.







Appendix A

gg box contribution

In SM, there are two non-vanishing helicity amplitude structures corresponding to the ones in BSM. They are [61]

$$M_{\text{SM}}^{+-+-} = M_{\text{SM}}^{-++-} = (-i)A\delta^{ab}\mathcal{F}(s, t, u) \quad (\text{A.0.1})$$

$$M_{\text{SM}}^{+- -+} = M_{\text{SM}}^{-++-} = (-i)A\delta^{ab}\mathcal{F}(s, u, t) \quad (\text{A.0.2})$$

where

$$\begin{aligned} \mathcal{F}(s, t, u) = & \left[1 + \frac{t-s}{u} \ln\left|\frac{t}{s}\right| + \frac{1}{2} \frac{s^2+t^2}{u^2} \ln^2\left|\frac{t}{s}\right| \right. \\ & \left. + i\pi \left\{ \frac{t-s}{u} + \frac{t^2+s^2}{u^2} \ln\left|\frac{t}{s}\right| \right\} \right] \\ \text{and } A = & 4\alpha\alpha_s \left[\sum_{j=1}^{n_f} Q_j^2 \right]. \end{aligned} \quad (\text{A.0.3})$$

The corresponding helicity amplitudes in the BSM case are [42]

$$M_{\text{SM}}^{+-+-} = M_{\text{SM}}^{-++-} = (-i)\frac{1}{2}\delta^{ab}\kappa^2\mathcal{D}'(s)u^2 \quad (\text{A.0.4})$$

$$M_{\text{SM}}^{+- -+} = M_{\text{SM}}^{-++-} = (-i)\frac{1}{2}\delta^{ab}\kappa^2\mathcal{D}'(s)t^2 \quad (\text{A.0.5})$$

where in the ADD model

$$\kappa^2\mathcal{D}'(s) = \frac{8\pi}{M_s^4} \left(\frac{\sqrt{s}}{M_s} \right)^{d-2} [2I(\Lambda/\sqrt{s}) - i\pi] \quad (\text{A.0.6})$$

The SM*GR+SM*GR interference corresponding to the first type helicity amplitude (eqn.[A.0.1]) is given by

$$\begin{aligned}
 [M_1^2] &= A \cdot \frac{1}{2} \cdot 8 \cdot u^2 \left[\mathcal{F}^*(s, t, u) \kappa^2 \mathcal{D}' s + \mathcal{F}(s, t, u) \kappa^2 \mathcal{D}'^*(s) \right] \\
 &= 32 \alpha_s \left[\sum_{j=1}^{n_f} Q_j^2 \right] \cdot \text{Re} \left[\mathcal{F}^*(s, t, u) \kappa^2 \mathcal{D}'(s) \right] \cdot u^2
 \end{aligned} \tag{A.0.7}$$

Similarly the SM*BSM interference part for the second type helicity amplitude (eqn.[A.0.2]) is given by

$$\begin{aligned}
 [M_2^2] &= A \cdot \frac{1}{2} \cdot 8 \cdot t^2 \left[\mathcal{F}^*(s, u, t) \kappa^2 \mathcal{D}' s + \mathcal{F}(s, u, t) \kappa^2 \mathcal{D}'^*(s) \right] \\
 &= 32 \alpha_s \left[\sum_{j=1}^{n_f} Q_j^2 \right] \cdot \text{Re} \left[\mathcal{F}^*(s, u, t) \kappa^2 \mathcal{D}'(s) \right] \cdot t^2
 \end{aligned} \tag{A.0.8}$$

The total SM*BSM interference contribution, including the helicity average, gluon color average for each gluon and the statistical average, is given by

$$M_{\text{SM*BSM}}^2 = \frac{1}{2} \frac{1}{4} \frac{1}{8} \frac{1}{8} \cdot 2 \cdot \{ [M_1^2] + [M_2^2] \} \tag{A.0.9}$$

Here the factor 2 comes because of the multiplicity of the helicity amplitude structures given in eqns.[A.0.1 and A.0.2].

Appendix B

Feynman rules

The propagator for the spin-2 KK modes is given by

$$P_G(q) = i B_{\mu\nu\rho\sigma} D(q) \quad (\text{B.0.1})$$

where $B_{\mu\nu\rho\sigma} = \eta_{\mu\rho}\eta_{\nu\sigma} + \eta_{\mu\sigma}\eta_{\nu\rho} - \frac{2}{n-1}\eta_{\mu\nu}\eta_{\sigma\rho}$ and $\eta_{\mu\nu}(q) = -g_{\mu\nu} + q_\mu q_\nu/q^2$. The tensors $C_{\mu\nu,\rho\sigma}$, $D_{\mu\nu,\rho\sigma}(p_1, p_2)$, $E_{\mu\nu,\rho\sigma}(p_1, p_2)$, $F_{\mu\nu\rho\sigma\lambda}(p_1, p_2, p_3)$ and $G_{\mu\nu,\rho\sigma\lambda\delta}$ used in the vertex factors are given by [6, 59] ¹

¹For the quark anti-quark gauge boson graviton vertex and the three gauge boson graviton vertex factors mentioned in [6] there will be an overall minus sign, which has been pointed out in [59].

$$C_{\mu\nu,\rho\sigma} = \eta_{\mu\rho}\eta_{\nu\sigma} + \eta_{\mu\sigma}\eta_{\nu\rho} - \eta_{\mu\nu}\eta_{\rho\sigma} , \quad (\text{B.0.2})$$

$$D_{\mu\nu,\rho\sigma}(p_1, p_2) = \eta_{\mu\nu}p_{1\sigma}p_{2\rho} - \left[\eta_{\mu\sigma}p_{1\nu}p_{2\rho} + \eta_{\mu\rho}p_{1\sigma}p_{2\nu} - \eta_{\rho\sigma}p_{1\mu}p_{2\nu} + (\mu \leftrightarrow \nu) \right] , \quad (\text{B.0.3})$$

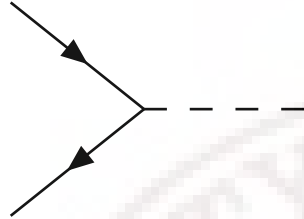
$$E_{\mu\nu,\rho\sigma}(p_1, p_2) = \eta_{\mu\nu}(p_{1\rho}p_{1\sigma} + p_{2\rho}p_{2\sigma} + p_{1\rho}p_{2\sigma}) - \left[\eta_{\nu\sigma}p_{1\mu}p_{1\rho} + \eta_{\nu\rho}p_{2\mu}p_{2\sigma} + (\mu \leftrightarrow \nu) \right] , \quad (\text{B.0.4})$$

$$F_{\mu\nu,\rho\sigma\lambda}(p_1, p_2, p_3) = \eta_{\mu\rho}\eta_{\sigma\lambda}(p_2 - p_3)_\nu + \eta_{\mu\sigma}\eta_{\rho\lambda}(p_3 - p_1)_\nu + \eta_{\mu\lambda}\eta_{\rho\sigma}(p_1 - p_2)_\nu + (\mu \leftrightarrow \nu) , \quad (\text{B.0.5})$$

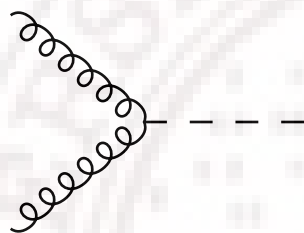
$$G_{\mu\nu,\rho\sigma\lambda\delta} = \eta_{\mu\nu}(\eta_{\rho\sigma}\eta_{\lambda\delta} - \eta_{\rho\delta}\eta_{\sigma\lambda}) + \left[\eta_{\mu\rho}\eta_{\nu\delta}\eta_{\lambda\sigma} + \eta_{\mu\lambda}\eta_{\nu\sigma}\eta_{\rho\delta} - \eta_{\mu\rho}\eta_{\nu\sigma}\eta_{\lambda\delta} - \eta_{\mu\lambda}\eta_{\nu\delta}\eta_{\rho\sigma} + (\mu \leftrightarrow \nu) \right] . \quad (\text{B.0.6})$$

All of these tensor are symmetric in $\mu \leftrightarrow \nu$.

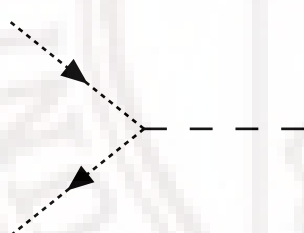
Following are the vertex factor for the gravitational interactions of spin-2 Kaluza-Klein modes with the SM fields.



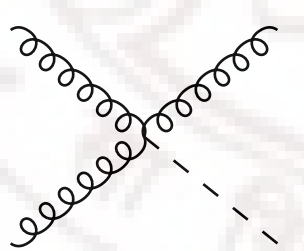
$$: -i\kappa/8 \left[\gamma_\mu (p_{1\nu} + p_{2\nu}) + \gamma_\nu (p_{1\mu} + p_{2\mu}) - 2\eta_{\mu\nu} (\not{p}_1 + \not{p}_2 - 2m_f) \right]$$



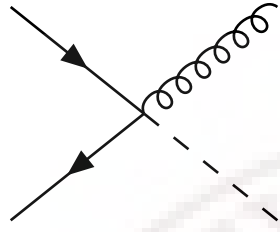
$$: -i\kappa/2 \delta^{ab} \left[(m_A^2 + p_1 \cdot p_2) C_{\mu\nu,\rho\sigma} D_{\mu\nu,\rho\sigma} (p_1 \cdot p_2) + \alpha^{-1} E_{\mu\nu,\rho\sigma} (p_1 \cdot p_2) \right]$$



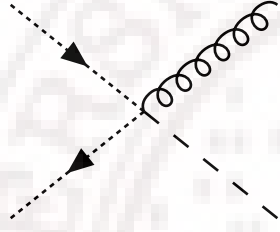
$$: -i\kappa/2 \left[(m_\phi^2 \eta_{\mu\nu} + C_{\mu\nu,\rho\sigma} p_1^\rho p_2^\sigma) \right]$$



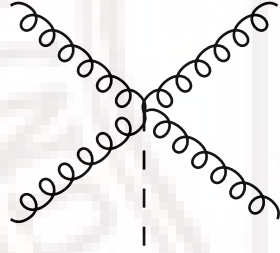
$$: -g\kappa/2 f^{abc} \left[C_{\mu\nu,\rho\sigma} (p_1 - p_2)_\lambda + C_{\mu\nu,\rho\lambda} (p_3 - p_1)_\sigma C_{\mu\nu,\sigma\lambda} (p_2 - p_3)_\rho + F_{\mu\nu,\rho\sigma\lambda} (p_1, p_2, p_3) \right]$$



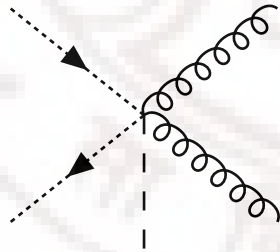
$$: -i g\kappa/4 T_{ij}^a [C_{\mu\nu,\rho\sigma} - \eta_{\mu\nu}\eta_{\rho\sigma}] \gamma^\sigma$$



$$: -i g\kappa/1 T_{ij}^a C_{\mu\nu,\rho\sigma} (k_1 + k_2)^\sigma$$



$$: -g^2\kappa/2 [f^{eac} f^{ebd} G_{\mu\nu,\rho\sigma\lambda\delta} + f^{eab} f^{ecd} G_{\mu\nu\rho\lambda\sigma\delta} \\ f^{ead} f^{ebc} G_{\mu\nu,\rho\sigma\delta\lambda}]$$



$$: -g^2\kappa/2 [C_{\mu\nu,\rho\sigma} \{T^a, T^b\}_{ij}]$$

where $\kappa = \sqrt{16\pi}/M_{Pl}$ in the case of ADD model and it is $\kappa = c_0 = k/M_{Pl}$ in the case of RS model.

Appendix C

Three body parametrization

In general for NLO computation using numerical techniques, the phase space integration is carried out using some multi-dimensional integration package like VEGAS. To do such integration, one has to have the three body phase space parametrization in which each of the 4-momentum components of all the final states are explicitly mentioned.

A typical NLO ($2 \rightarrow 3$) parton level process is given by

$$p_1 + p_2 \rightarrow p_3 + p_4 + p_5 \quad (\text{C.0.1})$$

where p_1, p_2 are the 4-momenta of the initial partons and p_3, p_4, p_5 are the 4-momenta of the final state partons. For simplification, we assume all the partons involved here are massless. The initial partons moving along the Z-axis are parameterized as

$$p_1 = \frac{\sqrt{s}}{2}(1, 0, 0, 1); \quad p_2 = \frac{\sqrt{s}}{2}(1, 0, 0, -1) \quad (\text{C.0.2})$$

where $s = (p_1 + p_2)^2$. To begin with one can consider the system of p_4 and p_5 as to correspond to a single particle whose mass is $p_{45}^2 = (p_4 + p_5)^2 \neq 0$. Then the above $2 \rightarrow 3$ process just corresponds to

$$p_1 + p_2 \rightarrow p_3 + p_{45} \quad (\text{C.0.3})$$

In any $2 \rightarrow 2$ process, both the initial and final state partons lie on a plane, the

4-momenta p_3 and p_{45} can easily be parameterized as

$$p_3 = E_3(1, \sin\theta, 0, \cos\theta); \quad p_4 = (E_{45}, -|\vec{p}|\sin\theta, 0, |\vec{p}|\cos\theta), \quad (\text{C.0.4})$$

where $E_3 = |\vec{p}|$ and E_{45} are the energies of p_3 and p_{45} system respectively and are calculated as

$$[(p_1 + p_2)^2 - p_3]^2 = (p_4 + p_5)^2 \quad (\text{C.0.5})$$

$$s - 2 E_3 \sqrt{s} = s_{45} \Rightarrow E_3 = \frac{s - s_{45}}{2\sqrt{s}} \quad (\text{C.0.6})$$

$$E_{45} = \sqrt{s} - E_3 \Rightarrow E_{45} = \frac{s + s_{45}}{2\sqrt{s}}. \quad (\text{C.0.7})$$

Here the particles p_3 and p_{45} are back to back and are along a direction Z' which is at an angle θ with the Z -axis along which the initial partons p_1 and p_2 are moving. For simplicity, one can directly work in that frame where this Z' is taken as the reference axis and towards the end one can make rotation transformation to come back to the actual Z -axis. In this new direction, the partons have the following parametrization

$$p_3 = |\vec{p}|(1, 0, 0, 1); \quad p_{45} = (E_{45}, 0, 0, -|\vec{p}|) \quad (\text{C.0.8})$$

Now the idea is to parameterize p_4 and p_5 in the rest frame of p_{45} and then boost these momenta to comes back to the centre of frame in which Z' is the reference directions. The rest frame of p_{45} itself is actually moving with a momentum of $|\vec{p}|$ and with an energy of E_{45} in the centre of mass frame of p_3 and p_{45} with new reference direction. Therefore the Lorentz boost parameters associated with are $\beta = |\vec{p}|/E_{45}$ and $\gamma = 1/\sqrt{1 - \beta^2}$. The 4-momenta of p_4 and p_5 in the rest frame of p_{45} can be parameterized as (here the momenta are denoted by asterisks)

$$p_4^* = \frac{\sqrt{s_{45}}}{2}(1, \sin\theta_1 \cos\phi_1, \sin\theta_1 \sin\phi_1, \cos\theta_1) \quad (\text{C.0.9})$$

$$p_5^* = \frac{\sqrt{s_{45}}}{2}(1, -\sin\theta_1 \cos\phi_1, -\sin\theta_1 \sin\phi_1, -\cos\theta_1), \quad (\text{C.0.10})$$

where θ_1 is the angle of p_4 momentum direction with Z' -direction and ϕ_1 is the azimuthal angle in the rest frame of p_{45} . The 4-momenta of p_4 in the centre of mass

frame of p_{45} and p_3 can easily be obtained from the Lorentz transformations using the above mentioned boost parameters as (here the componets are denoted by primes)

$$E'_4 = \gamma(E_4^* - \beta p_{4z}^*); \quad p'_{4z} = \gamma(p_{4z}^* - \beta E_4^*) \quad (\text{C.0.11})$$

$$E'_4 = \frac{1}{2}(E_{45} - |\vec{p}| \cos\theta_1) \quad p'_{4z} = \frac{1}{2}(E_{45} \cos\theta_1 - |\vec{p}|). \quad (\text{C.0.12})$$

Here under the boost only the z-component of the momentum and the energy are only modified. The transverse components p_{4x}^* and p_{4y}^* will remain unaffected. Hence $p'_{4x} = p_{4x}^*$, $p'_{4y} = p_{4y}^*$. Now we rotate the Z' direction by the angle θ to go back to the actual Z -direction along which the initial particles are moving. Now, under these rotations in the XZ plane, the p_{4x} and p_{4z} components will mix up (here the components are without any asterisks and primes)

$$\begin{pmatrix} p_{4x} \\ p_{4z} \end{pmatrix} = \begin{pmatrix} \cos\theta & \sin\theta \\ -\sin\theta & \cos\theta \end{pmatrix} \begin{pmatrix} p'_{4x} \\ p'_{4z} \end{pmatrix},$$

Under this rotations, the transverse component p_{4y} will be unaffected and is same as p'_{4y} . Finally we have

$$p_4^{(0)} = \frac{1}{2}(E_{45} - |\vec{p}| \cos\theta_1) \quad (\text{C.0.13})$$

$$p_4^{(1)} = p'_{4x} \cos\theta + p'_{4z} \sin\theta \quad (\text{C.0.14})$$

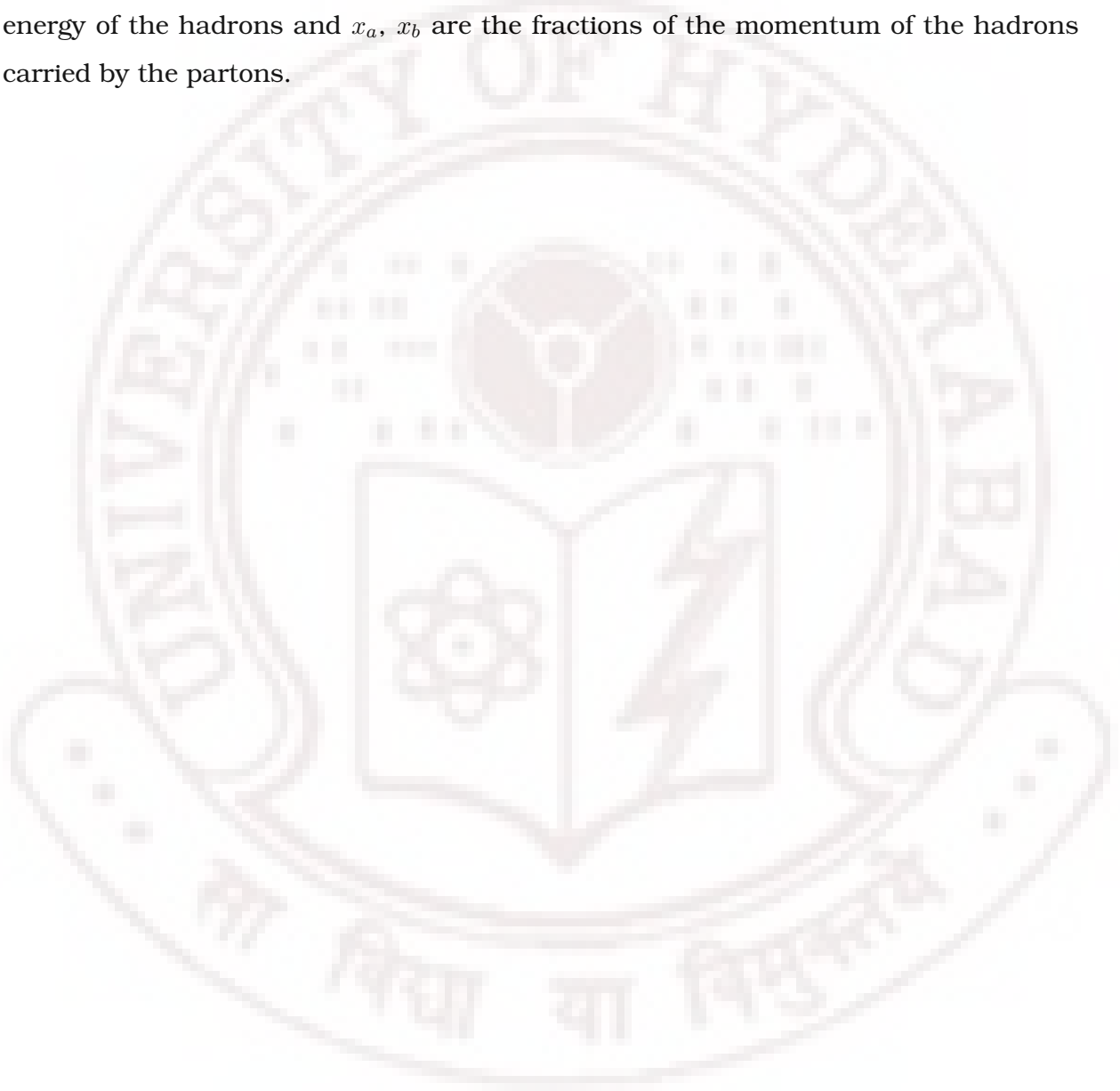
$$p_4^{(2)} = \frac{\sqrt{s_{45}}}{2} \sin\theta_1 \sin\phi_1 \quad (\text{C.0.15})$$

$$p_4^{(3)} = -p'_{4x} \sin\theta + p'_{4z} \cos\theta \quad (\text{C.0.16})$$

$$(\text{C.0.17})$$

where $p'_{4x} = \frac{\sqrt{s_{45}}}{2} \sin\theta_1 \cos\phi_1$ and $p'_{4z} = \frac{1}{2}(E_{45}\cos\theta_1 - |\vec{p}|)$. Here it should be noted that under the boosts or rotations, the angles also can chane to some other angles. But as per the numerical integration are considered, they are, after all, integration variables and will be integrated over in the full range. The frame dependency will not be there on them in that sense. The momentum p_5 can be obtained from the momentum conservation $p_5 = p_1 + p_2 - p_3 - p_4$. Finally, one can boost all these quantities to go

to the lab frame or the center of mass frame of the hadrons. The centre of mass frame of the partons, in the centre of mass frame of the hadrons, has a longitudinal momentum of $|\vec{P}_c| = (x_a - x_b) \sqrt{S}/2$ and an energy of $E_c = (x_a + x_b) \sqrt{S}/2$. Therefore the boost factors are $\beta_c = |\vec{P}|/E_c$ and $\gamma_c = 1/\sqrt{1 - \beta_c^2}$, where \sqrt{S} is the center of mass energy of the hadrons and x_a, x_b are the fractions of the momentum of the hadrons carried by the partons.



Other Publications

1. **Diphoton signals in theories with large extra dimensions to NLO QCD at hadron colliders**

M. C. Kumar, Prakash Mathews, V. Ravindran, Anurag Tripathi

Phys. Lett. B672 (2009) 45.

2. **Unparticles in diphoton production to NLO in QCD at the LHC**

M. C. Kumar, Prakash Mathews, V. Ravindran and Anurag Tripathi

Phys. Rev. D79 (2009) 075012; arXiv : 0804.4054 [hep-ph].

3. **Unparticle physics in diphoton production at the CERN LHC**

M.C.Kumar, Prakash Mathews, V.Ravindran and Anurag Tripathi

Phys. Rev. D77 (2008) 055013

Conferences/Schools attended

1. A topical meeting on **Beyond Standard Model Physics at the LHC**^{a 1} (bsmlhc) held at Indian Association for the Cultivation of the Science, Jadavpur, India during 15th to 17th January, 2009 .

2. Workshop on **Signaling the arrival of the LHC Era**^a

The Abdus-Salam International Centre for Theoretical Physics (I.C.T.P.), Trieste, Italy .

8th to 13th December, 2008.

3. Workshop on the **LHC and related Physics,**

Harish-Chandra Research Institute, Allahabad, India,

Sept. 20th - Oct 4th, 2008.

4. **Physics of Warped Extra Dimensions**^a,

^{1a} **Talk presented.**

Indian Institute of Technology Kharagpur, Kharagpur, India,
February, 2008.

5. **Workshop on High Energy Physics Phenomenology (WHEPPX)^a,**

Institute of Mathematical Sciences, Chennai, India,
January, 2008.

6. School on **QCD at the LHC,**

Harish-Chandra Research Institute, Allahabad, India,
November, 2007.

7. **SERC-THEP** main school,

University of Hyderabad, Hyderabad, India,
January, 2007.

8. **A topical meeting on Physics at LHC,**

Harish-Chandra Research Institute, Allahabad, India,
December, 2006.

9. **XVII DAE-BRNS High Energy Physics symposium,^a**

Indian Institute of Technology (I.I.T.) Kharagpur, Kharagpur, India,
December, 2006.

10. **SERC-THEP** main school, Indian Institute of Technology Kanpur, Kanpur, India,
December, 2004.

11. **SERC-THEP** preparatory school,

Institute of Mathematical Sciences, Chennai, India, October, 2004.

12. **(SERC)** preparatory school in Theoretical High Energy Physics **(THEP),**

University of Hyderabad, Hyderabad, India, December, 2003.

References

- [1] T. Appelquist, H. C. Cheng and B. A. Dobrescu, Phys. Rev. D **64** (2001) 035002 [arXiv:hep-ph/0012100].
- [2] N. Arkani-Hamed, S. Dimopoulos and G. R. Dvali, Phys. Lett. B **429** (1998) 263; I. Antoniadis, N. Arkani-Hamed, S. Dimopoulos and G. R. Dvali, Phys. Lett. B **436** (1998) 257; N. Arkani-Hamed, S. Dimopoulos, and G. Dvali, Phys. Rev. **D59**, (1999) 086004.
- [3] L. Randall and R. Sundrum, Phys. Rev. Lett. **83** (1999) 3370; W.D. Goldberger and M.B. Wise, Phys. Rev. Lett. **83** (1999) 4922.
- [4] M. Carmeli and T. Kuzmenko, arXiv:astro-ph/0110590.
- [5] T. Kaluza, Sitzungsber. Preuss. Akad. Wiss. Berlin (Math. Phys.) **1921** (1921) 966. T. Kaluza,
- [6] T. Han, J. D. Lykken and R. J. Zhang, Phys. Rev. D **59** (1999) 105006.
- [7] G. F. Giudice, R. Rattazzi and J. D. Wells, *Nucl. Phys.* **B544** (1999) 3.
- [8] E. A. Mirabelli, M. Perelstein, M. E. Peskin Phys. Rev. Lett. 82 (1999) 2236.
- [9] Prakash Mathews, Sreerup Raychaudhuri, K. Sridhar Phys. Lett. B450 (1999) 343; *ibid* Phys. Lett. B455 (1999) 115; *ibid* JHEP 0007 (2000) 008.
- [10] V. M. Abazov *et al.* [D0 Collaboration], Phys. Rev. Lett. **102** (2009) 051601

- [11] W.D. Goldberger and M.B. Wise, *Phys. Rev. Lett.* **83** (1999) 4922; *ibid Phys.Lett.* **B475** (2000) 275.
- [12] H. Davoudiasl, J.L. Hewett and T.G. Rizzo, *Phys. Rev. Lett* **84** (2000) 2080; *ibid. Phys. Rev.* **D63** (2001) 075004.
- [13] V. M. Abazov *et al.* [D0 Collaboration], *Phys. Rev. Lett.* **100** (2008) 091802 [arXiv:0710.3338 [hep-ex]].
- [14] C. D. Hoyle *et al.*, *Phys. Rev. D* **70** (2004) 042004
- [15] D. J. Kapner *et al.*, *Phys. Rev. Lett.* **98** (2007) 021101
- [16] S. J. Smullin *et al.*, *Phys. Rev. D* **72** (2005) 122001.
- [17] R. Spero *et al.*, *Phys. Rev. Lett.* **44** (1980) 1645; J. K. Hoskins *et al.*, *Phys. Rev. D* **32** (1985) 3084.
- [18] J.C. Long *et al.*, *Nature* 421, 922 (2003)
- [19] J. Chiaverini *et al.*, *Phys. Rev. Lett.* **90** (2003) 151101
- [20] E. G. Adelberger *et al.*, *Ann. Rev. Nucl. Part. Sci.* **53** (2003) 77
- [21] M. Azam, M. Sami, C. S. Unnikrishnan and T. Shiromizu, *Phys. Rev. D* **77** (2008) 101101
- [22] T. Banks and A. Zaks, *Nucl. Phys. B* **196** (1982) 189.
- [23] H. Georgi, *Phys. Rev. Lett.* **98** (2007) 221601 [arXiv:hep-ph/0703260].
- [24] Y. Nakayama, *Phys. Rev. D* **76**, 105009 (2007).
- [25] G. Mack, *Commun. Math. Phys.* **55**, 1 (1977).
- [26] B. Grinstein, K. A. Intriligator and I. Z. Rothstein, *Phys. Lett. B* **662** (2008) 367 [arXiv:0801.1140 [hep-ph]].

- [27] H. Georgi, Phys. Lett. B **650** (2007) 275 [arXiv:0704.2457 [hep-ph]].
- [28] K. Cheung, W. Y. Keung and T. C. Yuan, Phys. Rev. Lett. **99** (2007) 051803 [arXiv:0704.2588 [hep-ph]].
- [29] K. Cheung, W. Y. Keung and T. C. Yuan, AIP Conf. Proc. **1078** (2009) 156 [arXiv:0809.0995 [hep-ph]]. A. Rajaraman, AIP Conf. Proc. **1078**, 63 (2009) [arXiv:0809.5092 [hep-ph]], and references therein.
- [30] A. Bredenstein, A. Denner, S. Dittmaier and S. Pozzorini, JHEP **0808** (2008) 108 [arXiv:0807.1248 [hep-ph]].
- [31] L. Reina and S. Dawson, Phys. Rev. Lett. **87** (2001) 201804 [arXiv:hep-ph/0107101].
- [32] F. Febres Cordero, L. Reina and D. Wackeroth, Phys. Rev. D **74** (2006) 034007 [arXiv:hep-ph/0606102].
- [33] B. W. Harris and J. F. Owens, Phys. Rev. D **65** (2002) 094032 [arXiv:hep-ph/0102128].
- [34] E.L. Berger, E. Braaten and R.D. Field, Nucl. Phys. B **239**, 52 (1984); P. Aurenche, A. Douiri, R. Baier, M. Fontannaz and D. Schiff, Z. Phys. C **29**, 459 (1985); B. Bailey, J.F. Owens and J. Ohnemus, Phys. Rev. D **46**, 2018 (1992); B. Bailey and J.F. Owens, Phys. Rev. D **47**, 2735 (1993); B. Bailey and D. Graudenz, Phys. Rev. D **49**, 1486 (1994) [arXiv:hep-ph/9307368]; C. Balazs, E.L. Berger, S. Mrenna and C.-P. Yuan, Phys. Rev. D **57**, 6934 (1998) [arXiv:hep-ph/9712471]; C. Balazs and C.-P. Yuan, Phys. Rev. D **59**, 114007 (1999) [Erratum-ibid. D **63**, 059902 (1999)] [arXiv:hep-ph/9810319]; T. Binoth, J.P. Guillet, E. Pilon and M. Werlen, Phys. Rev. D **63**, 114016 (2001) [arXiv:hep-ph/0012191]; T. Binoth, arXiv:hep-ph/0005194. T. Binoth, J.P. Guillet, E. Pilon and M. Werlen, Eur. Phys. J. C **16**, 311 (2000) [arXiv:hep-ph/9911340].
- [35] E. Bonvin *et al.* [WA70 Collaboration], Z. Phys. C **41** (1989) 591.

- [36] E. Bonvin *et al.* [WA70 Collaboration], Phys. Lett. B **236** (1990) 523.
- [37] J. Alitti *et al.* [UA2 Collaboration], Phys. Lett. B **288** (1992) 386.
- [38] F. Abe *et al.* [CDF Collaboration], Phys. Rev. Lett. **70** (1993) 2232.
- [39] T. Binoth *et al.*, Eur. Phys. J. C **16** (2000) 311.
- [40] Z. Bern, L. J. Dixon and C. Schmidt, Phys. Rev. D **66** (2002) 074018 [arXiv:hep-ph/0206194].
- [41] C. Balazs *et al.*, Phys. Rev. D **76** (2007) 013009;
- [42] O. J. P. Eboli, T. Han, M. B. Magro and P. G. Mercadante, Phys. Rev. D **61** (2000) 094007 [arXiv:hep-ph/9908358];
- [43] K. m. Cheung and G. L. Landsberg, Phys. Rev. D **62** (2000) 076003 [arXiv:hep-ph/9909218];
- [44] O. J. P. Eboli, T. Han, M. B. Magro and P. G. Mercadante, Phys. Rev. D **61** (2000) 094007 [arXiv:hep-ph/9908358]; K. m. Cheung and G. L. Landsberg, Phys. Rev. D **62** (2000) 076003 [arXiv:hep-ph/9909218]; M. Luo, L. Wang and G. Zhu, Phys. Lett. B **672** (2009) 65 [arXiv:0812.0866 [hep-ph]]; M. C. Kumar, P. Mathews, V. Ravindran and A. Tripathi, Phys. Lett. B **672** (2009) 45 [arXiv:0811.1670 [hep-ph]].
- [45] P. Mathews, V. Ravindran, K. Sridhar and W. L. van Neerven, Nucl. Phys. B **713**, 333 (2005) [arXiv:hep-ph/0411018].
- [46] P. Mathews, V. Ravindran and K. Sridhar, JHEP **0510**, 031 (2005) [arXiv:hep-ph/0506158].
- [47] P. Mathews and V. Ravindran, Nucl. Phys. B **753**, 1 (2006) [arXiv:hep-ph/0507250].

- [48] M. C. Kumar, P. Mathews and V. Ravindran, Eur. Phys. J. C **49**, 599 (2007) [arXiv:hep-ph/0604135].
- [49] A. Abulencia *et al.* [CDF Collaboration], Phys. Rev. Lett. **97** (2006) 171802 [arXiv:hep-ex/0605101].
- [50] M. C. Kumar, P. Mathews, V. Ravindran and A. Tripathi, Phys. Rev. D **77** (2008) 055013 [arXiv:0709.2478 [hep-ph]]; M. C. Kumar, P. Mathews, V. Ravindran and A. Tripathi, arXiv:0804.4054 [hep-ph];
- [51] B. Bailey, J. F. Owens and J. Ohnemus, Phys. Rev. D **46** (1992) 2018.
- [52] FORM by J.A.M. Vermaseren, version 3.0 available from <http://www.nikhef.nl/form>.
- [53] R. K. Ellis, I. Hinchliffe, M. Soldate and J. J. van der Bij, Nucl. Phys. B **297** (1988) 221; L. Ametller, E. Gava, N. Paver and D. Treleani, Phys. Rev. D **32**, 1699 (1985);
D.A. Dicus and S.S.D. Willenbrock, Phys. Rev. D **37**, 1801 (1988).
- [54] M. C. Kumar, P. Mathews, V. Ravindran and A. Tripathi, Phys. Lett. B **672** (2009) 45 [arXiv:0811.1670 [hep-ph]].
- [55] S. Frixione, Phys. Lett. B **429** (1998) 369.
- [56] ATLAS Collaboration, ATLAS detector and physics performance. Technical design report. Vol. 2 (1999), CERN-LHCC-99-15.
- [57] CMS Collaboration, "CMS: The electromagnetic calorimeter, technical design report," report CERN/LHCC 97-33, CMS-TDR-4.
- [58] H. Flacher, M. Goebel, J. Haller, A. Hocker, K. Moenig and J. Stelzer, Eur. Phys. J. C **60** (2009) 543 [arXiv:0811.0009 [hep-ph]].
- [59] P. Mathews, V. Ravindran and K. Sridhar, JHEP **0408** (2004) 048 [arXiv:hep-ph/0405292].

- [60] J. Pumplin *et al.*, JHEP **0207** (2002) 012.
- [61] Z. Bern, L. J. Dixon and C. Schmidt, Phys. Rev. D **66** (2002) 074018 [arXiv:hep-ph/0206194].
- [62] S. D. Drell and T. M. Yan, Phys. Rev. Lett. **25** (1970) 316 [Erratum-ibid. **25** (1970) 902].
- [63] V. M. Abazov *et al.* [D0 Collaboration], arXiv:0904.0673 [hep-ex].
- [64] V. M. Abazov *et al.* [D0 Collaboration], arXiv:0901.2137 [hep-ex]. V. M. Abazov *et al.* [D0 Collaboration], Phys. Rev. D **76**, 052006 (2007)
- [65] G. Altarelli, R. K. Ellis and G. Martinelli, Nucl. Phys. B **157** (1979) 461.
- [66] T. Matsuura, S. C. van der Marck and W. L. van Neerven, Nucl. Phys. B **319** (1989) 570.
- [67] T. Matsuura, S. C. van der Marck and W. L. van Neerven, Phys. Lett. B **211**, 171 (1988).
- [68] T. Matsuura and W. L. van Neerven, Z. Phys. C **38** (1988) 623.
- [69] R. Hamberg, W. L. van Neerven and T. Matsuura, Nucl. Phys. B **359** (1991) 343 [Erratum-ibid. B **644** (2002) 403].
- [70] C. Anastasiou, L. J. Dixon, K. Melnikov and F. Petriello, Phys. Rev. Lett. **91** (2003) 182002
- [71] S. Alekhin Phys.Rev. D68 (2003) 014002.
- [72] A.D. Martin *et. al.*, Eur.Phys.J. C23 (2002) 73.
- [73] M. Bothe, Eur. Phys. J. C14 (2000) 285; W. T. Giele, S. Keller, Phys. Rev. D58 (1998) 094023; W. T. Giele, S. Keller, D. A. Kosower, hep-ph/0104052; S. I. Alekhin, Phys. Rev. D 63 (2001) 094022; CTEQ Collaboration: J. Pumplin *et al.*, JHEP 0207 (2002) 012; A. M. Cooper-Sarkar, J. Phys. G 28 (2002) 2669.

- [74] A.D. Martin *et. al.*, Eur.Phys.J. C28 (2003) 455.
- [75] A.D. Martin, R.G. Roberts, W.J. Stirling, R.S. Thorne PPP/01/37, DCPT/01/74, CERN-TH/2001-273, Cavendish-HEP-01/14 Journal-ref: Eur.Phys.J. C23 (2002) 73-87 and hep-ph/0110215.
- [76] V. M. Abazov *et. al.*, DØ Collaboration, Phy. Rev. Lett. 95 (2005) 091801.
- [77] C. D. Hoyle *et. al.*, Phys. Rev. **D70** (2004) 042004.
- [78] G. Altarelli and G. Parisi, Nucl. Phys. B **126** (1977) 298.
- [79] D. M. Hofman and J. Maldacena, JHEP **0805** (2008) 012 [arXiv:0803.1467 [hep-th]].
- [80] A. T. Alan, arXiv:0711.3272 [hep-ph].
- [81] P. Mathews and V. Ravindran, Phys. Lett. B **657** (2007) 198 [arXiv:0705.4599 [hep-ph]].
- [82] M. C. Kumar, P. Mathews, V. Ravindran and A. Tripathi, Phys. Rev. D **77** (2008) 055013 [arXiv:0709.2478 [hep-ph]].
- [83] M. C. Kumar, P. Mathews, V. Ravindran and A. Tripathi, Phys. Rev. D **79** (2009) 075012; arXiv:0804.4054 [hep-ph].
- [84] L. Randall and D. Tucker-Smith, Phys. Rev. Lett. **101** (2008) 221803 [arXiv:0806.1049 [hep-ph]].
- [85] L. A. Anchordoqui, H. Goldberg, D. Lust, S. Nawata, S. Stieberger and T. R. Taylor, Phys. Rev. Lett. **101** (2008) 241803 [arXiv:0808.0497 [hep-ph]].
- [86] P. Mathews, S. Raychaudhuri and K. Sridhar, JHEP **0007**, 008 (2000) [arXiv:hep-ph/9904232].
- [87] D. Atwood, S. Bar-Shalom and A. Soni, Phys. Rev. D **62** (2000) 056008 [arXiv:hep-ph/9911231].

- [88] D. K. Ghosh, P. Mathews, P. Poulose and K. Sridhar, JHEP **9911** (1999) 004 [arXiv:hep-ph/9909567].
- [89] B. L. Combridge, J. Kripfganz and J. Ranft, Phys. Lett. B **70** (1977) 234.
- [90] A. Bhatti *et al.*, J. Phys. G **36** (2009) 015004 [arXiv:0807.4961 [hep-ex]].
- [91] G. . Altarelli and M. L. . Mangano, “Standard model physics (and more) at the LHC. Proceedings, Workshop, Geneva, Switzerland, May 25-26, October 14-15, 1999,” D. Froidevaux and V. A. Mitsou, arXiv:0905.0258 [hep-ex];
- [92] G. F. Giudice, A. Strumia, Nucl. Phys. **B663** (2003) 377; G. F. Giudice, T. Plehn, A. Strumia, Nucl. Phys. **B706** (2005) 455.
- [93] V. M. Abazov *et. al.*, DØ Collaboration, Phy. Rev. Let. 95 (2005) 161602.
- [94] K. Cheung and G. Landsberg, Phys. Rev. **D62** (2000) 076003.